COMBINATORIAL SYNTHESIS OF NEW GFP- AND RFP-LIKE CHROMOPHORES AND THEIR PHOTOPHYSICAL PROPERTIES

A Dissertation
Presented to
The Academic Faculty

By

William Brett Fellows

In Partial Fulfillment
Of the Requirements for the Degree
Doctor of Philosophy in Chemistry

Georgia Institute of Technology

August, 2014

COMBINATORIAL SYNTHESIS OF NEW GFP- AND RFP-LIKE CHROMOPHORES AND THEIR PHOTOPHYSICAL PROPERTIES

Approved by:

Dr. Laren M. Tolbert, Advisor
School of Chemistry and Biochemistry
Georgia Institute of Technology

Dr. Charles Liotta
School of Chemistry and Biochemistry
Georgia Institute of Technology

Dr. David M. Collard
School of Chemistry and Biochemistry
Georgia Institute of Technology

Dr. Kyril Solntsev
School of Chemistry and Biochemistry
Georgia Institute of Technology

Dr. Wendy Kelly
School of Chemistry and Biochemistry
Georgia Institute of Technology

Dr. Julia Kubanek
School of Biology
Georgia Institute of Technology

Date Approved: May 27, 2014

ACKNOWLEDGEMENTS

I want to thank everyone who helped make this dissertation possible. First I want to thank Dr. Laren Tolbert for allowing me to be a member of his research group. He has been an invaluable presence in my professional and personal life in these past five years. His demeanor and extraordinary knowledge has kept me both grounded and motivated throughout my time at Georgia Tech. I am very grateful to have been his student. I would also like to thank Dr. Janusz Kowalik, a former research scientist in the group. He is one of the most knowledgeable people I have had the pleasure to meet and work with, and his help with synthetic work was more than I could have ever asked for. Dr. Kyril Solntsev is one of the most interesting people I have ever met, in addition to being a research scientist in the group. He has been a pleasure to work with and an excellent motivator. Additionally, I would like to thank the members of the Tolbert group, Juan Vargas, Jing Cheng, Nathan Jarnagin, Anthony Baldridge, E.-A. Weeks, and Brandon Sharp for all of their help and friendship throughout my graduate career.

Of course, I could not have gotten here without the help and support of my family. So, I would like to thank my mother (Joan Fellows), my brother (Joe Fellows), my grandmother (Ann Brown), and all of my extended family and friends. I would not have been able to accomplish any of this without their boundless help and support.

TABLE OF CONTENTS

LIST OF TABLES

LIST OF FIGURES

LIST OF SYMBOLS AND ABBREVIATIONS

Ac	Acetyl
AIE	Aggregation-Induced Emission
BDI	Benzylidenedimethylimidazolidinone
Bu	Butyl
BzOxz	Benzoxazole
$CDCl_3$	Deuterated Chloroform
DCM	Dichloromethane
DIPEA	Diisopropylethylamine
DMSO	Dimethylsulfoxide
Dodec	Dodecyl
DodecOBDI	Dodecyloxybenzylidenedimethylimidazolidinone
ESI	Electrospray Ionization
Et	Ethyl
GFP	Green Fluorescent Protein
HBDI	*p*-Hydroxybenzylidenedimethylimidazolidinone
Hept	Heptyl
Hex	Hexyl
HSA	Human Serum Albumin
iPr	*iso*-propyl
IR	Infrared
Me	Methyl

MHz	Mega Hertz
NBD	Nitrobenzoxadiazole
nm	Nanometer
NMR	Nuclear Magnetic Resonance
Oct	Octyl
nPr	*n*-propyl
p-OH-phenyl	*p*-hydroxyphenyl
Pent	Pentyl
Ph	Phenyl
pK_a	Acid-base Dissociation Constant
Pr	Propyl
RFP	Red Fluorescent Protein
ROBDI	*R*-Alkoxybenzylidenedimethylimidazolidinone
RP	Reprecipitation
SEM	Scanning Electron Microscopy
Tuat	Tautomerization
TBSCl	*tert*-Butyl dimethylsilylchloride
TEM	Transmission Electron Microscopy
TFA	Trifluoroacetic Acid
UV-Vis	Ultraviolet-Visible
λ	Wavelength
μm	Micrometer
Φ	Emission Quantum Yield

SUMMARY

A new synthetic methodology for the combinatorial preparation of C-terminus-modified Green and Red Fluorescent Protein chromophores is described. This method involves the modification of the previously reported [2+3] cycloaddition reaction scheme to incorporate new R^2 groups in the imidate used in the final step. This is achieved through two primary routes: (a) the imidation of nitriles using hydrochloric acid gas and (b) the *O*-alkylation of amides using a variant of Meerwein's Salt to provide conjugated imidates.

The preparation of fluorescent microcrystals and nanofibers from Green Fluorescent Protein chromophore derivatives via the reprecipitation method is also demonstrated. The properties of these microcrystals and nanofibers, especially in relation to the powder obtained from organic solvents, are also explored. Additionally, it is demonstrated that the size and shape of the microcrystals and nanofibers can be modulated with varying experimental conditions for RP.

A new class of AIE-active GFP chromophores is reported. These chromophores contain a benzoxazole group on the phenyl ring and varying lengths of alkyl chains on the imidazolidinone nitrogen. These benzoxazole-based chromophores exhibit unique properties in the solid state not previously observed for GFP chromophore derivatives, namely, a broadening of the excitation spectrum and red-shifting of the emission, likely caused by excimer formation. The crystal structure also reveals a unique "hot-dog" stacking motif.

Additionally, some projects which require further work are discussed at the end of the thesis. These include a stress-responsive GFP-based polymer and DNA-binding fluorophores.

CHAPTER 1

INTRODUCTION AND OVERVIEW

1.1 Motivation

The main objective of this work is the combinatorial synthesis of GFP- and RFP-like chromophores with different groups at the R^2 or "C-terminus" position of the chromophore (**Figure 1.7**), which was previously an inaccessible derivatization point for combinatorial synthesis. It is important to first define combinatorial chemistry, before further discussion of the subject. Combinatorial chemistry is the preparation of a large number of compounds in a single process. The library thus synthesized can be made as mixtures or a set of individual compounds. With this goal in mind, it is pertinent to discuss why such a library would be necessary or beneficial.

It has been previously demonstrated that GFP chromophores can work as ligands for a variety of proteins, including nuclear receptors.[17] Additionally, it has also been shown that a significant library of GFP chromophores can be easily screened for a variety of binding conditions.[18] However, in both of these cases, only GFP chromophores were used, and only those with derivatizations at the R^1 and R^{3-7} positions. It was shown in the nuclear receptor work that binding can sometimes be highly dependent on volume or shape, rather than specific structure of the ligand.[17] Thus, it would be of great significance to add R^2 to the derivatization points, not only increasing the variety of substituents but also the variety in volume and shape of the ligands. Of course, the R^2 derivatization point also opens an avenue to production of RFP-like chromophores, which

are significantly more useful in biological applications, due to the reduction in cell damage and background fluorescence, thanks to the lower energy necessary to excite the molecule. For these reasons, we decided to pursue a combinatorial method for synthesizing GFP- and RFP-like chromophores which incorporates derivatization at the R^2 position. This is the main thrust of the thesis, which is discussed at length in Chapter 2. Subsequent chapters discuss further investigations into the properties and applications of GFP chromophores.

1.2 Introduction to the Green Fluorescent Protein Chromophore

Since its discovery as a fluorescent element of the jellyfish *Aequorea victoria* in 1955 and first *in vitro* expression in the early 1990s, the green fluorescent protein (GFP) has seen widespread utilization as a biological marker.[1] The source of the GFP fluorescence has been shown to be the *p*-hydroxybenzylidenedimethylimidazolidinone (HBDI, **Figure 1.1**).[1]

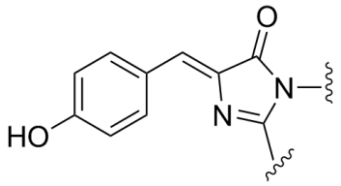

Figure 1.1: The GFP chromophore, HBDI.

The wild-type chromophore is formed post-translationally, through an auto-catalytic cyclization and subsequent autoxidation of the Ser-65, Tyr-66, and Gly-67 residues; formation of red fluorescent protein (RFP) chromophores arises from a further oxidation of the protein backbone (**Figure 1.2**).[1] Once formed, the chromophore is covalently anchored to the protein within an 11-stranded β-barrel, isolating it from the outside environment.[1] Through these covalent bonds and a network of hydrogen-bonds, the chromophore is rigidly held within the β-barrel thus providing the bright fluorescence.[2]

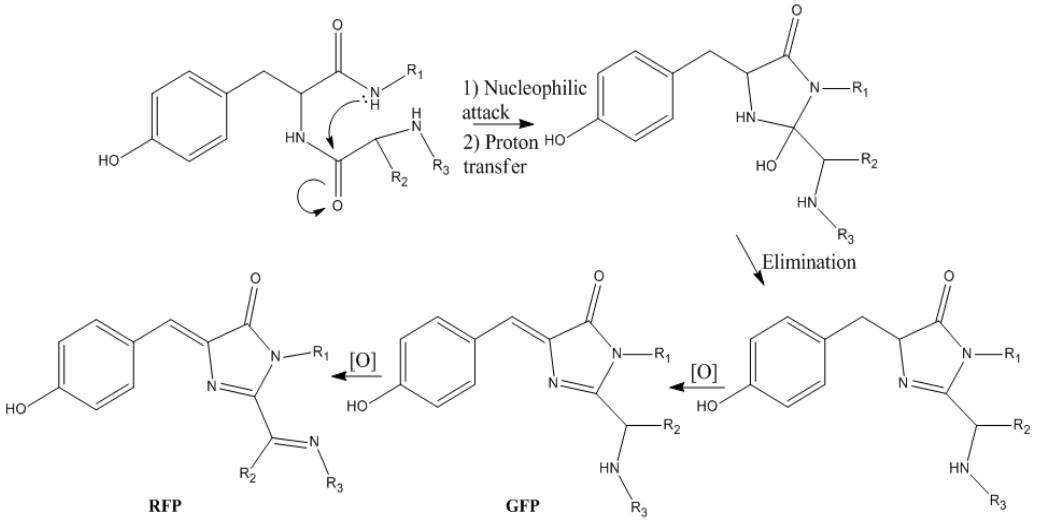

Figure 1.2: Biosynthesis of the GFP and RFP chromophores. R groups represent amino acid residues and the protein polypeptide backbone.

Upon removal of the chromophore from the β-barrel however, it shows poor fluorescence in solution. The Meech[3] and Tolbert[4] laboratories have shown that the low

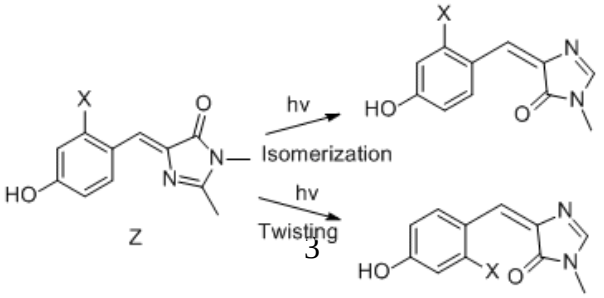

Figure 1.3: Twisting and double bond isomerization of HBDI.

fluorescence is due to twisting in the excited state, though the exact mechanism is highly debated. This twisting is responsible for efficient internal conversion, thus quenching fluorescence (**Figure 1.3**).[5] To that end, it has been demonstrated that encapsulation within a supramolecular cavity, a calixarene derivative known as an "octa-acid," limits the conformational freedom of the molecule upon complexation, and some of the fluorescence of HBDI derivatives is restored.[6] With the knowledge that the quantum yield differs by orders of magnitude when conformationally restricted versus in solution, we can utilize these chromophores as "turn-on" sensors for various applications. Baldridge and Tolbert have developed a selective human serum albumin (HSA) probe based on the GFP chromophore with a heptyl group at R^1, a hydroxyl group at R^3, and a diethylamino group at R^5 which shows a 70-fold enhancement of fluorescence upon binding to HSA.[7] Other substitution patterns were also developed and shown to selectively bind to nuclear receptors.[17] However, substitution at the R^2 position is notably absent. An additional set of chromophores that include R^2 substitutions could expand the diversity of the library and allow us to determine whether the binding is sensitive to these new variances in substitution. Therefore, we endeavored to complete the derivatization of the GFP chromophore, providing full substitution variability at all points of the parent molecule.

Furthermore, it has been shown that GFP chromophore derivatives with alkoxy groups on the phenyl ring (ROBDI) exhibit aggregate-induced emission (AIE), which can be altered by varying the chain length of the alkoxy group (**Figure 1.4**).[8] This phenomenon was also something we wished to invstigate, via new substitutions. The next

section discusses the methods commonly used to synthesize GFP chromophore derivatives, also called benzylidene imidazolidinones (BDIs).

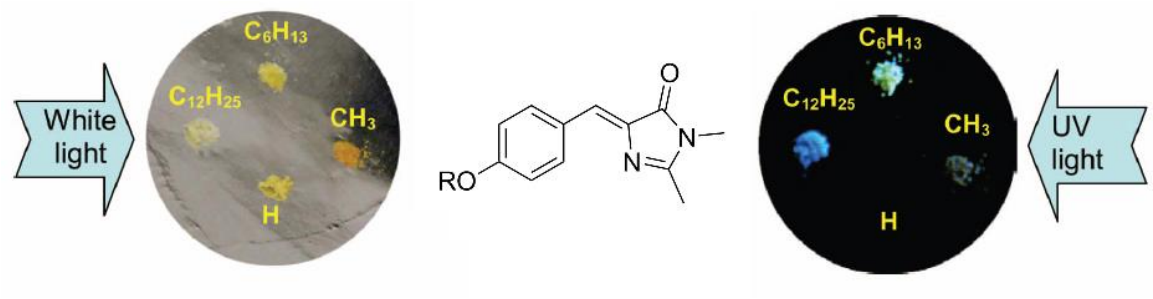

Figure 1.4: Photographs of ROBDI crystals under normal light and UV light. The ROBDI structure is shown in between (R = CH_3, C_6H_{13}, $C_{12}H_{25}$, or H).[8]

1.3 BDI Synthetic Methods

There are three methods commonly used for synthesizing GFP chromophores: the Erlenmeyer azlactone synthesis, a [2+3] dipolar cyclization method, and a Knoevenagel condensation. The [2+3] dipolar cyclization is a key focus of this work and will be discussed at length throughout both this introduction and Chapter 2; the Knoevenagel condensation reported by Burgess presents significant versatility, thus necessitating discussion;[9] and the Erlenmeyer azlactone synthesis[10, 11, 12] which is the most prominent of these methods, being used frequently in the literature,[9, 13, 14] will be discussed first, in the next section.

1.3.1 Erlenmeyer Azlactone Method

This method is a simple, two-step, high-yielding route to BDI derivatives, provided that there is good starting material availability.[10,11,12] The first step is a cyclization-condensation of *N*-acetyl glycine and an aromatic aldehyde in boiling acetic

anhydride, under basic conditions to yield the initial oxazolidinone. The intramolecular cyclization of *N*-acetyl glycine takes place first, followed by condensation with the aldehyde (**Figure 1.5**).

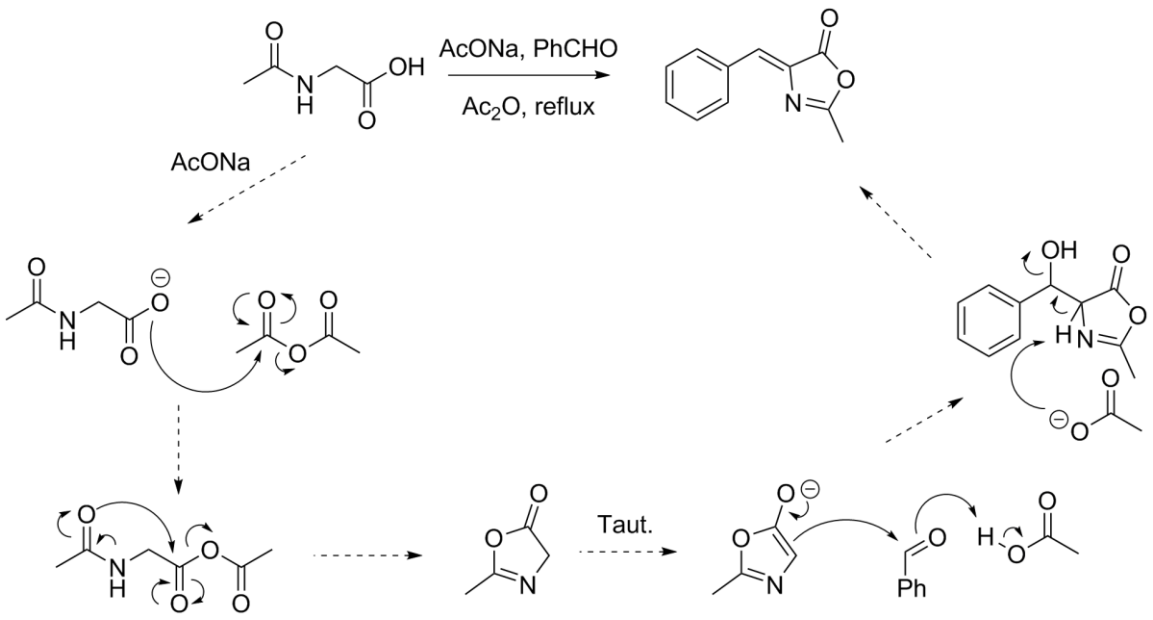

Figure 1.5: First step of the Erlenmeyer azlactone synthesis: cyclization-condensation reaction. Solid arrow: reaction. Dashed arrows: mechanism.

The second step is a ring-opening substitution reaction, with a primary amine acting as the nucleophile, followed by re-closing of the ring to transform the original oxazolidinone into an imidazolidinone (**Figure 1.6**).[10,11,12]

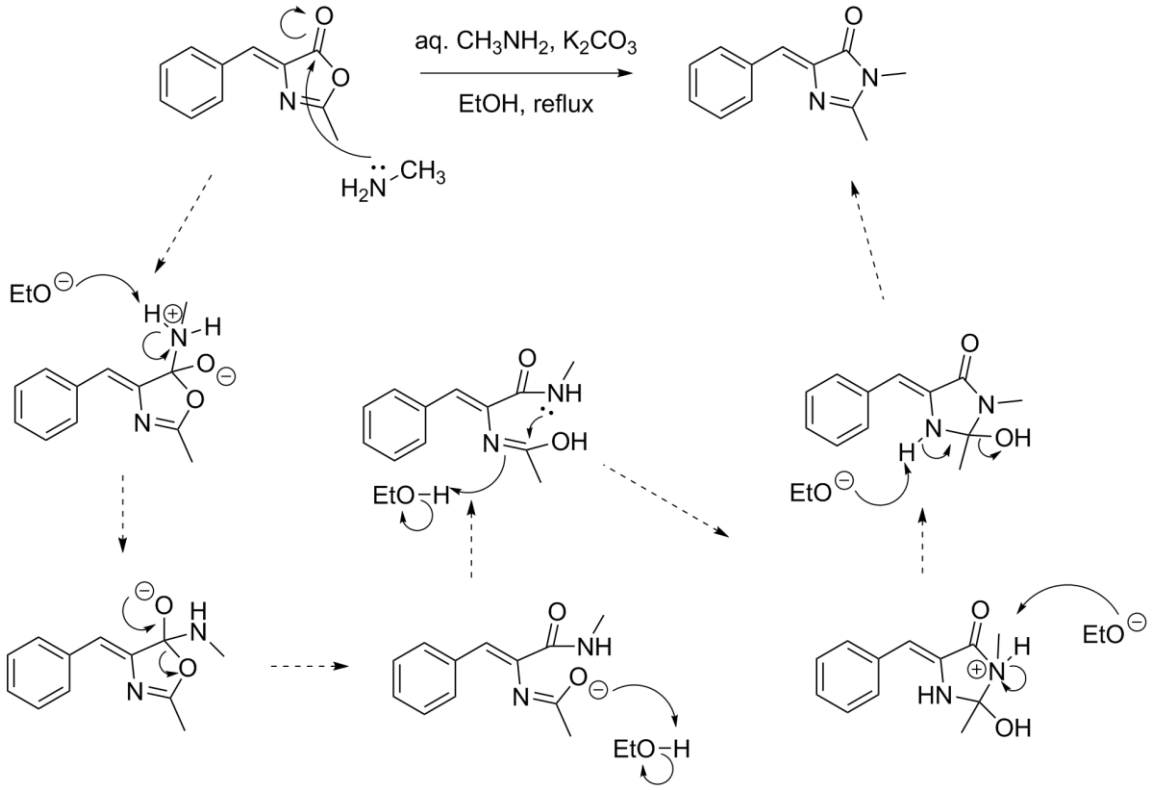

Figure 1.6: Second step of the Erlenmeyer azlactone synthesis: ring-opening and re-closing reaction. Solid arrow: reaction. Dashed arrows: mechanism.

This method is simple, short, and useful, in that it provides a two-step method for GFP chromophore derivatization at six positions, R^1 and R^{3-7} (**Figure 1.7**), utilizing commercially available aromatic aldehydes, primary amines, and *N*-acetyl glycine. Both steps require reflux, but the purification of the product in both steps is often achieved by simple recrystallization.

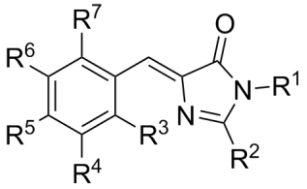

Figure 1.7: Generic BDI structure, where R groups represent all potential functionalization points.

1.3.2 Knoevenagel Condensation Method

The method presented by Burgess[9] involves first synthesizing the imidazolidinone ring through several steps, followed by a Knoevenagel condensation with an aromatic aldehyde. This method is similar to the Erlenmeyer azlactone synthesis, however, rather than using an oxazolidinone intermediate, the imidazolidinone is synthesized directly, in the initial steps (**Figure 1.8**). The imidazolidinone thus formed is then subjected to

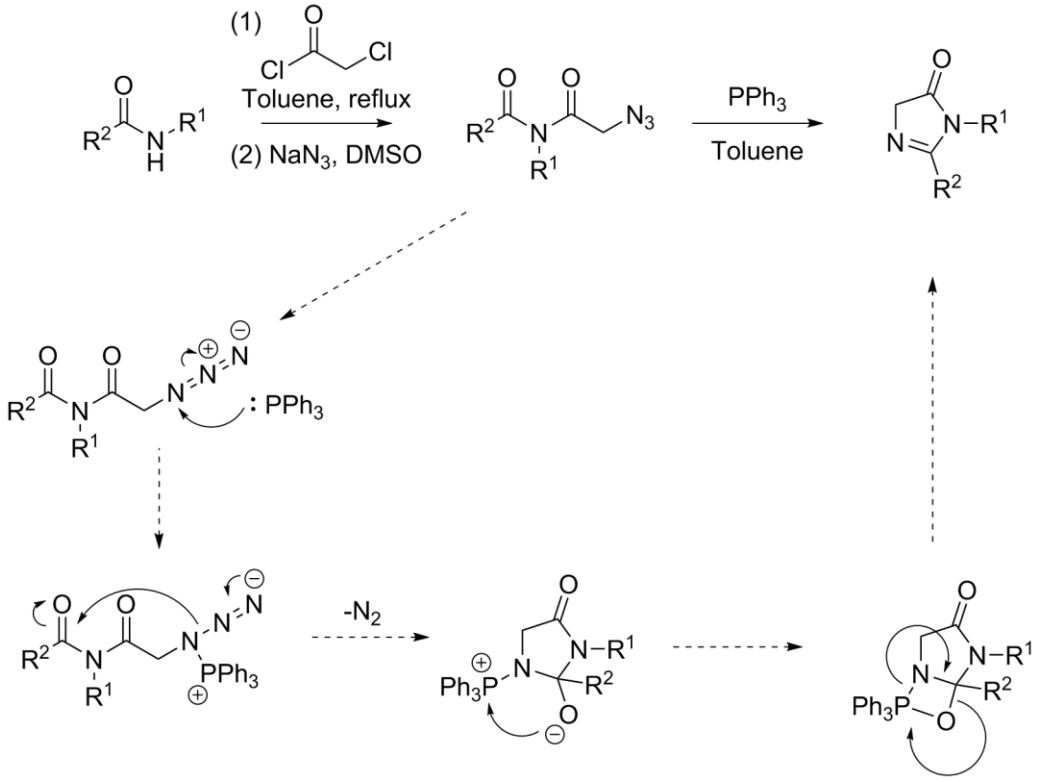

Figure 1.8: Imidazolidinone synthesis steps; dashed arrows show the mechanism for the cyclization step.

Knoevenagel condensation conditions with an aromatic aldehyde to yield the desired BDI (**Figure 1.9**). While this method is certainly lengthier than the Erlenmeyer azlactone synthesis, it is slightly milder, requiring only one reflux in toluene at 110 °C, whereas the latter requires two reflux steps, the first of which being a reflux in acetic anhydride at 140 °C and the second in ethanol at 78 °C. The subsequent steps, azidation, cyclization, and condensation, are all done at room temperature. Thus, the conditions are more tolerable of different functional groups.[9]

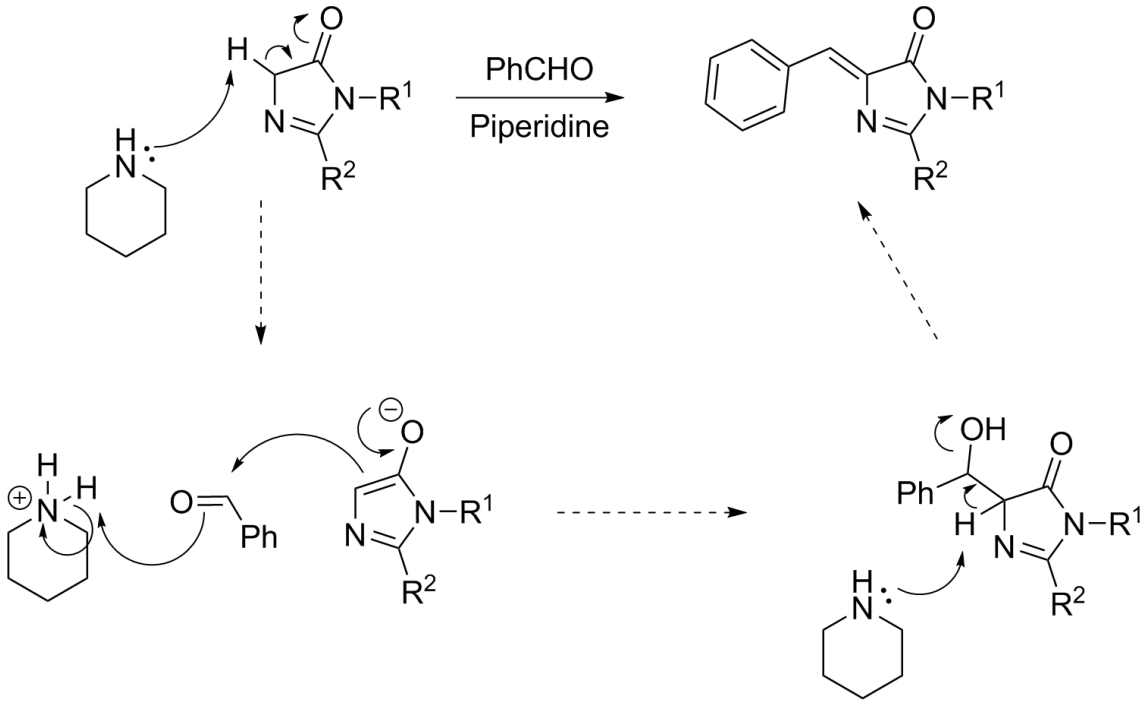

Figure 1.9: Knoevenagel condensation; dashed arrows show the mechanism.

1.3.3 [2+3] Cycloaddition Method

First reported by Bazureau in 1993,[15] the [2+3] cycloaddition method for synthesizing BDIs has seen significant use, since being demonstrated as a combinatorial method in 2010 by Baldridge, *et. al.*[16] The starting materials for this reaction are an aromatic imine and ethyl glycine acetimidate. The aromatic imine provides the R^1 and R^{3-}

[7] groups, while the imidate provides the R^2 group (**Figure 1.7**, R groups on the chromophore; **Figure 1.10**, R groups on cyclization precursors). The starting materials are made in two separate steps (**Figure 1.10**). These reactions are simple and do not require heating, cooling, or inert atmosphere.

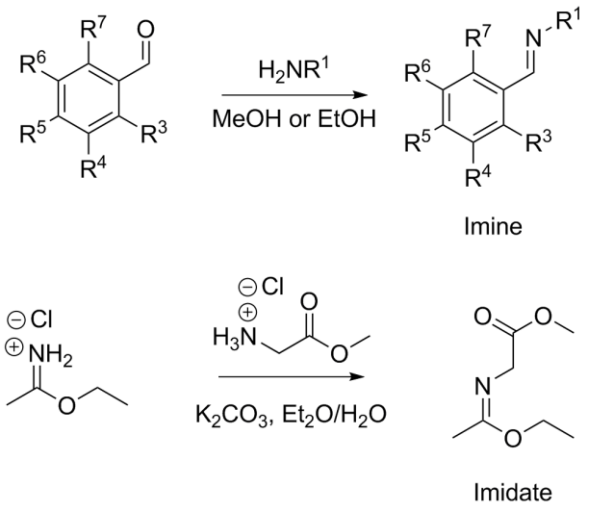

Figure 1.10: Synthesis of the cycloaddition precursors, the imine and imidate.

Once made, the imine and imidate are combined in ethanol and stirred at room temperature under atmosphere. A 1,3-dipolar cyclization then takes place, followed by ring opening and re-closing, to result in the precipitation of the chromophore product (**Figure 1.11**). The precipitated chromophore usually only requires filtration and washing with solvent for purification, though sometimes recrystallization or column chromatography is necessary.[16]

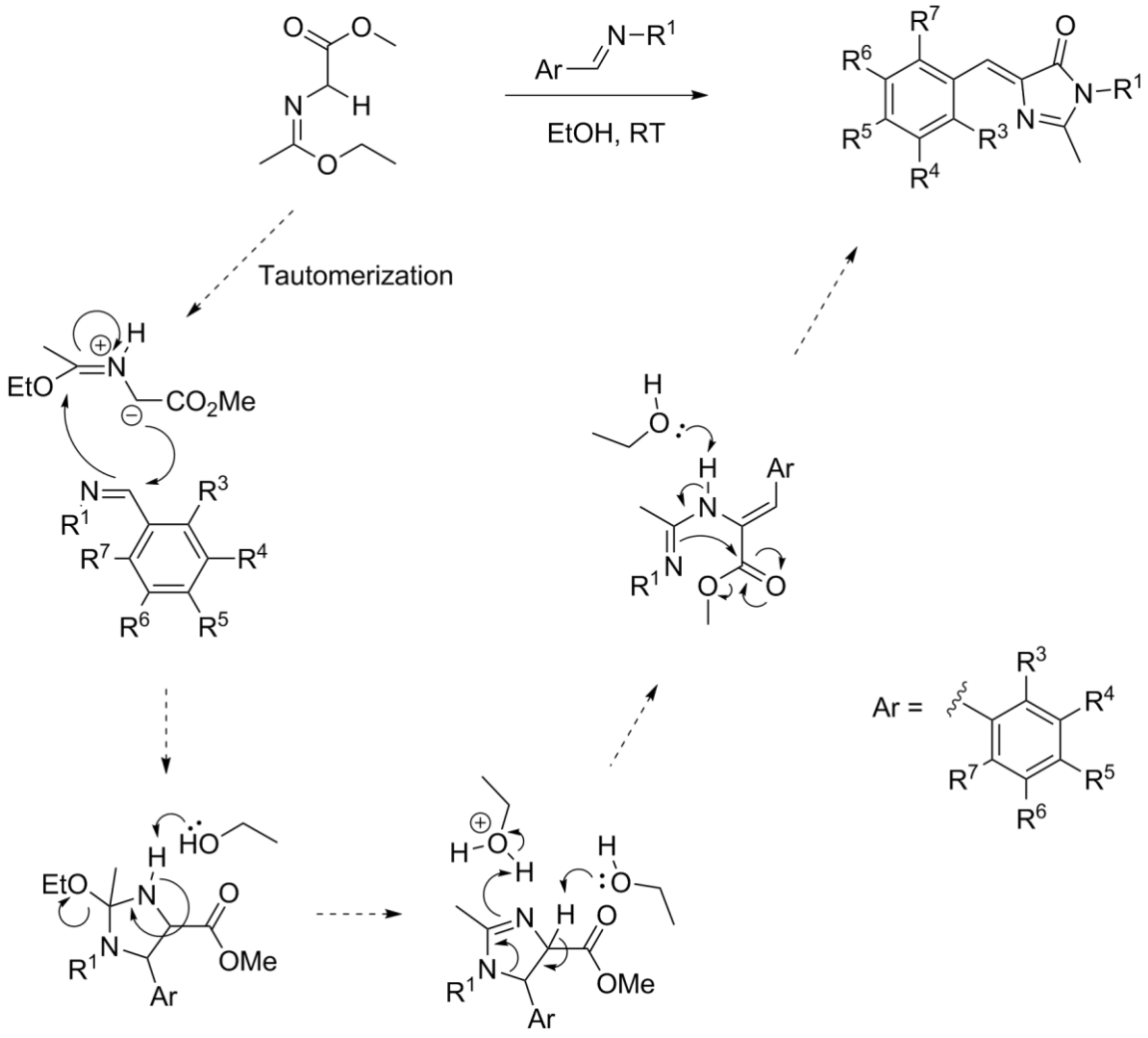

Figure 1.11: [2+3] Cycloaddition reaction. Dashed lines show the mechanism.

All methods discussed henceforth are related to the three methods described in this section. Their merits and drawbacks will be discussed at length in Chapter 2, in addition to their modification potential for our purposes. In particular, this work focuses on the R^2 position of the imidazolidinone ring.

1.4 References

[1] Zimmer, M. *Chem. Rev.* **2002**, *102*, 759-782.

[2] Ormö, M.; Cubitt, A. B.; Kallio, K.; Gross, L.A.; Tsien, R. Y.; Remington, S. J. *Science* **1996**, *273*, 1392-1395.

[3] Stoner-Ma, D.; Jaye, A. A.; Matousek, P.; Towrie, M.; Meech, S. R.; Tonge, P. J. *J. Am. Chem. Soc.* **2005**, *127*, 2864-2865.

[4] Usman, A.; Mohammed, O. F.; Nibbering, E. T. J.; Dong, J.; Solntsev, K. M.; Tolbert, L. M. *J. Am. Chem. Soc.* **2005**, *127*, 11214-11215.

[5] Liu, R. S. H. *Acc. Chem. Res.* **2001**, *34*, 555-562.

[6] Baldridge, A.; Samanta, S. R.; Jayaraj, N.; Ramamurthy, V.; Tolbert, L. M. *J. Am. Chem. Soc.* **2010,** *132*, 1498-1499.

[7] Baldridge, A.; Feng, S.; Chang, Y.-T.; Tolbert, L. M. *ACS Combi. Sci.* **2011**, *13*, 214-217.

[8] Dong, J.; Solntsev, K. M.; Tolbert, L. M. *J. Am. Chem. Soc.* **2009**, *131*, 662-670.

[9] Wu, L.; Burgess, K. *J. Am. Chem. Soc.* **2008**, *130*, 4089-4096.

[10] Erlenmeyer, E. *Justus. Liebigs. Ann. Chem.* **1893**, *275*, 1.

[11] Erlenmeyer, E. *Ber. Dtsch. Chem. Ges.* **1900**, *33*, 2036.

[12] Williams, D. L.; Ronzio, A. R. *J. Am. Chem. Soc.* **1946**, *68*, 647.

[13] Chen, K.-Y.; Cheng, Y.-M.; Lai, C.-H.; Hsu, C.-C.; Ho, M.-L.; Lee, G.-H.; Chou, P.-T. *J. Am. Chem. Soc.* **2007**, *129*, 4534-4535.

[14] He, X.; Bell, A. F.; Tonge, P. J. *Org. Lett.* **2002**, *4*, 1523.

[15] Lerestif, J. M.; Bazureau, J. P.; Hamelin, J. *Tet. Lett.* **1993**, *34*, 4639-4642.

[16] Baldridge, A.; Kowalik, J.; Tolbert, L. M. *Synthesis* **2010**, *14*, 2424-2436.

[17] Fluorescent GFP Chromophores as Potential Ligands for Various Nuclear Receptors by Duraj-Thatte, Anna, PhD., Georgia Institute of Technology, 2012, 222 pages; http://hdl.handle.net/1853/44764

[18] Lee, J.-S.; Baldridge, A.; Feng, S.; SiQiang, Y.; Kim, Y. K.; Tolbert, L. M.; Chang, Y.-T. *ACS Combi. Sci.* **2011**, *13*, 32-38.

CHAPTER 2

A NEW COMBINATORIAL METHOD FOR C-ALKYLATED GFP AND RFP CHROMOPHORE SYNTHESIS

2.1 Introduction - Current Literature Methods

As discussed in the previous chapter, the Erlenmeyer azlactone synthesis is the most common method for producing GFP-like chromophores.[14,15,16] Likewise, this method is often employed to furnish chromophores that are altered at the R^2 position,[1] also sometimes referred to as the C-terminus (**Figure 2.1**).

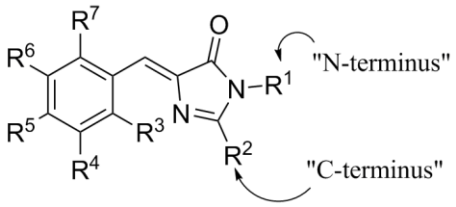

Figure 2.1: General structure of GFP and RFP chromophores

2.1.1 Erlenmeyer Azlactone Modification

The Erlenmeyer azlactone synthesis, as the most used method for GFP chromophore synthesis, is a clear choice for modification of the C-terminus position. The modifications necessary to the method are straightforward and require only the addition of two steps, starting from commercially available materials (**Figure 2.2**).[1]

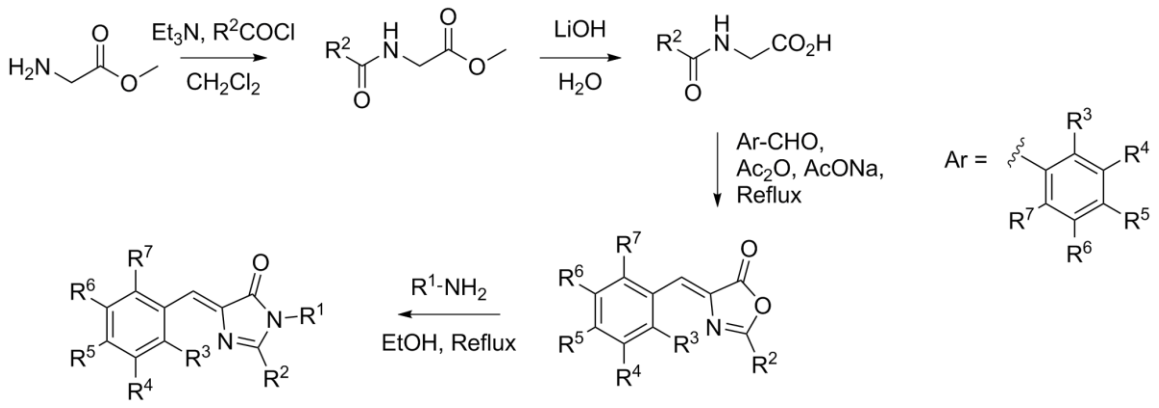

Figure 2.2: Erlenmeyer azlactone R^2 modifications

The two additional steps are added at the beginning, in order to integrate different R^2 groups into the scheme. The first step is the acylation of glycine methyl ester with the acid chloride of the desired R^2 carboxylic acid, using triethylamine as the base. The second step is simply the deprotection of the methyl ester, using one equivalent of lithium hydroxide in water. This furnishes the desired *N*-acylated glycine, similar to the *N*-acetyl glycine used as the starting material in the original scheme.

As a combinatorial method, this approach falls short, however. All of the steps are linear, which means that there are no branch points or convergent points at which to introduce new R groups. Therefore, to produce a chromophore with all new R groups, all steps must be repeated, starting from the commercially available R^2 acid, R^{3-7} aldehyde, and R^1 primary amine. If a variety of compounds with the same R^2 group is desired, the *N*-acylated glycine can be synthesized in bulk, but the final two steps must still be

performed in full, each time with a different R^1- and/or R^2-containing starting material. Considering that both of these steps require refluxing, it is a substantial time and glassware investment for the production of a large number of chromophores. Thus, it was decided that this was not the ideal method of choice for our purposes.

2.1.2 Knoevenagel Condensation Modification

The Knoevenagel condensation reported by Burgess in 2008 also presents a viable route for producing R^2-substituted chromophores, utilizing known chemistry through four steps (**Figure 2.3**).[2]

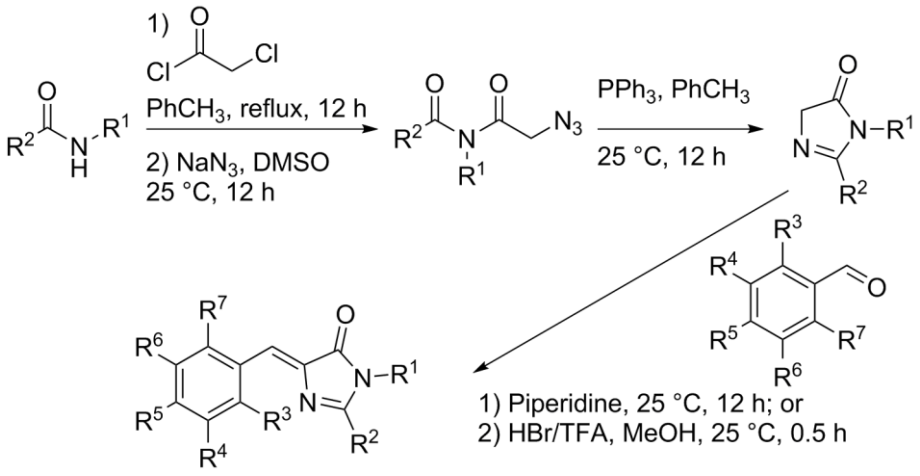

Figure 2.3: Knoevenagel condensation modifications

The first step, not shown in **Figure 2.3**, is the amidation of the R^2 acid with the R^1 primary amine, which can be accomplished using a variety of basic organic chemistry reactions. It should be noted, therefore, that this method is actually five steps, should the desired starting amide not be commercially available. The subsequent step is the acylation of the amide, using chloroacetyl chloride. The resulting imide is then subjected to nucleophilic substitution conditions, using sodium azide. The azoimide produced is

then cyclized using triphenylphosphine, as shown in **Figure 1.8**. The final step is the Knoevenagel condensation of the imidazolidinone with the desired aldehyde, as shown in **Figure 1.9**. It is notable that this final condensation can be either base-catalyzed or acid-catalyzed and is therefore more tolerant of different functional groups.

As a combinatorial method, this route also falls short, unfortunately. The most notable weakness is that R^1 and R^2 are combined in the very first step, which means that for any combination of different R^1 and R^2 groups, all steps in the route must be performed, since this route is completely linear. This weakness can be somewhat mitigated by producing a variety of imidazolidinones with different R^1 and R^2 groups in bulk and then performing the final condensation step with a variety of aldehydes, but this solution is less than ideal, at best. Therefore, once again, this method was not chosen for our purposes.

2.1.3 Oxidation and Wittig Method

Another method for producing chromophores with different groups at the R^2 position was reported by Lukyanov and Yampolsky in 2008.[3] This method involves the synthesis of chromophores with methyl groups at the R^2 position, followed by oxidation of this position to an aldehyde and subsequent Wittig reaction (**Figure 2.4**). This method also results in a double bond in the R^2 position, which produces a chromophore more like that of the RFP (**Figure 1.2**).

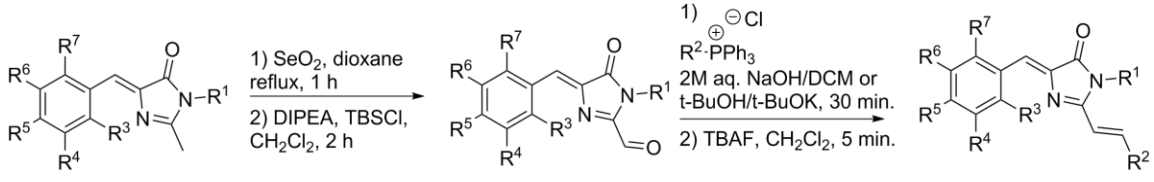

Figure 2.4: Oxidation and Wittig reaction route to RFP chromophores.

This is beneficial, since RFP chromophores are more advantageous for biological applications. Furthermore, since there are only two additional steps, the route is still fairly short. However, much like the previously discussed methods, this route is not without its drawbacks. First and foremost, it requires the initial synthesis of the chromophore, meaning this method is not integrated into the process but rather acts as an addendum. Therefore, all substituents are already determined, except for R^2. In order to make a combinatorial library using this method, it is basically required that one already exists, but wherein R^2 is always a methyl group. This is not ideal, as it is far more beneficial to be able to synthesize a combinatorial library from scratch, allowing for the integration of any R group at any position. Because of these drawbacks, this route is not well suited for our purposes.

2.1.4 Summary of Literature Methods

All of the current literature methods for synthesizing GFP/RFP chromophores with R^2 derivatization are lacking, when it comes to combinatorial goals. **Table 2.1** succinctly illustrates the shortcomings of these methods. It is clear that none of these methods provide any significant advantage over the others, in terms of combinatorial synthesis. They are all at least four steps, linear, R groups are combined throughout each scheme in different places, none of which provides an opportunity for efficient derivatization, and all require at least one reflux and column chromatography purification for each individual chromophore synthesized. All of these hindrances are unacceptable for a combinatorial approach and hamper the efficiency of such a route.

Table 2.1: Summary of the combinatorial shortcomings of available literature methods

	Tonge's Erlenmeyer Modification	Burgess's Condensation	Yampolsky/Lukyanov's Oxidation/Wittig
Number of Steps	4	4-5 (5, if R^2 is not methyl)	4-7 (depends on initial chromophore synthesis method)
Linear?	Yes	Yes	Yes
R group summary	All groups combined in final 2 steps	R^1 and R^2 combined in first step; R^{3-7} in final step	R^1 and R^{3-7} combined during chromophore synthesis; R^2 added in final 2 steps
Conditions	2 refluxes, 1-2 columns, 2 recrystallizations	1 reflux, 2 columns, 1 recrystallization	1-3 refluxes, 2 columns, 2 recrystallizations

Due to these significant drawbacks, it was decided that a new approach should be devised for the combinatorial synthesis of GFP/RFP chromophores involving R^2 derivatization.

2.2 Experimental Protocols

General Experimental

^{1}H NMR spectra were recorded with a Varian Mercury Vx 300 spectrometer operating at 300 MHz in $CDCl_3$ or DMSO-d_6, as indicated. ESI mass spectra were obtained using a

Micromass Quattro LC instrument. TLC was carried out on Analtech Uniplate Silica Gel GF plates. Column chromatography was performed using Sorbent Technologies 40–63 mm standard grade silica gel. The organic solvents and the reagents used in this study were used as received from commercial sources (Acros Organics, Fisher Scientific, Aldrich). Amides (**4**) were synthesized according to the literature procedure.[8]

General Procedure for Synthesis of Imidate Hydrochlorides from Nitriles (2): The appropriate nitrile (10 mL) was placed in a flask fitted with a gas inlet, outlet, and bubbler. Ethanol (1.02 eq.) and diethyl ether (100mL) were added, and HCl gas was bubbled into the flask while stirring at 0 °C for 2h. The reaction was stirred continuously and allowed to warm to room temperature overnight. The solution was evaporated until a solid was obtained, which was triturated with di-ethyl ether and filtered. The ethyl,[9] isopropyl,[9] butyl,[10] pentyl,[11] octyl,[11] phenyl,[9] and methyl[12] ether imidates were obtained in near quantitative yields and matched the spectra from the literature. The propyl imidate hydrochloride was purchased from Sigma-Aldrich.

Ethyl octanimidate hydrochloride (2, R = heptyl): White solid. ^{1}H NMR: (300 MHz, DMSO-d_6) δ 12.10 (s, br, 1H), 11.23 (s, br, 1H), 4.42 (q, J = 6 Hz, 2H), 2.60 (t, J = 6 Hz, 2H), 1.54 (pentet, J = 6 Hz, 2H), 1.29 (t, J = 6 Hz, 3H), 1.19 (m, 8H), 0.79 (t, J = 6 Hz, 3H).

General Procedure for the Synthesis of Alkyl Imidates (3): The appropriate imidate hydrochloride and glycine methyl ester hydrochloride were placed in a round bottom

flask with dichloromethane and triethylamine and allowed to stir for 30 minutes at room temperature. The resulting mixture was then washed with water (2 x equal volume) and brine (1 x equal volume), dried with magnesium sulfate, and the solvent was evaporated. The ethyl,[13] isopropyl,[13] and phenyl[13] imidates' ^{1}H NMR spectra were consistent with the literature data.

Methyl (E)-2-((1-ethoxypentylidene) amino)acetate (3, R = butyl): Colorless oil. ^{1}H NMR: (300 MHz, $CDCl_3$) δ: 4.03 (q, J = 6 Hz, 2H), 4.01 (s, 2H), 3.66 (s, 3H), 2.12 (t, J = 9 Hz, 2H), 1.45 (pentet, J = 6 Hz, 2H), 1.27 (sextet, J = 6 Hz, 2H), 1.18 (t, J = 6 Hz, 3H), 0.84 (t, J = 6 Hz, 3H)

Methyl (E)-2-((1-ethoxyhexylidene) amino)acetate (3, R = pentyl): Colorless oil. ^{1}H NMR: (300 MHz, $CDCl_3$) δ: 4.10 (q, J = 6 Hz, 2H), 4.07 (s, 2H), 3.73 (s, 3H), 2.18 (t, J = 6 Hz, 2H), 1.54 (pentet, J = 6 Hz, 2H), 1.30 (m, 4H), 1.25 (t, J = 6 Hz, 3H), 0.88 (t, J = 6 Hz, 3H)

Methyl (E)-2-((1-ethoxynonylidene) amino)acetate (3, R = octyl): Colorless oil. ^{1}H NMR: (300 MHz, $CDCl_3$) δ: 4.04 (q, J = 6 Hz, 2H), 4.00 (s, 2H), 3.66 (s, 3H), 2.11 (t, J = 6 Hz, 2H), 1.46 (pentet, J = 6 Hz, 2H), 1.21 (m, 10H), 1.18 (t, J = 6 Hz, 3H), 0.81 (t, J = 6 Hz, 3H)

Methyl (Z)-2-((1-ethoxy-2-methoxyethylidene)amino)acetate (3, R = methoxymethylene): Colorless oil. ^{1}H NMR: (300 MHz, $CDCl_3$) δ: 4.46 (q, J = 6 Hz, 2H), 4.36 (s, 2H), 3.70 (s, 2H), 3.37 (s, 3H), 3.26 (s, 3H), 1.33 (t, J = 6 Hz, 3H)

Methyl (E)-2-((1-ethoxybutylidene) amino) acetate (3, R = propyl): Colorless oil. ^{1}H NMR: (300 MHz, $CDCl_3$) δ: 4.10 (q, J = 6 Hz, 2H), 4.07 (s, 2H), 3.73 (s, 3H), 2.16 (t, J = 6 Hz, 2H), 1.56 (sextet, J = 6 Hz, 2H), 1.25 (t, J = 6 Hz, 3H), 0.92 (t, J = 6 Hz, 3H)

Methyl (Z)-2-((1-ethoxyoctylidene) amino)acetate (3, R = heptyl): Colorless oil. ^{1}H NMR: (300 MHz, $CDCl_3$) δ: 4.04 (q, J = 6 Hz, 2H), 4.00 (s, 3H), 3.66 (s, 3H), 2.11 (t, J = 6 Hz, 2H), 1.46 (pentet, J = 6 Hz, 2H), 1.21 (m, 8H), 1.18 (t, J = 6 Hz, 3H), 0.81 (t, J = 6 Hz, 3H)

General Procedure for the Synthesis of Conjugated Imidates (5): The appropriate amide (1.0 eq, neat if an oil, 1M in chloroform if a solid) was stirred at 50° C overnight with triethyloxonium hexafluorophosphate (1.3 eq). The reaction was worked up with 6M K_2CO_3, washed with water, dried with magnesium sulfate, and evaporated under reduced pressure to afford a pale yellow or colorless oil, which was used without further purification. In the case of the styryl R^2 group (R = phenyl, **Figure 2.10**), the resulting oil was purified by filtering through one inch of silica gel with 10% diethyl ether in hexane, yielding a colorless oil, after evaporation of solvent, which was used directly.

General Procedure for the Synthesis of C-substituted Chromophores (1): The appropriate imidate (1.1 equivalents) was combined with the imine in ethanol or methanol and stirred overnight at room temperature or 70 °C, as noted in the supporting information. A solid precipitated and was purified as noted in **Table 2.3**.

2.3 Results

As a method that is already inherently convergent, the [2+3] cycloaddition reaction reported by our group in 2010 was a prime candidate for investigation as a combinatorial method for R^2-derivatized chromophores.[4] The R^1 and R^{3-7} groups are combined in an initial imine-forming step, which is short and usually requires no purification.[4] The R^2 group, which in the existing method is always a methyl group, is introduced via an imidate also synthesized in only one, separate step, which takes under an hour and also usually requires no purification.[5] These intermediates are combined in one reaction, which yields the chromophore. The resulting chromophore generally precipitates during reaction and often requires very little, if any, purification (**Figure 2.5**).

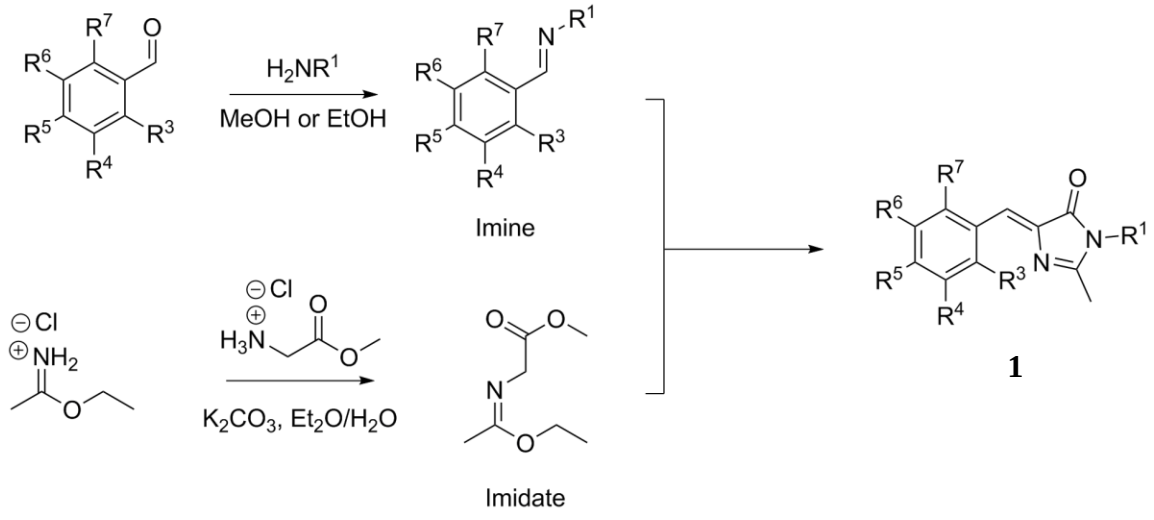

Figure 2.5: [2+3] Cycloaddition route to GFP chromophores

Clearly, this method is very beneficial, as the R^1 and R^{3-7} groups can be combined in one step and stored, creating a bank of imines from which to choose, while the R^2-containing starting material is made in bulk in a separate step. This presents the opportunity for synthesizing many chromophores all at once by pulling from the imine bank and combining fractions from the bulk imidate produced in the other step. The only challenge is to successfully synthesize the imidate, as the rest is known chemistry.[4]

2.3.1 Approach to Imidate Synthesis

There is one problem with the [2+3] cycloaddition approach to combinatorial synthesis of chromophores: there are only two commercially available ethyl imidate hydrochlorides, which is the starting material for the imidate synthesis step. The two commercially available ethyl imidate hydrochlorides are those which provide methyl and butyl R^2 groups. Therefore, in order to introduce a variety of R^2 substituents, ethyl imidate hydrochlorides must be synthesized in the laboratory. Availability of starting materials and the simplicity and reliability of the procedure led to the decision to produce the ethyl imidate hydrochlorides by reaction of the corresponding nitriles with hydrochloric acid gas and ethanol (**Figure 2.6**).[17]

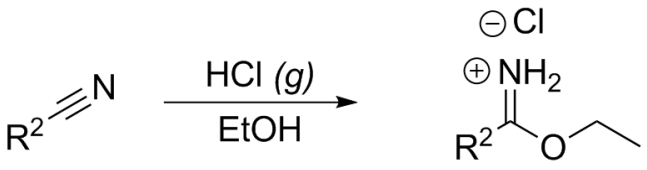

2

Figure 2.6: Ethyl imidate hydrochloride synthesis

With these ethyl imidate hydrochlorides in hand, we were then able to try the glycine nucleophilic substitution reaction (**Figure 2.5**, bottom left). Unfortunately, the new ethyl

imidate hydrochlorides were not tolerant of the aqueous conditions used in this reaction and provided very low yields (< 10%). Therefore, new conditions had to be devised. Anhydrous conditions, like those used by Bazureau's alternate method[5] of synthesizing imidates, were investigated. Bazureau's overnight reflux conditions were, however, too harsh, and it was discovered that the reaction reaches completion within thirty minutes at room temperature, affording good yields (70-93%, **Figure 2.7**).[6]

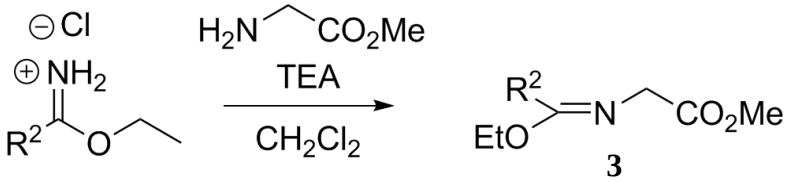

Figure 2.7: Anhydrous imidate synthesis

With these imidates now at our disposal, over 80 new GFP chromophores with different alkyl R^2 groups were synthesized via the [2+3] cycloaddtion reaction (**Figure 2.8**).

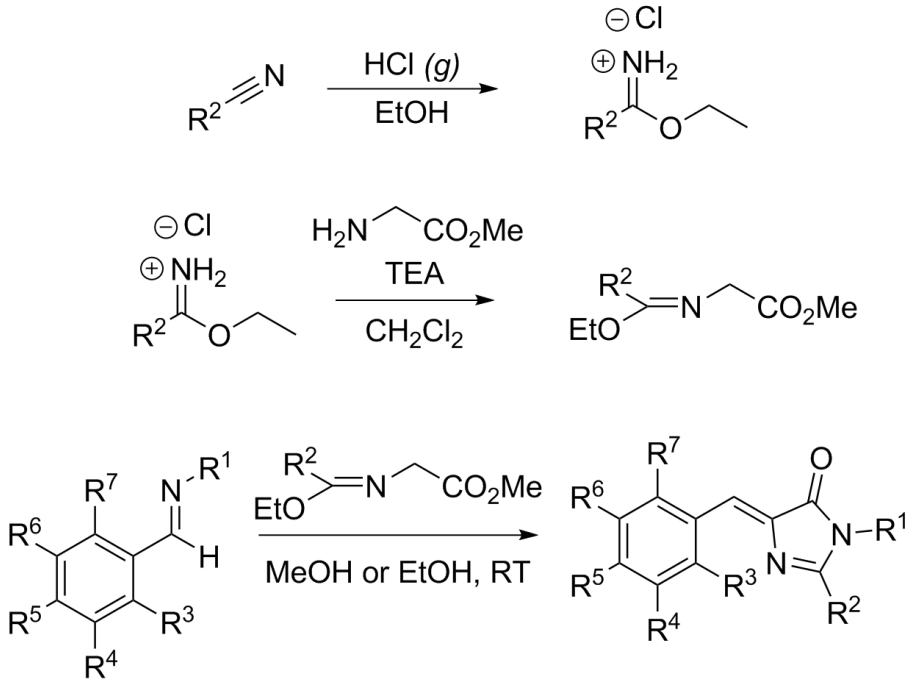

Figure 2.8: Full synthetic route to alkyl R^2 modified chromophores

As can be seen in **Figure 2.8**, this adds only one step to the overall synthetic scheme, which is the conversion of the nitrile to ethyl imidate hydrochloride. This is obviously beneficial, as it means that there are only 4 total steps, 3 of which are linear. Additionally, the R^1 and R^2 groups are not combined until the final step, and this method does not require reflux or column chromatography.

2.3.2 Conjugated Imidate for RFP-like Chromophore Synthesis

Another goal for us was to incorporate extended conjugation into the R^2 group, in order to gain access to RFP-like chromophores, combinatorially. Unfortunately, our approach to the synthesis of the alkyl R^2 imidates is not applicable to conjugated R^2 groups. As shown in **Figure 2.9**, hydrohalogenation takes place, rather than nucleophilic addition of ethanol.

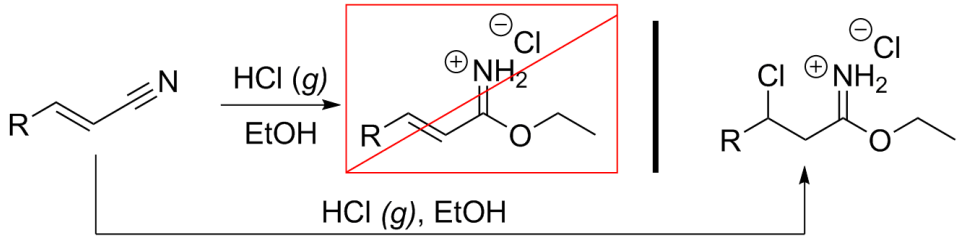

Figure 2.9: Failed HCl gas imidate synthesis

Therefore, another new method was necessary for producing the requisite conjugated imidates. After a literature search and extensive experimentation, a method was derived based on that which Doring reported in 2005 (see Experimental section for details).[7] The imidate is synthesized by *O*-alkylation of the corresponding amide, using a variant of Meerwein's Salt (**Figure 2.10**).[18]

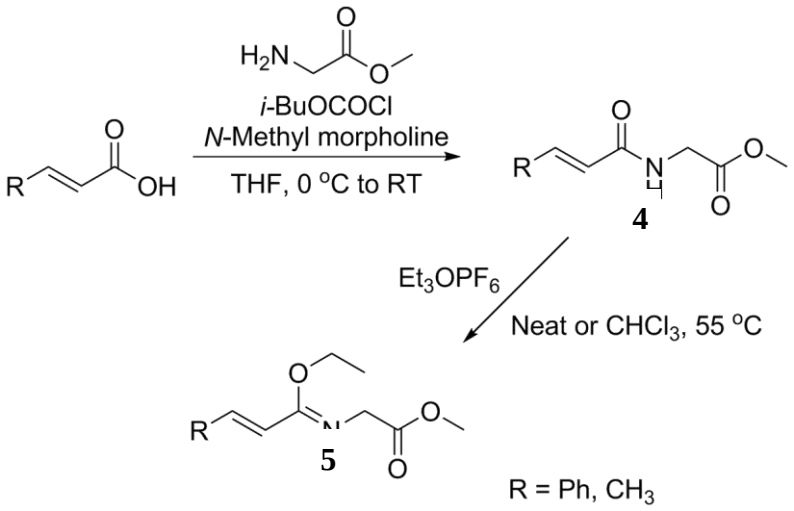

Figure 2.10: Imidate synthesis for conjugated R^2 groups

The conjugated imidates thus produced through this route were then used in the typical [2+3] cycloaddition conditions to provide RFP-like chromophores, with conjugation extended through the R^2 position (**Figure 2.11**).

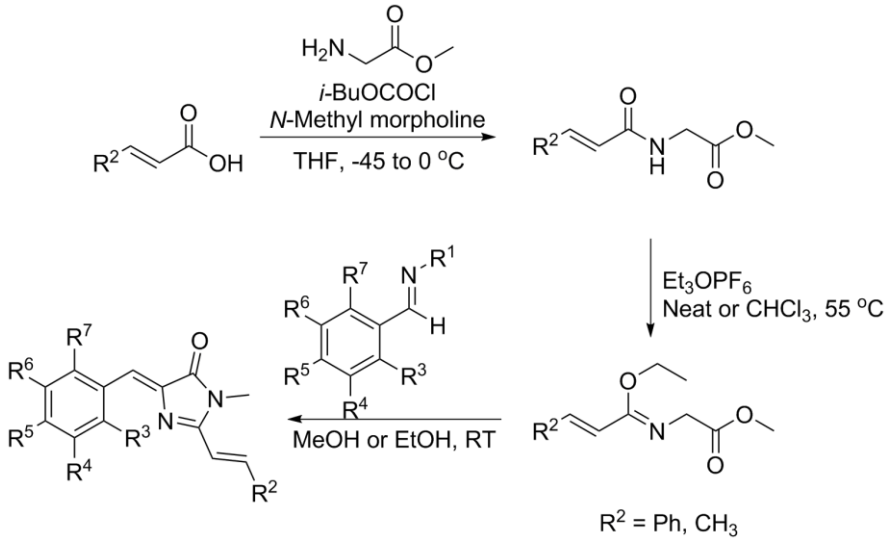

Figure 2.11: Full synthetic route to R^2-conjugated chromophores

Again, only one step is added to the overall scheme, for a linear total of 3 and overall total of four steps. The imidation step using the Meerwein's Salt variant takes the place of

the glycine nucleophilic substitution step, and the amidation step is the added step. As with the method for aliphatic R^2 groups, the R^1 and R^2 groups are combined in the final step and no reflux is required. Unfortunately, for some chromophores in which R^2 is a phenyl group, column chromatography is required. Additionally, for a more pure imidate, a short silica plug is required, which provides for a cleaner [2+3] cycloaddition reaction mixture.

Table 2.2 summarizes the library of GFP- and RFP-like chromophores synthesized in this work, indicating the substituents by their R group labels. Table 2.3 shows the yield and conditions of the final [2+3] cycloaddition step for each chromophore. ^{1}H NMR for all chromophores and ESI-MS and ^{13}C NMR for a representative selection of chromophores can be found in Appendix A.

Table 2.2: All chromophores synthesized to date of thesis submission.

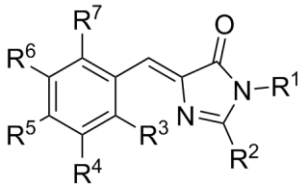

BDI #	R^1	R^2	R^3	R^4	R^5	R^6	R^7
1	Me	n-Pr	OH				
2	Me	n-Pr		OH			
3	Me	n-Pr			OH		
4	Me	n-Pr			$N(CH_3)_2$		
5	Me	n-Pr	CH_3				

BDI #	R^1	R^2	R^3	R^4	R^5	R^6	R^7
6	Me	n-Pr		CH_3			
7	Me	n-Pr			CH_3		
8	Me	n-Pr	CH_3		CH_3		
9	Me	n-Pr					
10	Me	Et					
11	Me	Heptyl					
12	$(CH_2)_2OCH_3$	Me		I			
13	Me	Me		I			
14	Me	$(CH)_2CO_2CH_3$			OH		
15	Me	Et	OH				
16	Me	Et			OH		
17	Me	Et			$N(CH_3)_2$		
18	Me	Pent	OH				
19	Me	Pent		OH			
20	Me	Pent			OH		
21	Me	Pent			$N(CH_3)_2$		
22	Me	Pent			CH_3		
23	Me	Bu		CH_3		CH_3	
24	Me	Bu					
25	Me	Bu			OH		
26	Me	Bu		CH_3			
27	Me	Bu			$N(Et)_2$		

BDI #	R^1	R^2	R^3	R^4	R^5	R^6	R^7
28	Me	Bu	CH_3				
29	Me	Bu	OH				
30	Me	Bu		OH			
31	Me	Bu			CH_3		
32	Me	Et	CH_3				
33	Me	Et		CH_3			
34	Me	Et			$N(Et)_2$		
35	Me	Et		CH_3	CH_3		
36	Me	Octyl					
37	Me	Octyl			Me		
38	Me	Octyl	Me				
39	Me	Octyl		Me			
40	Me	Octyl		Me	Me		
41	Me	Octyl		Me		Me	
42	Me	Octyl			$N(Et)_2$		
43	Me	Octyl	OH		$N(Et)_2$		
44	Me	Octyl			$N(Me)_2$		
45	Me	Octyl	OH				
46	Me	Octyl		OH			
47	Me	Octyl			OH		
48	Me	CH_2OMe		OH			
49	Me	CH_2OMe			$N(Me)_2$		

BDI #	R^1	R^2	R^3	R^4	R^5	R^6	R^7
50	Me	CH_2OMe	OH		$N(Et)_2$		
51	Me	Et		OH			
52	Me	Et			Me		
53	Me	Et	OH		$N(Et)_2$		
54	Me	Et		Me		Me	
55	$(CH_2)_2OH$	Me					
56	$(CH_2)_2OH$	Me			-CN		
57	Me	Pr		Me		Me	
58	Me	Pr			$N(Et)_2$		
59	Me	Pr		Me	Me		
60	Me	Pr	OH		$N(Et)_2$		
61	Me	iPr		Me	Me		
62	Me	iPr			$N(Me)_2$		
63	Me	iPr		Me			
64	Me	iPr					
65	Me	iPr			Me		
66	Me	iPr		OH			
67	Me	iPr			OH		
68	Me	Ph	OH		$N(Et)_2$		
69	Me	Me			p-OH-phenyl		
70	Me	Ph			OH		
71	Me	Ph		OH			

BDI #	R^1	R^2	R^3	R^4	R^5	R^6	R^7
72	Me	Ph	OH				
73	CH_2CO_2Me	Ph			$N(Me)_2$		
74	Me	Ph					
75	Me	Ph		Me			
76	Me	Heptyl	OH		$N(Et)_2$		
77	Me	Heptyl			OH		
78	Me	Heptyl		Me			
79	Me	Heptyl	Me				
80	Me	Heptyl		Me		Me	
81	Me	Heptyl		Me	Me		
82	Me	Heptyl			$N(Me)_2$		
83	Me	Heptyl	OH				
84	Me	Me			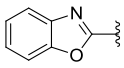		
85	Dodecyl	Me			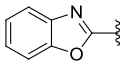		
86	Pentyl	Me			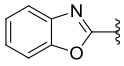		
87	Butyl	Me			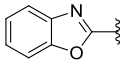		
88	$(CH_2)_3CO_2OH$	Me			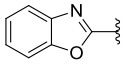		
89	Me	$(CH)_2Ph$			OMe		
90	Me	$(CH)_2CH_3$			$N(CH_3)_2$		
91	Me	$(CH)_2CH_3$			NO_2		
92	Me	$(CH)_2Ph$			NO_2		
93	hexyl	Me	2-naphthyl				

BDI #	R^1	R^2	R^3	R^4	R^5	R^6	R^7
94	dodecyl	Me	2-naphthyl				
95	Me	$(CH)_2Ph$			$N(CH_3)_2$		
96	Me	$(CH)_2Ph$			OH		

Table 2.3: Yields, isolation method, and reaction conditions for all chromophores synthesized. Reaction condition A: stirred overnight at room temperature in MeOH or EtOH. Reaction condition B: stirred overnight at 70 °C in EtOH. Solvents listed for isolation indicate solvent(s) used for the precipitation.

BDI #	Yield (%)	Isolation Method	Reaction Conditions
1	13.3	EtOH /H_2O	A
2	54.9	EtOH /H_2O	A
3	49.2	EtOH /H_2O	A
4	53.3	Hot EtOH trituration	A
5	14.7	MeOH /H_2O	A
6	30.6	MeOH /H_2O	A
7	10.2	Filtration	B
8	27.7	MeOH /H_2O	A
9	5.52	MeOH /H_2O	A
10	trace	Column chromatography	B
11	54.3	Column chromatography	Burgess Method[2]

BDI #	Yield (%)	Isolation Method	Reaction Conditions
12	59.7	Precipitated at 0°C; filtered	B
13	80.0	Filtration	B
14	48.8	Column chromatography	Lukyanov Method[3]
15	29.4	Filtration	A
16	27.7	Filtration	A
17	41.3	Filtration	A
18	32.1	Filtration	A
19	44.7	Filtration	A
20	43.2	Filtration	A
21	11.2	Filtration	A
22	trace	Filtration	A
23	11.7	Filtration	A
24	3.0	Filtration	A
25	57.2	Filtration	A
26	19.6	Filtration	A
27	31.0	Filtration	A
28	14.0	Filtration	A
29	16.8	Filtration	A
30	45.6	Filtration	A
31	16.6	Filtration	A

BDI #	Yield (%)	Isolation Method	Reaction Conditions
32	25.3	Filtration	B
33	33.4	Filtration	B
34	39.3	Filtration	B
35	32.2	Filtration	B
36	38.3	Filtration	A
37	56.6	Filtration	A
38	40.4	Filtration	A
39	15.7	Filtration	A
40	55.0	Filtration	A
41	50.6	Filtration	A
42	33.6	Filtration	A
43	44.1	Filtration	A
44	46.1	Filtration	A
45	68.3	Filtration	A
46	38.6	Filtration	A
47	36.0	Filtration	A
48	16.0	EtOH /H_2O	B
49	8.9	EtOH /H_2O	B
50	9.3	EtOH /H_2O	B
51	15.0	Extracted with DCM, evaporation, trituration with ether	A

BDI #	Yield (%)	Isolation Method	Reaction Conditions
52	39.0	EtOH/H_2O	A
53	16.0	EtOH/H_2O	A
54	34.0	EtOH/H_2O	A
55	49.3	Column chromatography	A
56	8.7	Column chromatography	A
57	66.7	EtOH/Et_2O	B
58	30.2	Et_2O	B
59	56.1	EtOH/Et_2O	B
60	66.6	EtOH/Et_2O	B
61	40.8	Evaporation, trituration with hexane	A
62	59.6	Evaporation, stirred with EtOH/H_2O for 3 days	A
63	37.7	Evaporation, trituration with hexane	A
64	27.2	Evaporation, stirred with EtOH/H_2O for 3 days	A
65	8.05	Evaporation, trituration with hexane	A

BDI #	Yield (%)	Isolation Method	Reaction Conditions
66	77.9	Evaporation, trituration with hexane	A
67	39.2	Evaporation, stirred with EtOH/H_2O for 24 hours	A
68	32.5	Filtration	B
69	59.4	EtOAc trituration	A
70	25.6	EtOH/H_2O	A
71	13.3	EtOH/Et_2O filtration	A
72	19.2	EtOH/H_2O	A
73	10.9	EtOH/Et_2O filtration	A
74	30.8	EtOH/H_2O	A
75	24.1	EtOH/H_2O	A
76	20.1	Evaporation, trituration with Et_2O	A
77	19.9	Et_2O filtration	A
78	14.3	Evaporation, trituration with Et_2O	A
79	32.0	Evaporation, trituration with hexane	A
80	58.8	Evaporation, trituration with	A

BDI #	Yield (%)	Isolation Method	Reaction Conditions
		hexane	
81	11.5	Evaporation, trituration with hexane	A
82	12.1	Et_2O filtration	A
83	84.3	Evaporation, trituration with hexane	A
84	40.8	Et_2O filtration	A
85	N/A	Evaporation, trituration with hexane	A
86	N/A	Evaporation, trituration with hexane	A
87	N/A	Evaporation, trituration with hexane	A
88	N/A	Evaporation, trituration with hexane	A
89	49.5	Column chromatography	A
90	16.0	Filtration	A
91	54.3	Filtration, boiling MeOH trituration	A
92	51.2	Filtration, Et_2O wash	A

BDI #	Yield (%)	Isolation Method	Reaction Conditions
93	N/A	N/A	A
94	15.3	Evaporation, placed in freezer, trituration with hexane	A
95	9.7	Column, MeOH trituration	A
96	21.3	Filtration, Et_2O wash	A

2.4 Conclusions

In conclusion, the synthesis of a new class of R^2-derivatized GFP- and RFP-like chromophores was accomplished via a new combinatorial route. These results were accomplished by addition of a single step to the route. In the case of alkyl R^2 groups, this step was simply making new ethyl imidate hydrochlorides via reaction with hydrochloric acid gas and ethanol; the following step was then slightly modified to be anhydrous, in order to accommodate the new functional groups. For conjugated R^2 groups, the additional step was an amidation step, but the subsequent step was a replacement of the usual glycine substitution, instead using a variant of Meerwein's Salt to transform the amide to the desired imidate. These results show that R^2-modified GFP- and RFP-like chromophores can be synthesized combinatorially, using a convergent, shorter route than those previously demonstrated in the literature.

2.5 References

[1] He, X.; Bell, A. F.; Tonge, P. J. *Org. Lett.* **2002**, *4*, 1523.

[2] Wu, L.; Burgess, K. *J. Am. Chem. Soc.* **2008**, *130*, 4089-4096.

[3] Yampolsky, I.; Kislukhin, A. A.; Amatov, T. T.; Shcherbo, D.; Potapov, V. K.; Lukyanov, S.; Lukyanov, K. A. *Bioorg. Chem.* **2008**, *36*, 96-104.

[4] Baldridge, A.; Kowalik, J.; Tolbert, L. M. *Synthesis* **2010**, *14*, 2424-2436.

[5] Lerestif, J. M.; Perrocheau, J.; Tonnard, F.; Bazureau, J. P.; Hamelin, J. *Tetrahedron* **1995**, *51*, 6757-6774.

[6] Fellows, W. B.; Kowalik, J.; Tolbert, L. M. "A New Combinatorial Method for C-alkylated GFP and RFP Chromophore Synthesis." *Submitted*.

[7] Bluhm, M. E.; Folli, C.; Pufky, M. K.; Walter, O.; Doring, M. *Organometallics* **2005**, *24*, 4139-4152.

[8] Brochu, J.-L.; Prakesch, M.; Enright, G. D.; Leek, D. M.; Arya, P. *J. Comb. Chem.* **2008**, *10*, 405-420.

[9] Berger, O.; Wein, S.; Duckert, J.-F.; Maynadier, M.; Fangour, S. E.; Escale, R.; Durand, T.; Vial, H.; Vo-Hoang, Y. *Bioorg. Med. Chem. Lett.* **2010**, *20*, 5815-5817.

[10] Goebel, M.; Staels, B.; Unger, T.; Kintscher, U.; Gust, R. *Chem. Med. Chem.* **2009**, *4*, 1136-1142.

[11] Hooley, R. J.; Rebek, Jr., J. *Org. Lett.* **2007**, *7*, 1179-1182.

[12] Ellingboe, J. W.; Collini, M. D.; Quagliato, D.; Chen, J.; Antane, M.; Schmid, J.; Hartupee, D.; White, V.; Park, C. H.; Tanikella, T.; Bagli, J. F. *J. Med. Chem.* **1998**, *41*, 4251-4260.

[13] Morel, F.; Lerestif, J. M.; Bazureau, J. P.; Hamelin, J. *Heteroatom Chem.* **1996**, *3*, 187-194. Our conditions are similar to this method; see Experimental section of this chapter for details.

[14] Erlenmeyer, E. *Justus. Liebigs. Ann. Chem.* **1893**, *275*, 1.

[15] Erlenmeyer, E. *Ber. Dtsch. Chem. Ges.* **1900**, *33*, 2036.

[16] Williams, D. L.; Ronzio, A. R. *J. Am. Chem. Soc.* **1946**, *68*, 647.

[17] Hunter, M. J.; Ludwig, M. L. *J. Am. Chem. Soc.* **1962**, *84*, 3491-3504.

[18] Wagner, B.; Schumann, D.; Linne, W.; Koert, U.; Marahiel, M. A. *J. Am Chem. Soc.* **2006**, *128*, 10513-10520.

CHAPTER 3

MICROCRYSTALS WITH ENHANCED EMISSION PREPARED FROM HYDORPHOBIC ANALOGUES OF THE GREEN FLUORESCENT PROTEIN CHROMOPHORE VIA REPRECIPITATION

The research highlighted within this chapter represents a collaboration between the Tolbert lab at Georgia Tech, in Atlanta, and the lab of Dr. Suzanne Fery-Forgues at The University of Toulouse, ITAV, in Toulouse, France. Throughout this collaboration, the synthesis and design of chromophores was performed within the Tolbert lab and the reprecipitation experiments were performed in the Fery-Forgues lab. Data analysis and manuscript preparation were equally shared between the two collaborating labs.

3.1 Introduction

In the last ten years, there has been significant effort toward the study of organic luminescent nano- and micromaterials, due to their potential applications in biological sciences,[2-5] as chemical and biochemical sensors,[5-9] and in optical and optoelectronic engineering.[9-13] Among these, a new class of materials which are weakly emissive in solution but luminescent in the solid state has seen significant attention. This phenomenon is referred to as aggregation-induced emission (AIE).[14,15] Consequently,

these materials avoid the notorious problem of fluorescence quenching that occurs for most dyes when passing from dilute solutions to the aggregated state.[16,17] The behavior of these compounds can be explained as follows. Although molecules that display the AIE phenomenon belong to various chemical families, their design principle generally involves the presence of aromatic groups connected by rotatable single bonds. Excitation energy is dissipated in solution via free rotation of the aromatic groups, resulting in a conical intersection/internal conversion and, as a result, a loss of fluorescence efficiency. At the same time, enhanced emission in the solid state has been associated with molecular planarization and restricted molecular motions. The AIE effect has also been assigned to a variety of other mechanisms including the cancellation of competitive photochromic mechanisms, prevention of exciton diffusion, J-aggregate formation, protection of the fluorophores from specific interactions with the solvent, or to a synergistic combination of these effects.

Very recently, the Tolbert lab has developed a series of new compounds that demonstrate the AIE phenomenon.[18] They are analogues of the green fluorescent protein (GFP)[19-21] chromophore, that is, derivatives of *p*-hydroxybenzylidenedimethylimidazolidinone (HOBDI, Figure 1). By manipulating various substituents on the phenyl group, our aim is now to use aggregates of these compounds as micro- or nanomaterials by analogy with fluorescent nanoparticles. This approach requires a methodology for spontaneous production of particles using simple methods for general applicability. Specifically, for applications as bioprobes, a mild method to generate suspensions of organic micro- and

nanoparticles directly usable in biological media is required. In this context, the reprecipitation (RP) method, developed primarily by Nakanishi and co-workers,[22,23] and extensively used during the past decade, is of great interest. RP consists of dissolving the organic compound (which is insoluble or weakly soluble in water) in a water-miscible solvent and pouring a small volume of this concentrated solution into a large volume of water under vigorous stirring. The abrupt solvent change prompts the hydrophobic organic compound to precipitate, thus leading to the formation of an aqueous suspension of nano- and microparticles that can be directly used for biological applications. These particles can also be filtered, dried, stored, and used for numerous other applications. Notably, the RP conditions are very far from equilibrium, since nucleation takes place at very high level of supersaturation. The shape and size of the micro/nanoparticles produced by RP often differ from those obtained by classical recrystallization. However, the possible influence of these parameters on the AIE fluorescence properties has not yet been studied.

The first section of this portion of the chapter clarifies the influence of the RP conditions on the AIE fluorescence properties. The RP method is particularly well suited for hydrophobic molecules and, as such, was chosen for our work with the hexyloxy and dodecyloxy derivatives of the GFP chromophore (HexOBDI and DodecOBDI, respectively, **Figure 3.1**).

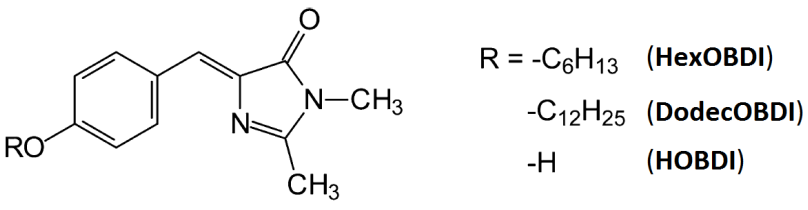

Figure 3.1: Alkoxy chromophores used in this work

These molecules have previously demonstrated solid state emission[18] and represent potential candidates for the preparation of micro- and/or nano-particles usable in aqueous biological media. In the first portion of this work, the RP process was adapted to these compounds. A distinct advantage of the method is that several experimental parameters can be varied to control the morphology and size of the particles produced. Experiments were thus carried out at three different temperatures, as well as in the absence and in the presence of an additive, specifically poly(acrylic acid) (PAA), which proved to be very useful in a previous work to influence the RP of nitrobenzoxadiazole (NBD) derivatives.[24] A variety of techniques were used to monitor and characterize the formation of particles from HexOBDI and DodecOBDI. The second portion of this section of the chapter illustrates the fluorescence properties of the particles produced by RP as compared to those of the microcrystalline powders of the same compounds obtained through crystallization in an organic solvent.

3.2 Experimental

Materials. *N*-hexyloxybenzylidenedimethylimidazolinone (HexOBDI) and *n*-dodecyloxybenzylidenedimethylimidazolinone (DodecOBDI) were synthesized by alkylation of HOBDI as previously described.[18] In addition to the traditional method of HOBDI synthesis described in Ref. 25, this precursor was also prepared using the novel high-yield method developed at Georgia Tech.[26] The samples used for spectroscopic measurements were checked for purity by HPLC. For RP, acetonitrile (Merck, HPLC grade) and high-pressure demineralized water (resistivity 18.3 MΩ cm) prepared with a

Milli-Q apparatus (Millipore) were used as solvents. Poly(acrylic acid) (Average MW = 100 000, 35% in H_2O) and propionic acid were purchased from Aldrich.

Apparatus. An HPLC/MS system (AutoPurif, Waters) equipped with a UV−vis diode array and ES mass spectrometer was used at the Chemistry Platform of ITAV. Columns were Phenomenex Gemini C18 and an acetonitrile/water mixture gradient (from 95:5 to 0:100 in 10 min) containing 0.05% formic acid was used as the eluent. To obtain dry powders of reprecipitated compounds, RP was performed with 1250 mL of suspension in the experimental conditions described in the text. The precipitate was then collected by filtration on 200 nm Millipore Nylon filters and dried under vacuum at 50 °C. For DodecOBDI in the presence of PAA, the suspension was centrifuged at 10,000 rpm for 30 min at 5 °C and most of the supernatant was discarded before filtration. This process allowed a sufficient amount of compound to be recovered before the Nylon filter was clogged by small particles. ^{1}H NMR spectra were recorded on a Bruker AVANCE 500 spectrometer operating at 500.13 MHz and the IR spectra were measured on a Nexus Thermonicolet at the “Services Communs de l′UniversitéPaul Sabatier de Toulouse." The X-ray powder diffraction patterns were performed in the “Service Diffraction X du LCC Toulouse." These were collected in transmission mode, on capillary samples, on a θ-θ XPert Pro Panalytical diffractometer, with λ (Cu Kα1, Kα2) = 1.54059, 1.54439 Å. Extraction of peak positions for indexing was performed with a fitting program, available in the PC software package Highscore+ supplied by Panalytical.

The shape and size of the reprecipitated compounds were examined with a Zeiss Axioskop fluorescence microscope equipped with an Andor Luca camera. The excitation

wavelength was 350−380 nm, and the emission wavelength was set at above 400 nm, using suitable filters. Alternatively, samples were illuminated at 430−450 nm and the emission wavelength was collected above 500 nm. The microcrystals grown in methanol were observed at low magnification on a Macrofluo Leica Z16APO fluorescence microscope equipped with a black and white Roper camera (Imaging Platform of ITAV). Transmission and scanning electron microscopy (TEM and SEM, respectively) were performed at the "Service Commun de Microscopie Electronique de l′Université Paul Sabatier". For TEM, a JEOL JEM 1400 electron microscope equipped with an SIS Megaview III camera was used. To prepare the TEM samples, the carbon grids were soaked in an aqueous suspension containing the alkyl-OBDI derivatives, after RP was complete. The samples were revealed with a drop of ammonium molybdate aqueous solution (2%, pH 5) as a contrasting agent and allowed to dry for 48 h under vacuum at 60 °C. SEM was carried out with a JEOL JSM 6700F apparatus. The powder sample was deposited on a self-adhesive tape and metalized with platinum. UV−vis absorption spectra were recorded on a Hewlett-Packard 8452A diode array spectrophotometer.

Spectroscopic measurements were conducted at 22 °C in a temperature-controlled cell. Corrected steady state fluorescence spectra were recorded with a Photon Technology International (PTI) Quanta Master 1 spectrofluorometer, using cells of 1 cm or 1 mm optical pathway. The fluorescence quantum yields (Φ_F) were determined using the classical formula: $\Phi_{Fx} = (A_s F_x n_x^2 \Phi_{Fs})/(A_x F_s n_s^2)$, where *A* is the absorbance at the excitation wavelength, *F* is the area under the fluorescence curve, and n is the refraction index.[27] Subscripts *s* and *x* refer to the standard and to the sample of unknown quantum

yield, respectively. Coumarin 6 in absolute ethanol (Φ_F = 0.78) was used as a standard.[27] Fluorescence quantum yields were measured by exciting the samples near their absorption maxima. Solid state photoluminescence quantum yields were recorded on a Xenius SAFAS spectrofluorometer equipped with a $BaSO_4$ integrating sphere and a Hamamatsu R2658 detector. Solid samples were deposited on a metal support and luminescence spectra were corrected. The excitation source was scanned in order to evaluate the reflected light for the empty sphere (L_a), the samples facing the source light (L_c), and the sample out of the irradiation beam (L_b). The fluorescence spectra were recorded with the sample facing the source light (E_c) and out from the direct irradiation (E_b). The PM voltage was adapted to the measurement of reflected light and emission spectra, respectively, and proper correction was applied to take into account the voltage difference. The absolute photoluminescence quantum yield values (Φ_P) were determined by a method based on the one developed by de Mello et al.,[28] using the formula: $\Phi_P = [E_c - (1 - \alpha)E_b]/ \alpha L_a$ with $\alpha = 1 - (L_c/L_b)$.

3.3 Results and Discussion

Preparation of Micro/Nanoparticles Using the RP Method

Stock solutions of HexOBDI and DodecOBDI (2 × 10−3 M) in acetonitrile were prepared. A 40 μL portion was rapidly injected into a volume of 1.96 mL of water or water containing 0.738% (7.38 × 10^{-5} M) PAA, previously conditioned at desired temperature, and the mixture was left under vigorous magnetic stirring. The dye

concentration in the mixture was 4×10^{-5} M, the fraction of acetonitrile in water being 2% v/v. In all cases, the mixture became rapidly cloudy and fluorescent.

Monitoring by Optical Spectroscopy. RP was monitored by UV−vis absorption spectroscopy to determine the duration of the process and possibly get an initial idea about the mechanism of particle formation. Experiments in water alone at room temperature were investigated first. For HexOBDI, the absorption spectrum showed a progressive decrease in absorbance, with almost no wavelength shift (**Figure 3.2a**). Such a variation of absorbance is generally associated with the formation of particles and their precipitation.[24,29] The process was almost complete in 12 minutes. For DodecOBDI, no spectral evolution was noted after the first few minutes (**Figure 3.2b**). Such behavior has been observed for highly hydrophobic compounds that form small particles almost instantly when placed in a weakly solvating solvent.[30]

Next, the effect of PAA was investigated. For HexOBDI, by comparison with the experiment run in water alone, the presence of PAA induced a weaker decrease in absorbance and a significant increase of the baseline (**Figure 3.2c**), suggesting formation of small particles that remain in suspension. A red shift of 10 nm was also noted. The duration of the process was almost unchanged. For DodecOBDI, the presence of PAA induced remarkable spectral variations (**Figure 3.2d**). The initial spectrum was blue-shifted, and the absorbance was smaller than in water alone. Over 16 min, the absorption spectrum recovered the shape and intensity previously observed at the end of the experiment run in the absence of PAA, and the absorbance was further decreased (**Figure 3.2d**, inset). These variations indicated the involvement of a complex phenomenon before precipitation of the particles. Control experiments conducted with propionic acid at an

equivalent carboxylic acid concentration produced precipitation close to that observed in the absence of additive, suggesting the importance of the polymer structure in the above experiments.

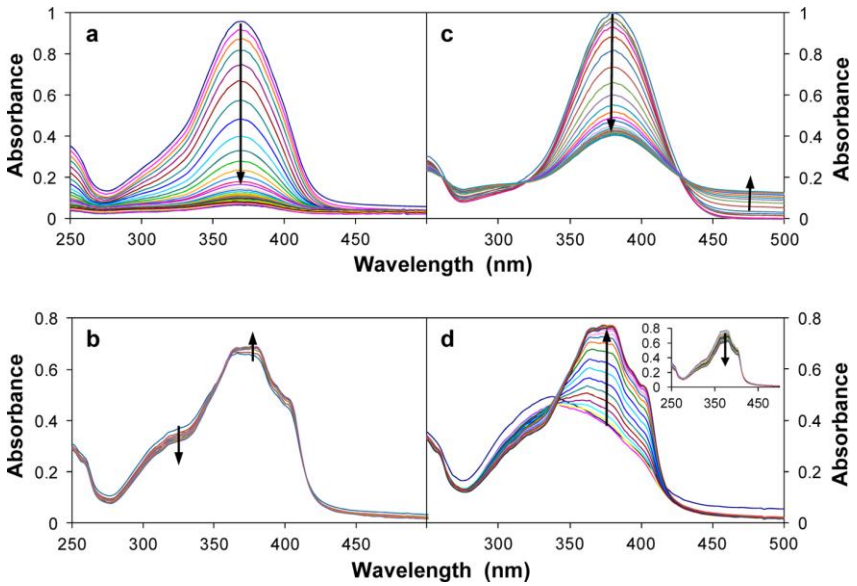

Figure 3.2: Evolution of the UV/vis absorption spectrum of HexOBDI and DodecOBDI ($4 \times 10{-}5$ M) during RP at 22 °C in water containing 2% v/v CH_3CN in the absence (spectra a and b, respectively) and presence of poly(acrylic acid) 0.738% (spectra c and d, respectively). One measurement every 30 s for spectra (a) and (c), every 2 min for (b), and every min for (d). The inset of (d) shows the absorbance decrease taking place from 16 to 30 min after onset.

Plotting the absorbance variation at 370 and 380 nm (for HexOBDI and DodecOBDI, respectively) versus time allowed the RP kinetics to be visualized[24,29] (Figures S1 and S2, Supporting Information of Ref. 1). The curves showed a rapid evolution and then leveled off. For both dyes, the shape of the curve recorded in the presence of PAA was similar to that in water alone. However, an initial induction period clearly appeared and the RP process lasted slightly longer in the presence of PAA. It thus seems that the whole RP process remained the same, but the presence of the polymer slowed down nucleation and crystal growth.

The molecules under investigation displayed the unusual property of emission in the solid state but not in dilute solution. It was thus instructive to monitor the kinetics of the RP process by fluorimetry. The RP process of HexOBDI in the presence of PAA seemed particularly suitable. In fact, the absorption curves displayed a quasi-isosbestic point at 316 nm. Excitation at this wavelength avoided correction for absorbance variation. Moreover, the inner-filter effect was constant and absorbance at this wavelength was low (A ≈ 0.17), which allowed linear detection of fluorescence. The variation of the fluorescence intensity was monitored over 30 min. The appearance and growth of an emission peak at 448 nm was observed (**Figure 3.3a**). Plotting the fluorescence intensity variation versus time generated a curve inverse to that of the corresponding absorbance curve (**Figure 3.3b**). This clearly indicated that the variations detected by both absorption and fluorescence spectroscopy corresponded to the formation of particles.

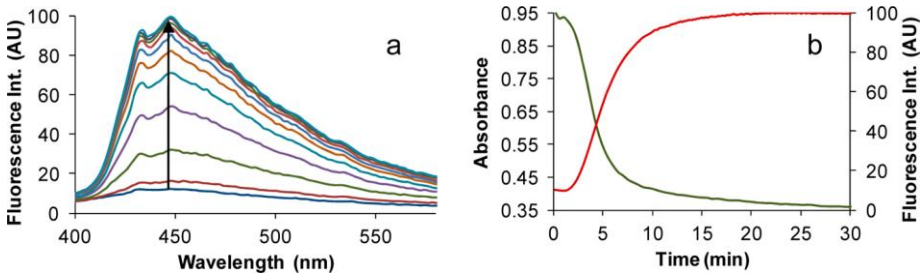

Figure 3.3: Kinetics of the RP process of HexOBDI (4×10^{-5} M) at 22 °C in aqueous medium containing poly(acrylic acid) 0.738% and 2% v/v CH3CN. (a) Variation of the emission spectrum with λ_{ex} = 316 nm (quasi-isosbestic point), one curve every 3 min. The peak at 432 nm is a scattering peak from excitation. (b) Plot of absorbance at 370 nm (green line) and fluorescence at 450 nm (red line) versus time.

In our experience, when changes were no longer detected by optical spectroscopy during RP, the suspensions remained stable for many hours. When crystalline particles

were formed, crystal growth actually continued by Ostwald ripening, but it was very slow and allowed quite reproducible measurements to be performed. In the present case, spectroscopy indicated that the initial formation of particles was quite rapid at room temperature (10−30 min, according to the dye and presence of PAA). As some variations could be observed when RP was conducted at different temperatures, the mixtures were systematically examined more than 2 h after onset of RP in the following work. The observations were very reproducible.

Observations by Fluorescence Microscopy of the RP Mixture Prepared in the Absence of Additive at Various Temperatures. RP was performed in water alone at 4, 22, and 38 °C to study the effect of temperature. A drop of the RP mixture was placed between two glass slides and examined with a fluorescence microscope. Excitation was performed with UV light (350−380 nm), and the emission recorded above 400 nm. Particles emitting a turquoise-green light were observed in both samples. Alternatively, when the samples were excited with blue light (430−450 nm) with recording emission above 500 nm, particles appeared yellow. The main tendency of both compounds was to give microcrystalline plates via the RP method (**Figure 3.4**). The shape of platelet crystals was more regular for HexOBDI than for DodecOBDI, and twinned microcrystals were frequently encountered in the former case. In all samples, the particle size and shape were heterogeneous. When RP was carried out at 4 °C, the HexOBDI sample was characterized by a large number of needlelike microcrystals, most of them very thin and agglomerated, others having larger dimensions and showing the result of heterogeneous nucleation (also see Figure S3 in the Supporting Information of Ref 1). At 22 °C, elongated plates measuring 10−25 μm long and 2 μm wide were formed, together with

smaller crystals. At 38 °C, most of the microcrystals appeared as wide platelets with irregular shapes. Similarly, DodecOBDI formed thin needles at 4 °C and bigger microcrystals at increasing RP temperature. At 38 °C, various populations of particles coexisted. It is noteworthy that many crystals emitted more strongly on the edges than in the center, a phenomenon already encountered for other dye microcrystals and attributed to waveguiding.[24,27,31] Interestingly, for DodecOBDI, the microcrystals were accompanied at all temperatures by a diffuse network of very thin nanofibers (**Figure 3.5a**).

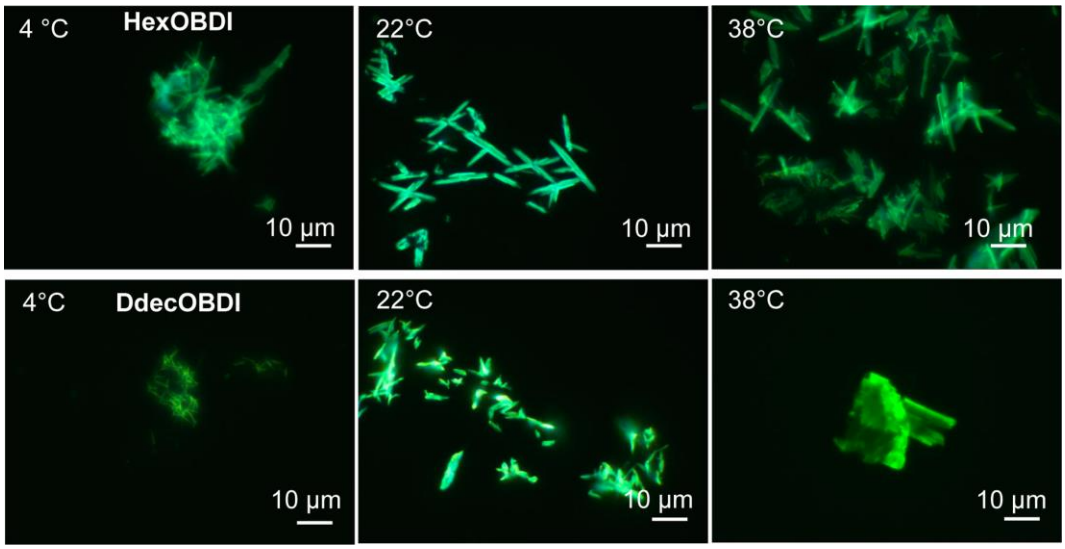

Figure 3.4: Fluorescence microscopy images of HexOBDI (top) and DodecOBDI (bottom) at 4×10^{-5} M after RP in water with 2% v/v acetonitrile at 4 °C, 22 and 38 °C. Excitation with UV light.

The microcrystals of both dyes appeared to undergo a change under the microscope UV light beam; they became round, and the fluorescence vanished. Moreover, the fibrils disappeared almost instantaneously upon irradiation with UV light (**Figure S4**, Supporting Information of Ref. 1). Both observations indicate the occurrence of a photochemical reaction. This phenomenon can be related to a recent study[32] in which

some HOBDI dye derivatives were observed to undergo photoinduced [2 + 2] cycloaddition in the crystalline state, and thus to become nonfluorescent. However, photo-oxidation cannot be ruled out. Two reasons at least may explain why photobleaching was slower for microcrystals than for fibrils. First, in the microcrystals, the surface molecules can act as an internal filter to protect the microstructure against light penetration and, possibly, oxygen access. Second, molecular packing may also differ in fibrils and in microcrystals, making the former more sensitive to photochemical reaction, as was noted for polymorphs.[32] The photoreaction was slower with blue light, presumably because the sample did not absorb much at this wavelength.

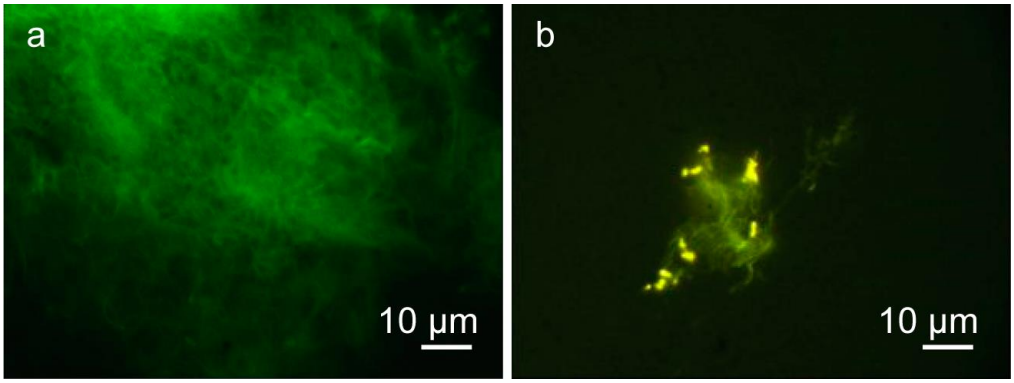

Figure 3.5: Fluorescence microscopy image of the nanofiber network observed in a sample of DodecOBDI at 4×10^{-5} M after RP in water with 2% v/v acetonitrile. (a) RP at 4 °C, excitation with UV light. (b) RP in the presence of PAA at 22 °C, excitation with blue light.

Observations by Electron Microscopy. To get additional structural information, samples prepared at 22 °C were studied by transmission electron microscopy (TEM). RP was performed as described above, and a drop of the sample was deposited on a grid, dried and stained by a contrasting agent. Particles were observed, most of them containing sharp edges typical of crystals. Elongated crystals similar to those observed by fluorescence microscopy (Figure S5a and b, Supporting Information, Ref 1), as well as

small crystals (Figure S5c, Supporting Information, Ref 1) were found in both samples. Twinned crystals were also observed in HexOBDI samples (Figure S6, Supporting Information, Ref 1). Crystallinity was confirmed by a clear electron diffraction spectrum (Figure S5b and c, Supporting Information, Ref 1). Samples of DodecOBDI also clearly revealed the presence of nanofibers (Figure S5d, Supporting Information, Ref 1), which vanished under the electron beam when attempting to get an electron diffraction pattern.

The samples were also examined by scanning electron microscopy (SEM). To do so, 25 mL of dye solution at 2×10^{-3} M in acetonitrile was poured into 1.225 L of distilled water. The resulting particles were filtered, dried under vacuum at 45 °C, and metalized before the SEM studies. For both dyes, SEM revealed the presence of elongated platelets with irregular outlines, the thickness of which was about 350−500 nm (Figure S7, Supporting Information, Ref 1). The platelets were slightly shorter than the ones observed by fluorescence microscopy, but this can be explained by the fact that hydrodynamics conditions, and particularly stirring, are very different due to the volumes used.

Observation and Characterization of the RP Mixture Prepared in the Presence of PAA. RP was carried out at 22 °C in aqueous medium containing poly(acrylic acid) 0.738%, and the resulting suspension was observed by fluorescence microscopy. Generally, the microcrystal size was reduced in the presence of PAA. For HexOBDI, only agglomerates of small microcrystals (3 μm in their largest dimension) were observed. For DodecOBDI, a large number of fibrils were observed, forming a sort of diffuse network between the microcrystals (**Figure 3.5b**). Dry samples were also examined by SEM (**Figure 3.6**). SEM confirmed that the HexOBDI sample contained

microcrystals similar to those observed in the absence of PAA. In contrast, the microcrystals of DodecOBDI were much rarer and markedly smaller, with a thickness between 100 and 200 nm, and they coexisted with a dense fibrous network.

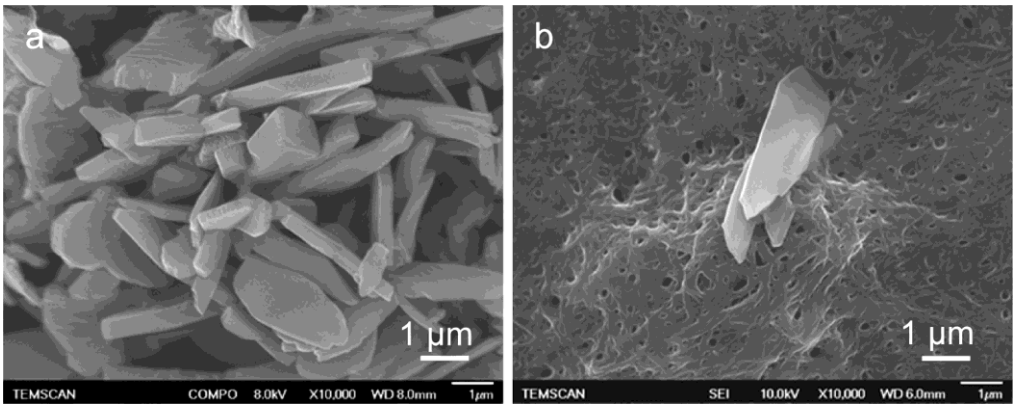

Figure 3.6: Scanning electron microscopy images of the samples of (a) HexOBDI and (b) DodecOBDI (4 × 10−5 M) after RP in aqueous medium with 2% v/v acetonitrile at 22 °C in the presence of 0.738% PAA.

To learn more about the role of PAA on the formation of microcrystals and fibrils, a sufficiently large amount of particles was prepared in the same concentration conditions as specified above, filtered on Millipore, rinsed with deionized water, and dried under vacuum. A portion of this solid was dissolved in deuterated methanol and analyzed by ^{1}H NMR at 500 MHz. No peaks were detected between 5.5 and 6.8 ppm, where the characteristic signals of PAA appear[33] (Figures S8 and S9, Supporting Information, Ref 1). Another portion of this solid was analyzed by FTIR and compared with pristine compounds. For HexOBDI, no difference was found between the sample processed with PAA and the reference, while for DodecOBDI a broadening of the 2500−3500 cm^{-1} region and of the peak at 1705 cm^{-1} may indicate the residual presence of some PAA in the sample (Figure S10, Supporting Information, Ref. 1).

Finally, X-ray powder diffraction patterns of HexOBDI and DodecOBDI reprecipitated with PAA were recorded and compared with pristine compound. All the samples showed well resolved peaks, indicating their crystalline nature. Most of the diffraction peaks of the reprecipitated and pristine powder were superimposable (Figure S11, Supporting Information, Ref. 1) and in perfect agreement with the theoretical XRPD pattern calculated from X-ray analysis data[18] using the Mercury software. The crystal packing mode was thus retained during the RP process, and it was not affected by the presence of PAA.

Considerations on the Crystal Structure and Observation of Pristine Powders by SEM

The RP method mainly led to microcrystals. Consequently, before going further, it seemed pertinent to recall the crystal packing mode of these compounds. Growing single crystals of HexOBDI and DodecOBDI in organic solvents was relatively easy and their crystal structure obtained by X-ray analysis has been published and discussed.[18] Both compounds crystallized in the triclinic $P\bar{1}$ system. The crystal morphology was determined using the Bravais Friedel Donnay and Harker (BFDH) theory in the Mercury software[34] (**Figure 3.7** and Supporting Information Figure S12, Ref. 1). For both compounds, the heteroatoms were accessible on the main faces, making them relatively polar. The difference was that two faces (110 and −1−10) of the DodecOBDI crystal were much more apolar than the corresponding faces on the DodecOBDI crystal, due to the presence of the long alkyl chains.

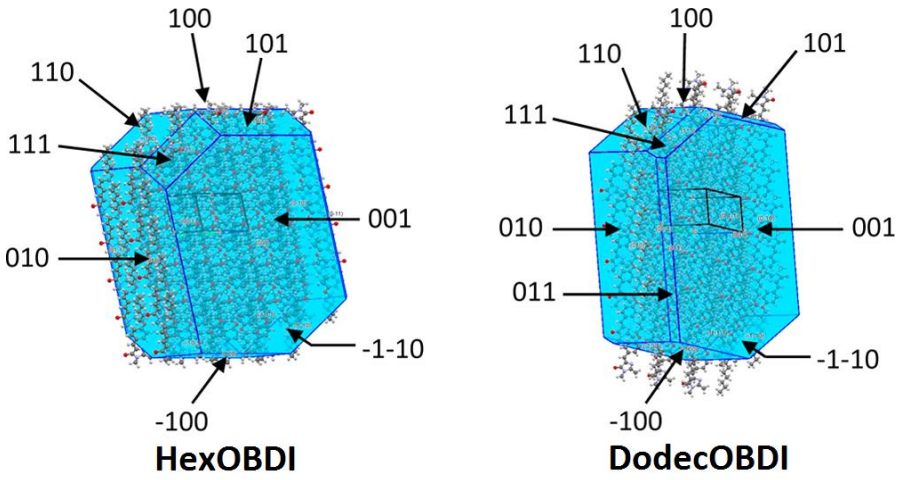

Figure 3.7: Crystal morphology of HexOBDI and DodecOBDI predicted from X-ray analysis data[18] using the Mercury software,[34] with indexation of the main faces.

The pristine powders resulting from crystallization in ethyl acetate were observed by SEM (**Figure 3.8**). It appeared that these powders were constituted by agglomerates of slightly elongated, relatively thick crystals. Many of these crystals were close to the morphology predicted by BFDH theory. Although crystals of better quality would be necessary to distinguish the faces unambiguously, it can be supposed for example that the hexagonal face that ends the crystal of **Figure 3.8b** could be the (001) face, the side faces could be (010), (110), (100), and (0−10), while the (111) and (101) faces would be inexistent. In this case, the axis of maximum elongation would be *z*.

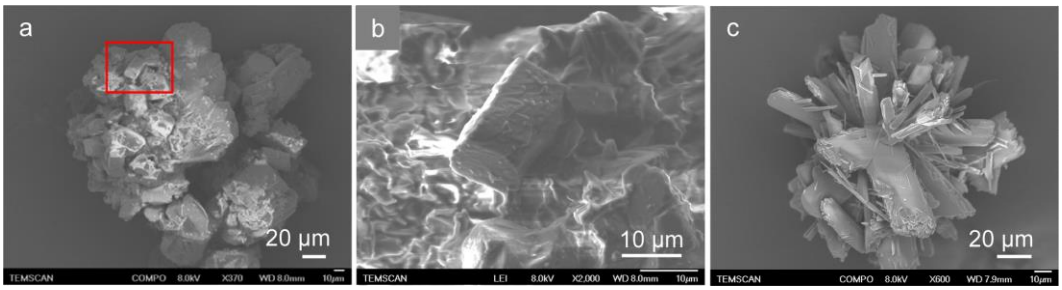

Figure 3.8: Scanning electron microscopy images of (a) HexOBDI with magnification of the red rectangle (b) and (c) DodecOBDI pristine powder crystallized in ethylacetate.

For the sake of comparison, the compounds were recrystallized in methanol. Very flat microcrystals, elongated for HexOBDI and rectangular for DodecOBDI, were obtained (Figure S13, Supporting Information, Ref. 1). The platelet crystals obtained by RP in water were very different from the models and from the pristine crystals obtained in ethyl acetate, but they were close to the flat crystals obtained in methanol, except for size. This observation suggests that the crystal morphology was controlled by solvent polarity. Given the shape of the platelets obtained in methanol and water, the main face could be (001) and the axis of maximum elongation would then be *x* for crystals grown in polar media.

Photoluminescence Properties

The HexOBDI and DodecOBDI compounds used for the study of the optical properties were purified and checked by HPLC, in order to obtain samples as pure as possible. In particular, possible traces of HOBDI, which was used as the precursor for synthesis and constitutes the major cause of impurity, were removed.

The RP process resulted in well-characterized microcrystals. Their luminescence properties in suspension and as powders were investigated and compared with those of pristine microcrystalline powders (**Figure 3.9**). Additionally, it was instructive to make a comparison with pristine compounds that contain a known amount of HOBDI.

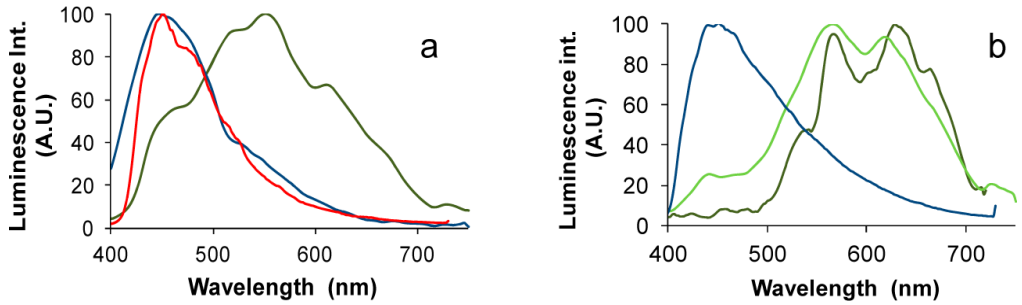

Figure 3.9: Selected emission spectra of (a) HexOBDI and (b) DodecOBDI: Normalized fluorescence spectra of the suspensions of the compounds reprecipitated in water with 2% v/v acetonitrile at 22 °C (blue lines), photoluminescence spectra of the pristine microcrystalline powders (dark green lines), HexOBDI issued from RP with PAA (red line), and DodecOBDI with 2% HOBDI. λ_{ex} = 370 nm.

Fluorescence of Microcrystal Aqueous Suspensions. The fluorescence spectra of the suspensions were recorded directly after RP, using the same method as for solutions. This gave information about the properties of native microcrystals. The present system lends itself well to this type of study, because AIE-active compounds were virtually nonfluorescent in solution and little interference from dissolved fluorophores was likely to occur. Cells of 1 cm and 1 mm optical path length were used for HexOBDI and DodecOBDI, respectively, keeping the absorbance below 0.1 and at around 0.07, respectively. The emission spectrum obtained for HexOBDI exhibited a single structureless band with a maximum at 450 nm and was quite close to that obtained in the presence of PAA (see **Figure 3.3**). The spectrum of DodecOBDI was only slightly broader than that of HexOBDI. It is noteworthy that the shape of both spectra hardly varied with changing the excitation wavelength between 300 and 420 nm (Figure S13, Supporting Information, Ref. 1). The excitation spectra are shown and discussed in the Supporting Information of Ref. 1 (Figure S14). The fluorescence quantum yields of the

suspensions were obtained and found to be around 0.07 and 0.01 for HexOBDI and DodecOBDI, respectively. However, the measurement of fluorescence spectra in turbid media is particularly difficult and subject to many artifacts.[35] Consequently, these values must be considered with circumspection and only their order of magnitude can be reasonably relied upon.

Photoluminescence of Dry Microcrystals Obtained by RP and Pristine Compounds. The photoluminescence spectra of powders were recorded using a spectrofluorometer equipped with an integrating sphere. The dry powders of HexOBDI and DodecOBDI prepared by RP in water alone were examined, together with HexOBDI prepared in the presence of PAA. These compounds were nearly colorless powders that generated bluish light upon excitation with a hand-held UV lamp. The photoluminescence spectrum of the two former samples was broader than that of the reprecipitated compounds in suspension, while the spectrum of HexOBDI prepared in the presence of PAA was superimposable. The photoluminescence quantum yields were 0.026, 0.019, and 0.035, respectively, by exciting at 370 nm with a 20 nm bandpass, and they were weakly dependent on the excitation wavelength and bandpass.

Pristine HexOBDI appeared as a bright yellow powder, strongly emitting in the pale yellow, while DodecOBDI was an orange powder, which emitted in the orange yellow with lower intensity. Exciting the HexOBDI and DodecOBDI powders at 370 nm generated emission spectra that were much broader than those of the corresponding reprecipitated compounds. The photoluminescence quantum yields, obtained with a broad

bandpass (20 nm at excitation and 10 nm at emission), were found to be 0.046 and 0.022 for HexOBDI and DodecOBDI, respectively. The quantum yield varied with variation of the excitation wavelength or excitation bandpass.

Finally, pristine powders containing 2% HOBDI were examined. Their photoluminescence spectra and quantum yield were found to be close to those of the pure compounds. Increasing the amount of HOBDI in HexOBDI to 33% led to a brown powder that was poorly emissive under the hand-held UV lamp. The photoluminescence of this sample was weak, and the spectrum was strongly shifted to the red. It is noteworthy that all doped compounds observed with the fluorescence microscope showed microcrystals that homogeneously emitted in a wide span of wavelengths. No domains presenting a particular emission were distinguished.

The hydrophobic derivatives of the GFP chromophore studied in this work are excellent candidates for the preparation of micro/nanoparticles via the RP method. The natural tendency of these compounds is to produce elongated platelets in water. By comparison with the compounds crystallized in ethyl acetate, the modification of the crystal habit can be attributed to a solvent effect. Presumably, water molecules strongly interact with the hydrophilic faces and prevent growing of these faces. Since slow-growing faces are the most developed, hydrophilic faces develop more than hydrophobic faces when crystals grow in water. The experimental conditions are related to small differences in the size and shape of the resulting particles. For instance, the microcrystals get smaller with decreasing temperature. This effect can be explained by the dye supersaturation at low temperature, inducing a fast nucleation process.

The presence of PAA also affects the RP process. Comparison with propionic acid shows that the polymeric structure is necessary for this effect to take place. In water at pH 5, an appreciable fraction of the carboxylic groups are ionized (the pK_a of PAA is 4.3).[36] This is also the case for the monocarboxylic acid (pK_a 4.87), but the difference is that the whole polymer carries a substantial charge due to the large number of carboxylate group per polymer molecule.[37] Such a polyion has the property of structuring the neighboring water molecules and increasing the viscosity of the medium. Moreover, the carboxylate groups constitute a multiplicity of anchoring points and favor electrostatic interactions with polar surfaces. In the present case, the polymer clearly slowed down the kinetics of microcrystal formation for both dyes, and from a practical point of view, it allowed the size of the microcrystals to be reduced and, possibly, controlled, without any detectable change in the crystal packing mode. This effect can also partly be attributed to the increased viscosity of the medium due to PAA that reduces the diffusion of dye molecules. Additionally, direct interaction probably takes place between PAA and DodecOBDI, as suggested by the spectacular variation in crystal size, the increased formation of fibers and the traces of polymer detected by IR spectroscopy in the precipitate issued from RP. This effect has been encountered in the preparation of microcrystals from NBD dyes.[24] It is quite complex and mainly attributable to the polymer adsorbing on the crystal faces and inhibiting crystal growth, without variation in the crystal packing mode. This type of interaction would allow the changes observed during the kinetics of crystal formation to be interpreted. Indeed, the small particles stay longer in suspension and the negative coating prevents agglomeration, thus delaying precipitation. The complex phenomenon observed for monitoring the RP of DodecOBDI

in the presence of PAA could also be explained. As a matter of fact, the HexOBDI and DodecOBDI molecules are rather similar, and it seems unlikely that only one of them interacts with the polymer in the dissolved state. All attempts to give evidence to an interaction between PAA and the DodecOBDI molecules dissolved in various mixtures of water and organic solvents were unfruitful. It was also imagined that the observed effect could be attributed to a specific solvation effect around DodecOBDI molecules when passing from acetonitrile to water, with the homogenization of the solvent being slowed down by the viscosity of the medium in the presence of PAA. However, this hypothesis was ruled out by the very weak solvatochromism of DodecOBDI, as already reported.[25] Consequently, we attribute the variations shown in **Figure 3.2d** to the interaction of clusters in solution or nanocrystals with PAA, followed by crystal growth and subsequent precipitation. Interaction would be visible at the beginning of the RP process because the proportion of surface molecules in very small particles is significant with respect to those of the bulk. Interaction would become gradually less obvious as crystals grew. It can be supposed that the phenomenon was observed for DodecOBDI and not for HexOBDI because the crystal faces of the two compounds have different polarity and thus the strength of interaction with PAA was different. The same hypothesis would also allow the increased formation of nanofibers to be explained in the case of DodecOBDI. If the development of the polar faces was inhibited by adsorption of PAA while the two apolar faces kept growing, the result would be the formation of fiber-like crystals.

The assumption that the nanofibers of DodecOBDI are crystalline relies on the observation that no amorphization was detected on the corresponding XRPD pattern. However, in the absence of any direct proof of crystallinity such as an electron diffraction

pattern, the possibility that the fibers are amorphous must also be considered. In this case, their formation could not be anticipated, because only a small number of organic molecules with low molecular weight spontaneously produced nanofibers by the RP method.[9,30,38−44] The nanofiber formation seems to be related here to the presence of the dodecyl chain. This observation is in line with the widely acknowledged statement that the presence of an alkyl chain is a facilitating factor,[9] although contrary examples can be found.[30] The observation that PAA strongly favors the formation of nanofibers is interesting from both a fundamental and applied point of view. Controlling the formation of fluorescent nanofibers via RP is still challenging, although remarkable attempts of rationalization have recently been made in this field.[11] This control frequently requires the use of additives. The RP method is easy to implement and could be useful to produce nanofibers, in view of numerous applications, for example in new technology devices and in the field of fluorescent chemical and biochemical sensors.[9,11,12]

The optical properties of these dyes in solution and in the solid state have already been reported.[18,25] It has been proposed that the fluorescence quenching observed in various solvents at room temperature arises from a nonadiabatic transition induced by the free rotation around the exomethylene double bond in the excited state. In contrast, the dramatic emission enhancement that characterizes the solid state has been attributed to "freezing" of the planar conformation of the dyes, resulting in effective conjugation between the donor and acceptor groups. The crystal packing mode, where head-to-head π-stacking is avoided, is similar for both dyes and favorable for light emission.

In the present study, it was interesting to compare the fluorescence spectra of the suspensions with photoluminescence spectra of the dry reprecipitated compounds and the

pristine crystalline powders. The emission spectra of the suspensions and reprecipitated compounds of both dyes were centered at around 450 nm, although the signal was nonnegligible above 550 nm. These spectra were almost independent of excitation wavelength, implying that they contained virtually one fluorescent species, the formation of which was directed by the RP conditions that are very far from equilibrium. In contrast, photoluminescence spectra of the pristine compounds were broader than the fluorescence spectra of the suspensions, and their quantum yield varied with changes in the excitation wavelength and bandpass. It has already been shown that the emission spectrum of these compounds was strongly dependent on the excitation wavelength. Actually, a previous solid-state study has been carried out on pristine microcrystalline powders and on thin films formed by heating the dyes above the melting point and rapidly cooling down to room temperature. The presence of two major emissive species, emitting, respectively, at around 460 and 550 nm, was established.[18] The solid samples of our dyes prepared in organic solvents seem to be inhomogeneous. Many hypotheses can be considered to try explaining this observation. (i) Two phases differing by their conformation or molecular arrangement, that is, polymorphs, appear in these preparation conditions. However, the same peaks were found in the XRPD patterns of both the reprecipitated HexOBDI and pristine powder, indicating that the same crystalline phase is present in both samples, and a second crystalline phase was not detected. In this case, the presence of a small amount of amorphous compound should be considered. (ii) Emission at long wavelengths arises from surface defects. It can be imagined that some crystal faces are more prone than others to generate defects or solvent inclusions, and these faces would appear preferentially during the slow crystallization of the sample in organic

solvents. The agglomeration of microcrystals could also favor the formation of defects. (iii) The presence of impurities must also be considered. This is the reason why compounds that contain known amounts of HOBDI were studied. These crystals were uniformly emitting, thus suggesting that the compounds were cocrystallized. The photoluminescence spectra of the compounds doped with 2% HOBDI were not very different from those of the purified compounds. At low concentration, HOBDI does not seem to be the main cause of spectral deformations. This is no longer the case at high concentration. The more HOBDI in the compounds, the more colored they were: for instance, a sample of HexOBDI containing 33% HOBDI was brownish. The emission spectrum showed a strong contribution in the red and a weak intensity. This can be explained by the fact that HOBDI absorbed the fraction of blue light emitted by HexOBDI and DodecOBDI, but this energy was totally lost because this compound is nonemissive.[18] In contrast, long wavelengths passed through the crystal, while the overall emission was strongly decreased. (iv) Finally, it can also be thought that reabsorption between molecules of the same type plays a major role. The solid-state emission spectrum of HexOBDI and DodecOBDI molecules is broad and extends till the red region. But a population of molecules can absorb light between 400 and 500 nm, even if their extinction coefficient is weak at these wavelengths. Consequently, part of the light emitted at short wavelengths by HexOBDI and DodecOBDI is reabsorbed, and only partially re-emitted. The result is that the short-wavelength contribution of the crystal emission spectrum decreases for the benefit of the red contribution. This reabsorption phenomenon is strongly reminiscent of that encountered for NBD derivatives, for which

it was shown that reabsorption was accompanied by waveguiding taking place in a preferred direction of the crystals.[29] Such a process could explain why, in the present work, the compounds drastically change emission properties depending on the crystallization conditions, that is to say, with varying the crystal morphology and thickness.

3.4 Conclusions

This study demonstrates that synthetic analogues of the GFP chromophore are good candidates for preparing AIE-active organic fluorescent microcrystals and nanofibers via the RP method. Platelet microcrystals and nanofibers were obtained, the shape and size of which can be modulated with varying the experimental conditions. It should therefore be possible to adjust the experimental parameters of the RP method to prepare homogeneous samples, in view of the desired application. The two compounds that were chosen for this study exhibit a modest photoluminescence quantum yield after RP. Moreover, the smallest particles are quite unstable in water under light irradiation. These two points are critical for practical applications. However, a large number of HOBDI derivatives have already been synthesized.[26,32,45,46] Some of them are much more emissive than HexOBDI and DodecOBDI, and more stable from a photochemical point of view. We will continue to study the emission properties of their particles produced using the RP method. Alternatively, other preparation methods are under investigation, in particular, drop-casting that can be used for compounds less hydrophobic than the ones studied above.

From a general point of view, the RP of AIE-active compounds allows the fluorescence of native crystals to be examined in the suspension without any interference from dissolved molecules. Evidence was given for the dependence of the photoluminescence properties on the crystal size and morphology. The present study did not allow ascertaining the involvement of polymorphs. However, as is true of most of AIE compounds, HexOBDI and DodecOBDI are characterized by a single bond between aromatic groups, and could then take many conformations. The presence of distinct polymorphs is presently being searched for in other dyes of the same family whose optical properties significantly depend on the nature of their preparation.[18] The RP method could then be an effective tool to direct the formation of only one species. It must be emphasized that polymorphism-dependent emission of AIE-active compounds has only recently been reported.[47–49] Examples are still rare, and the case of the GFP chromophore has not yet been considered. Finally, due to their unusual optical properties, such AIE-active compounds could also be exceptional tools for the study of crystal growth, and work is in progress in this direction.

3.5 References

[1] Fery-Forgues, S.; Veesler, S.; Fellows, W. B.; Tolbert, L. M.; Solntsev, K. M. *Langmuir* **2013**, *29*, 14718-14727.

[2] Yu, Y.; Feng, C.; Hong, Y.; Liu, J.; Chen, S.; Ng, K. M.; Luo, K. Q.; Tang, B. Z. *Adv. Mater.* **2011**, *23*, 3298-3302.

[3] Yang, Y.; An, F.; Liu, Z.; Zhang, X.; Zhou, M.; Li. W.; Hao, X. *Biomaterials* **2012**, *33*, 7803-7809.

[4] Parthasarathy, V.; Fery-Forgues, S.; Campioli, E.; Recher, G.; Terenziani, F.; Blanchard-Desce, M. *Small* **2011**, *7*, 3219-3229.

[5] Fery-Forgues, S. *Nanoscale* **2013**, *5*, 8428-8442.

[6] Che, Y.; Zang, L. *Chem. Comm.* **2009**, *34*, 5106-5108.

[7] Tao, S.; Li, G.; Yin, J. *J. Mater. Chem.* **2007**, *17*, 2730-2736.

[8] Monnier, V.; Dubuisson, E.; Sanz-Menez, N.; Boury, B.; Rouessac, V.; Ayral, A.; Pansu, R. B.; Ibanez, A. *Microporous Mesoporous Mater.* **2010**, *132*, 531-537.

[9] Fery-Forgues, S.; Fournier-Noel, C. Organic fluorescent nanofibers and submicrometer rods. In *Nanofibers*; Kumar A. Ed.; In-Techweb: Rijeka, Croatia, 2010, pp 383-404. ISBN 978-953-7619-86-2; DOI: 10.5772/45660; http://www.sciyo.com/books/show/title/nanofibers.

[10] Patra, A.; Chandaluri, Ch. G.; Radhakrishnan, T. P. *Nanoscale* **2012**, *4*, 343-359.

[11] Zhao, Y. S.; Fu, H.; Peng, A.; Ma, Y.; Liao, Q.; Yao, J. *Acc. Chem. Res.* **2010**, *43*, 409−418.

[12] Jagannathan, R.; Irvin, G.; Blanton, T.; Jagannathan, S. *Adv. Funct. Mater.* **2006**, *16*, 747−753.

[13] Schiek, M.; Balzer, F.; Al-Shamery, K.; Brewer, J. R.; Lützen, A.; Rubahn, H.-G. *Small* **2008**, *4*, 176−181.

[14] Hong, Y.; Lam, J. W. Y.; Tang, B. Z. *Chem. Soc. Rev.* **2011**, *40*, 5361−5388.

[15] Zhang, S.; Qin, A.; Sun, J.; Tang, B. Z. *Prog. Chem.* **2011**, *23*, 623−636.

[16] Krasovitkii, B. M.; Bolotin, B. M. Organic Luminescent Materials; VCH: Weinheim, Germany, 2002.

[17] Birks, J. B. Photophysics of Aromatic Molecules; Wiley: London, 1970.

[18] Dong, J.; Solntsev, K. M.; Tolbert, L. M. *J. Am. Chem. Soc.* **2009**, *131*, 662−670.

[19] Zimmer, M. *Chem. Rev.* **2002**, *102*, 759−781.

[20] Tsien, R. Y. *Annu. Rev. Biochem.* **1998**, *67*, 509−544.

[21] Green Fluorescent Protein: Properties, Applications, and Protocols, 2nd ed.; Chalfie, M.; Kain, S. R., Eds.; Wiley-Interscience; Hoboken, NJ, 2005.

[22] Oikawa, H.; Nakanishi, H. In Single Organic Nanoparticles; Masuhara, H., Nakanishi, H., Sasaki, K.,Eds.; Springer-Verlag: Berlin, 2003.

[23] Kasai, H.; Nalwa, H. S.; Oikawa, H.; Okada, S.; Matsuda, H.; Minami, N.; Kakuda, A.; Ono, K.; Mukoh, A.; Nakanishi, H. *Jpn. J. Appl. Phys.* **1992**, *31*, L1132−L1134.

[24] Abyan, M.; Bertorelle, F.; Fery-Forgues, S. *Langmuir* **2005**, *21*, 6030−6037.

[25] Dong, J.; Solntsev, K. M.; Tolbert, L. M. *J. Am. Chem. Soc.* **2006**, *128*, 12038−12039.

[26] Baldridge, A.; Kowalik, J.; Tolbert, L. M. *Synthesis* **2010**, *14*, 2424−2436.

[27] Reynolds, G. A; Drexhage, K. H. *Opt. Commun.* **1975**, *13*, 222−225.

[28] de Mello, J. C.; Wittmann, H. F.; Friend, R. H. *Adv. Mater.* **1997**, *9*, 230−232.

[29] Bîrlă, L.; Bertorelle, F.; Rodrigues, F.; Badré, S.; Pansu, R.; Fery-Forgues, S. *Langmuir* **2006**, *22*, 6256−6265.

[30] Ghodbane, A.; D'Altério, S.; Saffon, N.; McClenaghan, N. D.; Scarpantonio, L.; Jolinat, P.; Fery-Forgues, S. *Langmuir* **2012**, *28*, 855−863.

[31] Takazawa, K.; Kitahama, Y.; Kimura, Y.; Kido, G. *Nano Lett.* **2005**, *5*, 1293−1296.

[32] Naumov, P.; Kowalik, J.; Solntsev, K. M.; Baldridge, A.; Moon, J.-S.; Kranz, C.; Tolbert, L. M. *J. Am. Chem. Soc.* **2010**, *132*, 5845−5857.

[33] Ahuja, P.; Sarkar, R.; Jannin, S.; Vasos, P. R.; Bodenhausen, G. *Chem. Comm.* **2010**, *46*, 8192−8194.

[34] Bruno, J.; Cole, J. C.; Edgington, P. R.; Kessler, M.; Macrae, C. F.; McCabe, P.; Pearson, J.; Taylor, R. *Acta Crystallogr.* **2002**, *B58*, 389−397.

[35] Oelkrug, D. Fluorescence spectroscopy in turbid media and tissues. In Topics in fluorescence spectroscopy: probe design and chemical sensing; Lakowicz, J. R., Ed.; Plenum Press: New York, 1994; pp 223−253.

[36] Wall, F. T.; deButts, E. H. *J. Chem. Phys.* **1949**, *17*, 1330−1334.

[37] Leaist. *J. Solution Chem.* **1989**, *18*, 421−435.

[38] Zhao, Y. S.; Xu, J.; Peng, A.; Fu, H.; Ma, Y.; Jiang, L.; Yao, J. *Angew. Chem., Int. Ed.* **2008**, *47*, 7301−7305.

[39] Yu, H.; Qi, L. *Langmuir* **2009**, *25*, 6781−6786.

[40] An, B.-K.; Gihm, S. H.; Chung, J. W.; Park, C. R.; Kwon, S.-K.; Park, S. Y. *J. Am. Chem. Soc.* **2009**, *131*, 3950−3957.

[41] Li, S.; He, L.; Xiong, F.; Li, Y.; Yang, G. *J. Phys. Chem. B* **2004**, *108*, 10887−10892.

[42] Fu, H.; Xiao, D.; Yao, J.; Yang, G. *Angew. Chem., Int. Ed.* **2003**, *42*, 2883−2886.

[43] Zhang, X. J.; Zhang, X. H.; Shi, W. S.; Meng, X. M.; Lee, C.; Lee, S. T. *J. Phys. Chem. B* **2005**, *109*, 18777−18780.

[44] Onodera, T.; Oshikiri, T.; Katagi, H.; Kasai, H.; Okada, S.; Oikawa, H.; Terauchi, M.; Tanaka, M.; Nakanishi, H. *J. Cryst. Growth* **2001**, *229*, 586−590.

[45] Lee, J.-S.; Baldridge, A.; Feng, S.; SiQiang, Y.; Kim, Y. K.; Tolbert, L. M.; Chang, Y.-T. *ACS Comb. Sci.* **2011**, *13*, 32−38.

[46] Baranov, M. S.; Solntsev, K. M.; Lukyanov, K. A.; Yampolsky, I. V. *Chem. Comm.* **2013**, *49*, 5778−5780.

[47] Yoon, S.-J.; Park, S.-Y. *J. Mater. Chem.* **2011**, *21*, 8338.

[48] Wei, R.; Song, P.; Tong, A. *J. Phys. Chem. C* **2013**, *117*, 3467−3474.

[49] Gu, X.; Yao, J.; Zhang, G.; Yan, Y.; Zhang, C.; Peng, Q.; Liao, Q.; Wu, Y.; Xu, Z.; Zhao, Y.; Fu, H.; Zhang, D. *Adv. Funct. Mater.* **2012**, *22*, 4862−4872.

CHAPTER 4

SOLID STATE EMISSION PROPERTIES OF BENZOXAZOLE-BASED GREEN FLUORESCENT PROTEIN CHROMOPHORE DERIVATIVES

The research highlighted within this chapter represents a collaboration between the Tolbert lab at Georgia Tech, in Atlanta, and the lab of Dr. Suzanne Fery-Forgues at The University of Toulouse, ITAV, in Toulouse, France. Throughout this collaboration, the synthesis and design of chromophores was performed within the Tolbert lab and the reprecipitation experiments were performed in the Fery-Forgues lab. Data analysis, fluorescence and kinetic measurements, and manuscript preparation were equally split between the two collaborating labs.

4.1 Introduction

As discussed in the previous chapter, AIE-active compounds have seen considerable attention lately, due to their numerous potential applications in biological sciences,[1-4] for chemical and biochemical sensors,[4-8] and for optical and optoelectronic engineering.[8-12] GFP chromophore derivatives have gained repute as AIE-active fluorophores, as reported by the Tolbert lab[13] and in Chapter 3;[14] we have also developed a new class of AIE-active GFP chromophores based on the incorporation of a benzoxazole (BzOxz) group on the phenyl ring (**Figure 4.1**). However, unlike the previous chapter, this chapter is not focused on RP methods and observations. Indeed, the

discussion in this chapter is centered on a unique phenomenon observed when taking solid state fluorescence measurements on these compounds as a pristine powder.

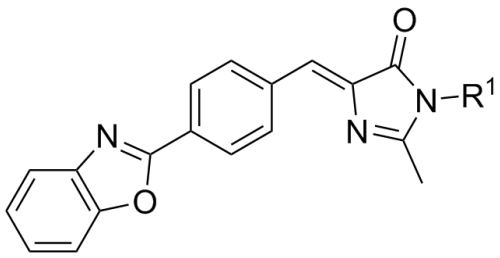

Figure 4.1: General structure of BzOxz-containing chromophores

These chromophores all share the general structure presented in **Figure 4.1**, with the R^1 group being alkyl chains of a different length for each derivative (R^1 = methyl, dodecyl, pentyl, and butyl for compounds 84, 85, 86, and 87, respectively, as labeled in **Table 2.2**).

Unlike the dyes described in the original AIE-active GFP chromophore report,[13] these derivatives do not only "turn on" fluorescence in the solid state, yielding a red-shifted emission from longer-wavelength excitation. Instead, they exhibit drastic changes in excitation and emission properties, when compared to those of the same materials in solution. We believe this spectroscopic phenomenon to be caused by formation of an excimer. To our knowledge, such radical changes in spectral properties have not been reported for GFP-like chromophores.

4.2 Experimental

General

Synthesis. Chromophores for this work (**BDI 84-87**, **Table 2.2**) were synthesized using the [2+3] cycloaddition reaction first reported in 2010 by the Tolbert lab[16] and discussed extensively throughout Chapter 2. ^{1}H NMR spectral data for each synthesized derivative indicates a high level of purity (Appendix A).

Spectroscopy. Fluorescence lifetimes were measured using an Edinburgh Instruments time-correlated single photon counting (TCSPC) system. In this measurement, two picosecond excitation pulse diode lasers (LDH-P-C-375 and LDH-P-C-470) with different wavelengths (372 nm and 467 nm) were used as excitation light sources. The detection system consisted of a high speed MicroChannel Plate PhotoMultiplier Tube (MCP-PMT, Hamamatsu R3809U-50) and TCSPC electronics. Ultraviolet-visible spectra were recorded on a Perkin Elmer Lambda19 spectrophotometer. Measurements of solid-state photoluminescence were carried out using the front face emission scan mode on a Jobin-Yvon FluoroLog-3 spectrofluorimeter. The entrance/exit slits of the monochromators were adjusted to the proper fluorescence intensity of each sample. Crystalline powder samples were placed between quartz plates. Solution spectra were carried out on the same Jobin-Yvon FluoroLog-3 spectrofluorimeter.

4.3 Results

Chromophores 84-87 are all weakly fluorescent in solution, with an absorbance maximum of approximately 370 nm and an emission maximum of about 450 nm. This behavior is typical of GFP chromophore derivatives.[16, 17] This implies that the

benzoxazole (BzOxz) group has very little effect, if any, on the spectroscopic properties of the molecules, in solution. In the solid state, however, this is clearly not the case (**Figure 4.2**).

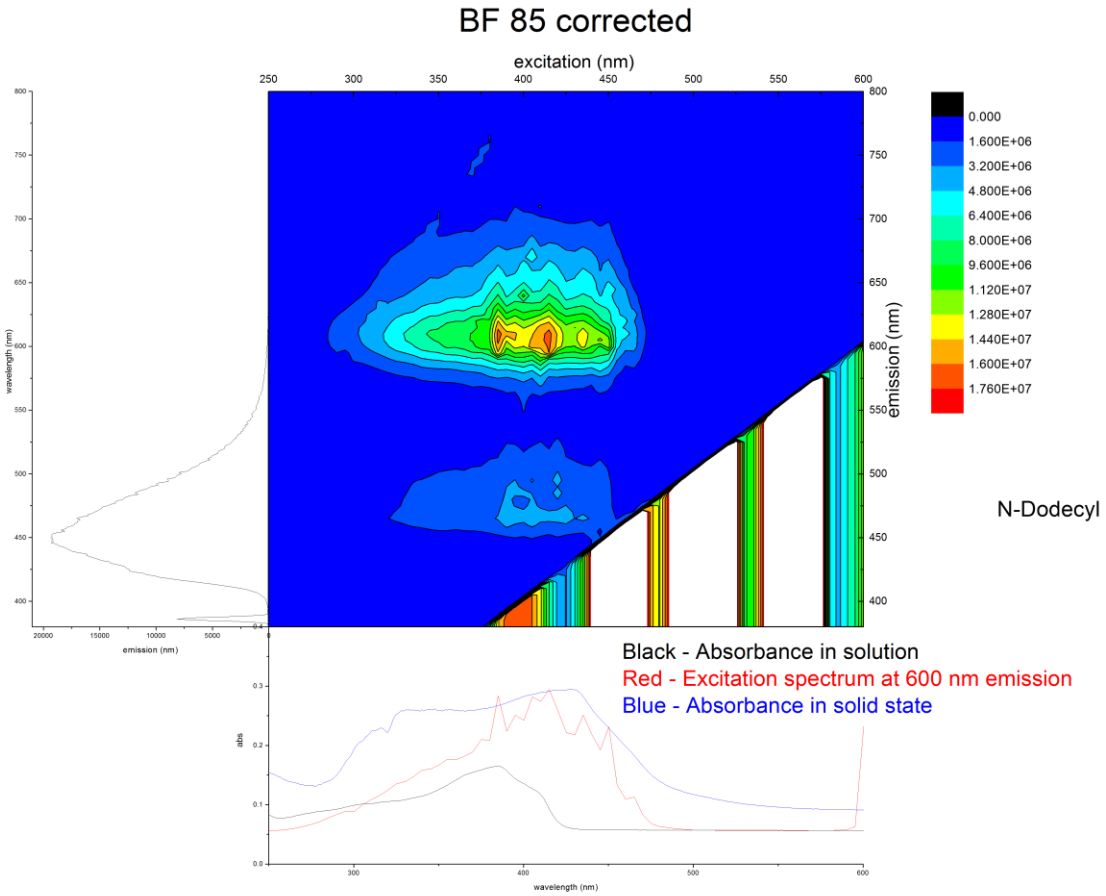

Figure 4.2: Steady-state fluorescence (left) and absorbance (bottom, black) spectra for compound 85 in solution. Also shown are the absorbance in the solid state (bottom, blue), the 3D solid state spectrum (center), and the excitation spectrum at 600 nm emission extracted from the 3D plot (bottom, red).

As can be seen in **Figure 4.2**, the *N*-dodecyl derivative shows a clear shift in emission from ~450 nm to ~600 nm, when comparing the solid state spectrum to the solution spectrum. Additionally, the excitation range has expanded in the solid state to

include both longer and shorter wavelengths. This is of major importance, because to our knowledge this expansion in the excitation region has not been observed before, in GFP chromophore analogs. Also of note is the presence, in the solid state spectrum, of the original emission and excitation curves observed in solution. These values appear to be conserved in the solid state, although at a much lower intensity than the new, red-shifted values. The other long-chain derivatives, where R^1 = butyl and pentyl, also display these red-shifted emission and excitation values (see Appendix B). These red-shifted emission and excitation values must be caused by an excimer formed in the solid state, due to the aggregation of the molecules.

Interestingly, compound 84 (R^1 = methyl) displays these same trends, but the intensity of the excitation and emission curves in solution which appear in the solid state are approximately the same as the new red-shifted values (**Figure 4.3**). The excimer observed in the long-chain derivatives appears to be present in the methyl derivative, but the intensity is far lower than that of the long-chain derivatives. This is not surprising, as the solid powder is very weakly fluorescent, compared to that of the long chain derivatives, under a hand-held UV lamp.

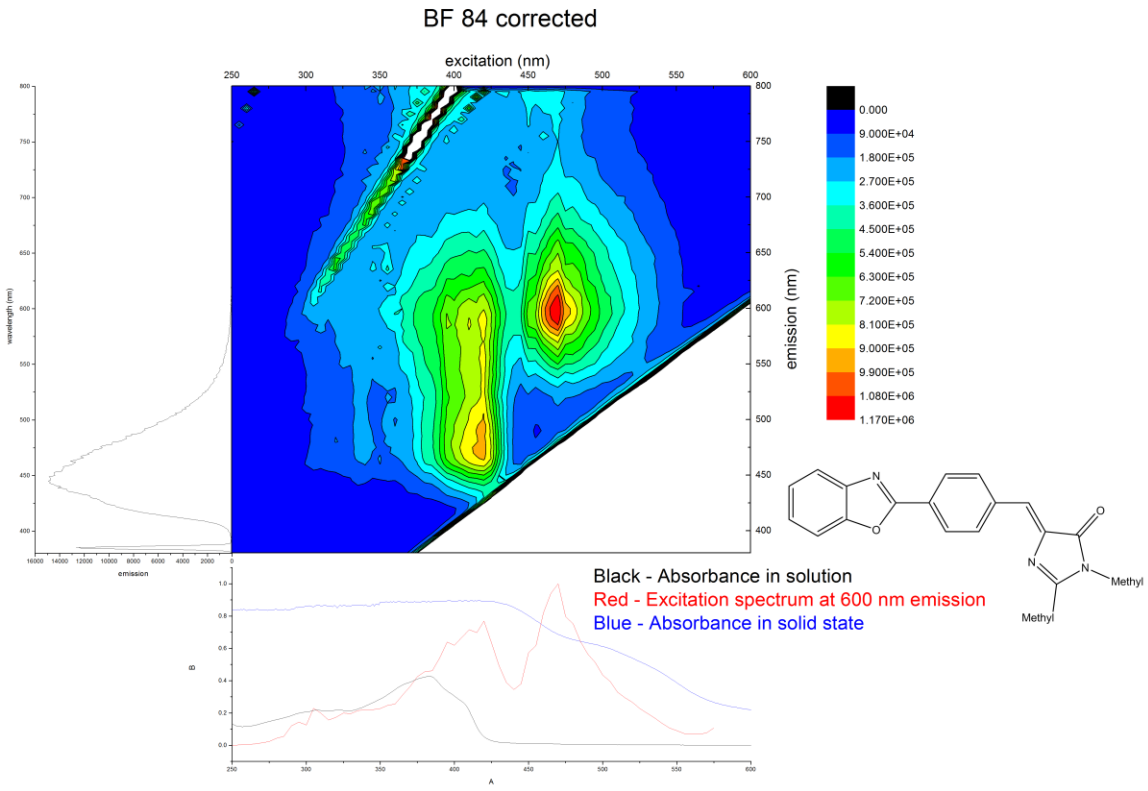

Figure 4.3: Steady-state fluorescence (left) and absorbance (bottom, black) spectra for compound 84 in solution. Also shown are the absorbance in the solid state (bottom, blue), the 3D solid state spectrum (center), and the excitation spectrum at 600 nm emission extracted from the 3D plot (bottom, red).

This change in the spectroscopic properties is very unique, compared to those previously reported, which exhibit only a tight red-shift in both emission and excitation.[13] Also of note is that this phenomenon cannot be caused simply by the presence of long alkyl chains on the imidazolidinone ring, because as reported by Shen, *et al.*,[18] introduction of long alkyl chains at the C-terminus does not result in drastic changes in absorbance or emission. Therefore, these dramatic changes in spectral properties must be caused by a combination of both the presence of the BzOxz moiety on the phenyl ring, perhaps in correlation to the alkoxy derivatives reported by the Tolbert group in 2009,[13]

and the long alkyl chain, which has been demonstrated to raise intensity of emission.[18] It is also particularly noteworthy that all four of the compounds discussed herein exhibit this excimeric behavior, regardless of the size of the alkyl chain (**Figures 4.1, 4.2, B.1, and B.2**).

Kinetic measurements in the solid state indicated that the lifetimes of the red-shifted species were far longer than those of the shorter-wavelength emitting species (**Figure 4.3**), as exemplified by the *N*-dodecyl chromophore.

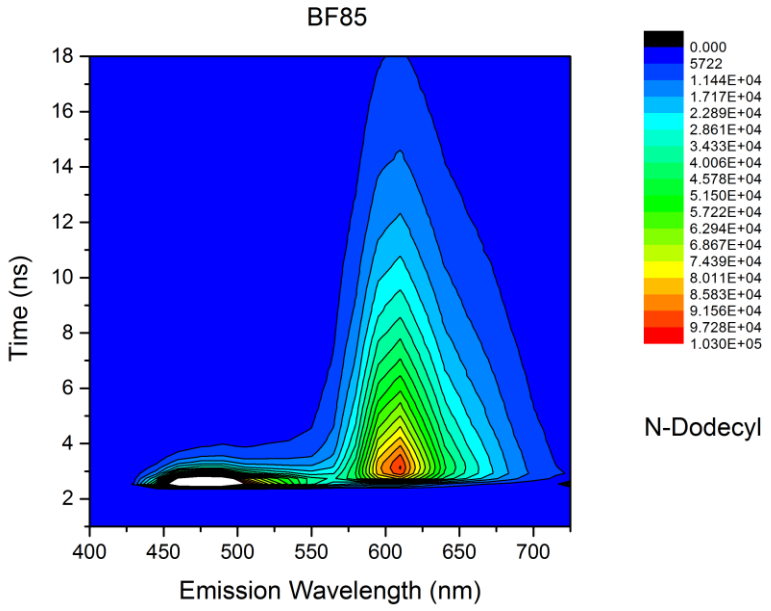

Figure 4.4: Kinetic spectrum of compound 85, taken with 372 nm laser excitation.

The trend of longer lifetime for the red-shifted emission is conserved throughout the series of compounds, however, with shorter alkyl chains, the lifetimes also become shorter, as can be seen by contrasting the kinetic spectra of the *N*-dodecyl chromophore (**Figure 4.3**) with that of the *N*-methyl chromophore (**Figure 4.4**). For the kinetic spectra of all compounds, see Appendix B.

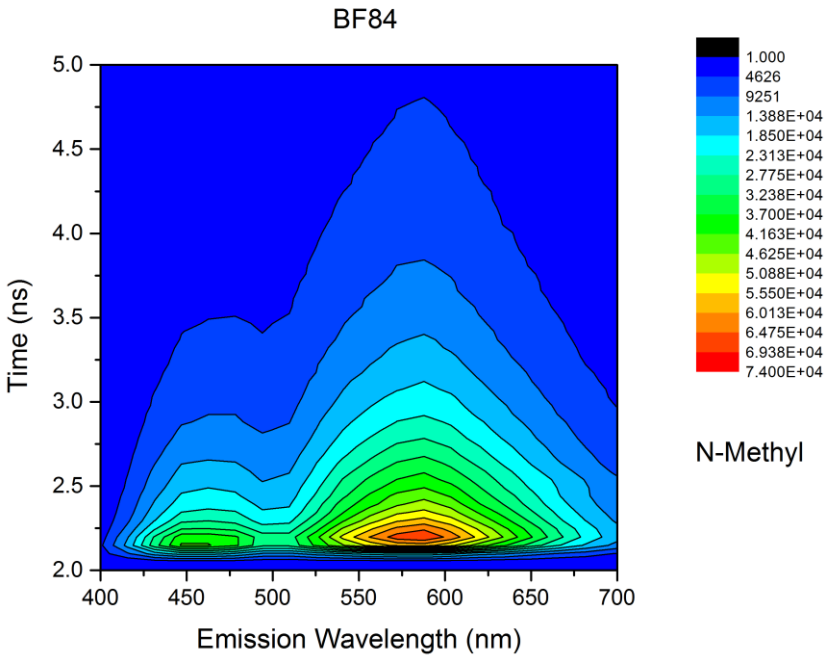

Figure 4.5: Kinetic spectrum of compound 84, taken with 372 nm laser excitation.

These results are also consistent with Shen's observations that with a longer alkyl chain on the imidazolidinone ring, a longer lifetime is observed.[18] However, it must be stressed that Shen did not observe the red-shifted emission and excitation broadening, as we do. This difference in lifetimes is most well depicted the linear curves from the emission maxima (**Figure 4.6**). Furthermore, it can be seen that the red-shifted, excimer emission maxima are much longer lived than the bluer monomer emission.

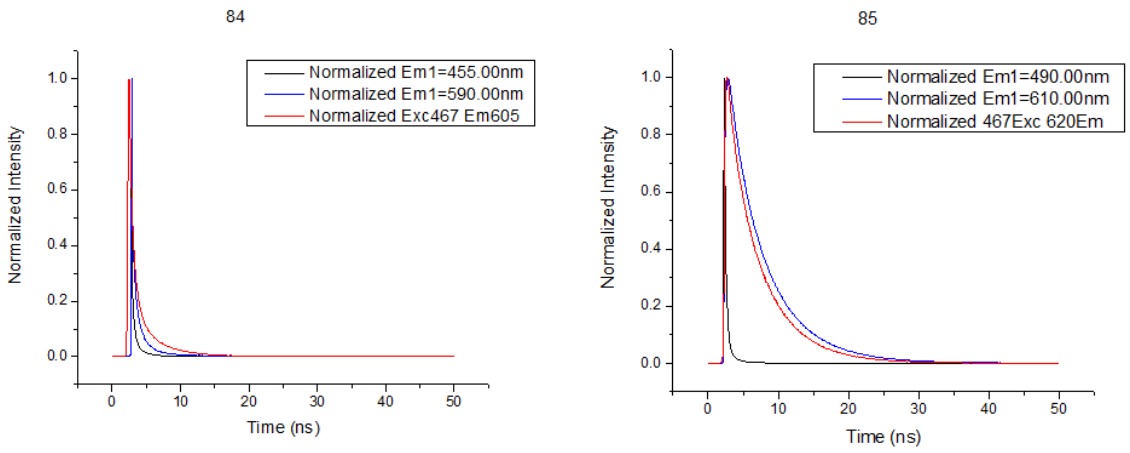

Figure 4.6: Normalized linear curves extracted from the emission maxima of **Figures 4.4 and 4.5**.

The most surprising observation regarding these compounds, however, is what we saw in the crystal structures. Each compound exhibits a unique crystal structure, with different packing for each individual derivative. The *N*-butyl chromophore (BDI 87) shows a head-to-head stacking motif (**Figure 4.7**) with very little overlap of the aromatic moieties, due to horizontal slippage (**Figure 4.8**).

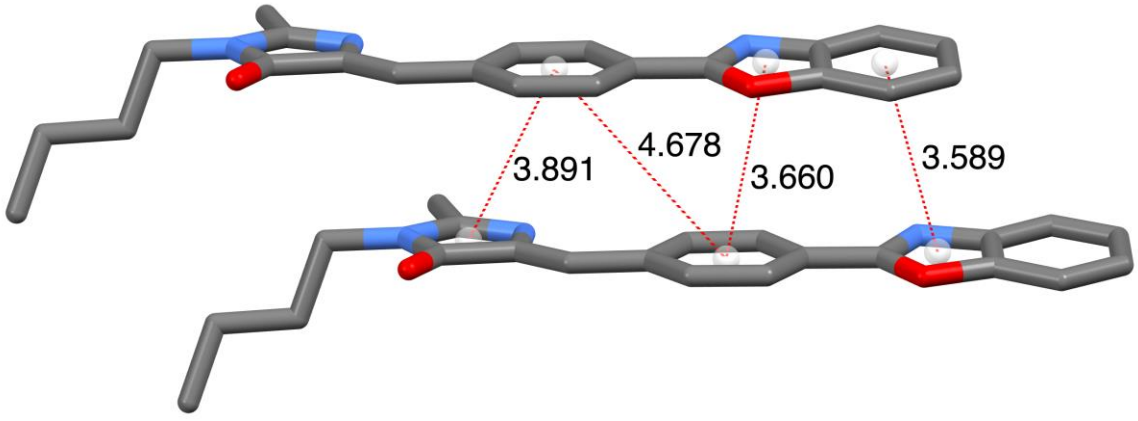

Figure 4.7: Side view of the crystal structure of BDI 87. Distances shown in angstroms.

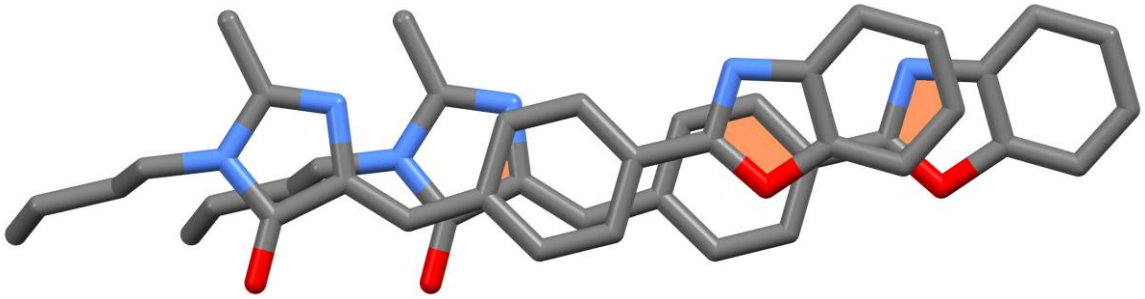

Figure 4.8: Top-down view of the crystal structure of BDI 87. Overlap of aromatic moieties highlighted in orange.

The *N*-pentyl derivative (BDI 86), on the other hand, shows a head-to-tail stacking motif (**Figure 4.9**), with no overlap of aromatic moieties (**Figure 4.10**). Upon closer look, however, it can be seen that there is some overlap of the aromatic moieties of the top and bottom molecules.

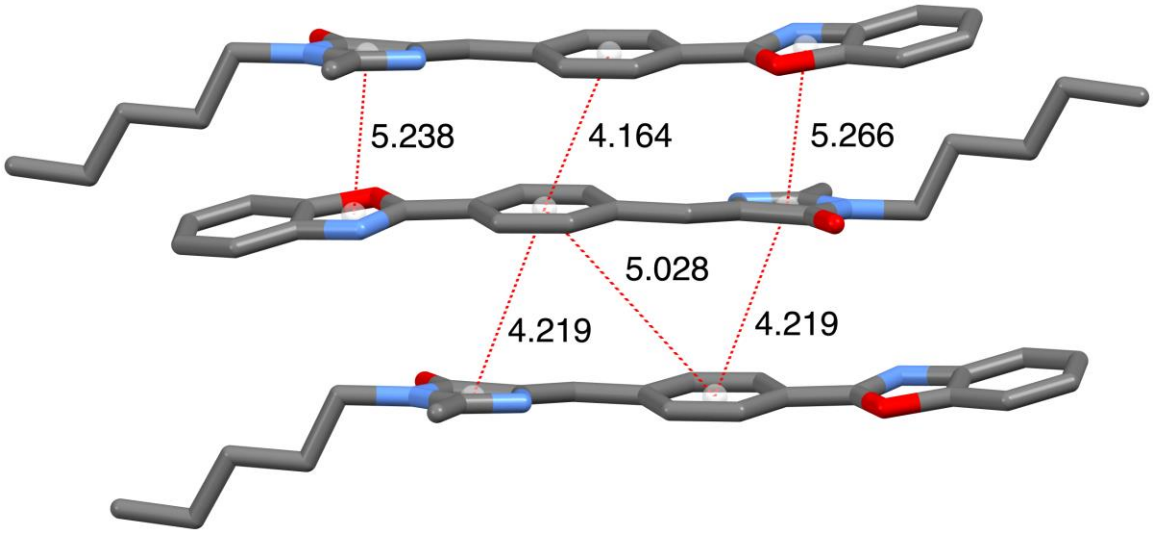

Figure 4.9: Side view of the crystal structure of BDI 86. Distances shown in angstroms.

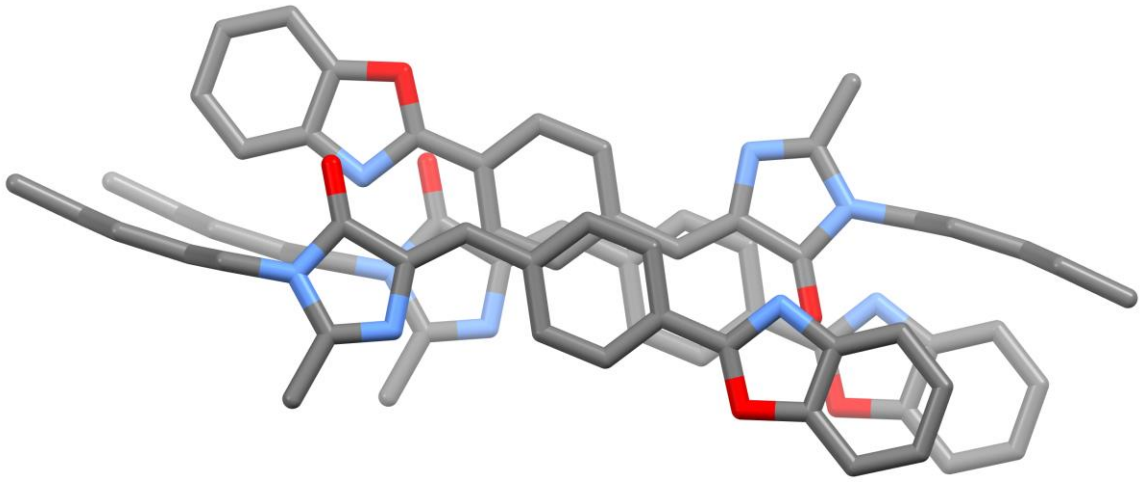

Figure 4.10: Top-down view of the crystal structure of BDI 86. Depth is indicated by color saturation.

The *N*-dodecyl chromophore (BDI 85) also a shows head-to-tail stacking motif (**Figure 4.11**) and no overlap of aromatic moieties between adjacent molecules (**Figure 4.12**). However, there is again significant overlap between the top and bottom molecules.

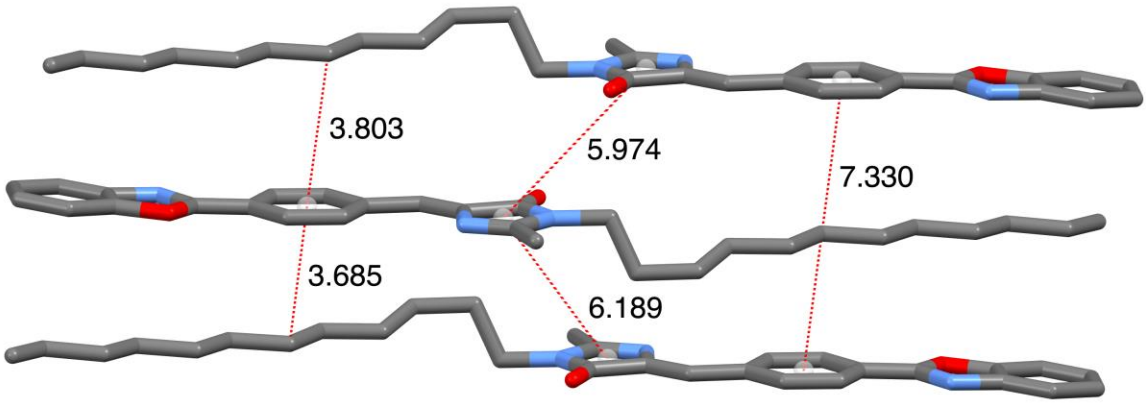

Figure 4.11: Side view of the crystal structure of BDI 85. Distances shown in angstroms.

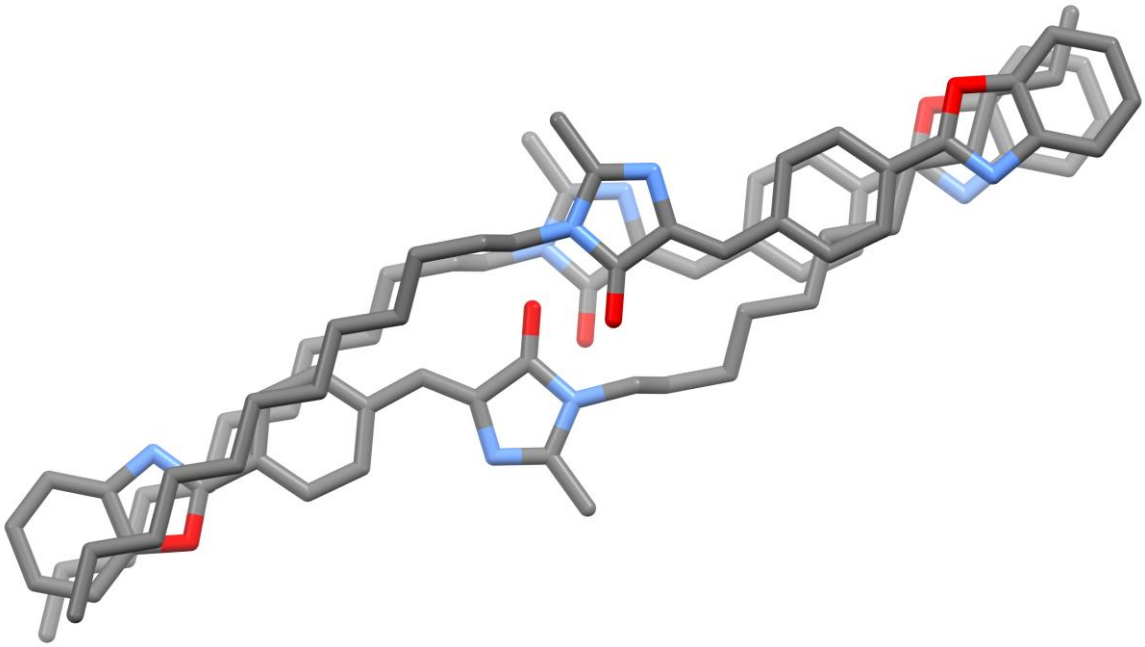

Figure 4.12: Top-down view of the crystal structure of BDI 85. Depth is indicated by color saturation.

This lack of interaction between adjacent molecules, yet good overlap between every other molecule, is what has led us to term this type of stacking as "hot dog stacking." The unique aspect of the hot dog stacking is that this means the excimer involves interaction through the intervening alkyl chains, which to our knowledge has never previously been observed.

4.4 Conclusions

In conclusion, a new class of GFP chromophore derivatives based on incorporation of a BzOxz group is presented which exhibits spectral properties characteristic of excimer formation, in addition to AIE behavior in the solid state. These derivatives merge the qualities of the C-terminus long-chain chromophores reported by Shen,[18] as they show increased fluorescence intensity in the solid state and longer lifetimes, and those of the phenyl alkoxy chromophores reported by the Tolbert group, as

they show significant red-shifting of emission and absorption in the solid state.[13] However, these derivatives are unique in that they not only red-shift the excitation, but it is also broadened, which is a phenomenon not previously seen with these types of chromophores. Additionally, we observe a new stacking motif, hot dog stacking, which results in a potential new class of excimers.

4.5 References

[1] Yu, Y.; Feng, C.; Hong, Y.; Liu, J.; Chen, S.; Ng, K. M.; Luo, K. Q.; Tang, B. Z. *Adv. Mater.* **2011**, *23*, 3298-3302.

[2] Yang, Y.; An, F.; Liu, Z.; Zhang, X.; Zhou, M.; Li. W.; Hao, X. *Biomaterials* **2012**, *33*, 7803-7809.

[3] Parthasarathy, V.; Fery-Forgues, S.; Campioli, E.; Recher, G.; Terenziani, F.; Blanchard-Desce, M. *Small* **2011**, *7*, 3219-3229.

[4] Fery-Forgues, S. *Nanoscale* **2013**, *5*, 8428-8442.

[5] Che, Y.; Zang, L. *Chem. Comm.* **2009**, *34*, 5106-5108.

[6] Tao, S.; Li, G.; Yin, J. *J. Mater. Chem.* **2007**, *17*, 2730-2736.

[7] Monnier, V.; Dubuisson, E.; Sanz-Menez, N.; Boury, B.; Rouessac, V.; Ayral, A.; Pansu, R. B.; Ibanez, A. *Microporous Mesoporous Mater.* **2010**, *132*, 531-537.

[8] Fery-Forgues, S.; Fournier-Noel, C. Organic fluorescent nanofibers and submicrometer rods. In *Nanofibers*; Kumar A. Ed.; In-Techweb: Rijeka, Croatia, 2010, pp 383-404. ISBN 978-953-7619-86-2; DOI: 10.5772/45660; http://www.sciyo.com/books/show/title/nanofibers.

[9] Patra, A.; Chandaluri, Ch. G.; Radhakrishnan, T. P. *Nanoscale* **2012**, *4*, 343-359.

[10] Zhao, Y. S.; Fu, H.; Peng, A.; Ma, Y.; Liao, Q.; Yao, J. *Acc. Chem. Res.* **2010**, *43*, 409−418.

[11] Jagannathan, R.; Irvin, G.; Blanton, T.; Jagannathan, S. *Adv. Funct. Mater.* **2006**, *16*, 747−753.

[12] Schiek, M.; Balzer, F.; Al-Shamery, K.; Brewer, J. R.; Lützen, A.; Rubahn, H.-G. *Small* **2008**, *4*, 176−181.

[13] Dong, J.; Solntsev, K. M.; Tolbert, L. M. *J. Am. Chem. Soc.* **2009**, *131*, 662−670.

[14] Fery-Fogues, S.; Veesler, S.; Fellows, W. B.; Tolbert, L. M.; Solntsev, K. M. *Langmuir* **2013**, *29*, 14718-14727.

[15] Baldridge, A.; Kowalik, J.; Tolbert, L. M. *Synthesis* **2010**, *14*, 2424-2436.

[16] Solntsev, K. M.; Poizat, O.; Dong, J.; Rehault, J.; Lou, Y.; Burda, C.; Tolbert, L. M. *J. Phys. Chem. B* **2008**, *112*, 2700-2711.

[17] Kummer, A. D.; Kompa, C.; Niwa, H.; Hirano, T.; Kojima, S.; Michel-Beyerle, M. E. *J. Phys. Chem. B* **2002**, *106*, 7554-7559.

[18] Shen, X.; Huang, G.; Li, K.; Zhang, G.; Zhang, D. *Sci. China Chem.* **2013**, *9*, 1197-1203.

CHAPTER 5

SUMMARY AND FUTURE WORK

5.1 Summary

In Chapter 2, a new synthetic methodology for the combinatorial preparation of C-terminus-modified Green and Red Fluorescent Protein chromophores is described.[1] This method involves the modification of the previously reported [2+3] cycloaddition reaction scheme[2] to incorporate new R^2 groups in the imidate used in the final step. This is achieved through two primary routes: (a) the imidation of nitriles using hydrochloric acid gas and (b) the *O*-alkylation of amides using a variant of Meerwein's Salt to provide conjugated imidates.

Chapter 3 demonstrates the preparation of fluorescent microcrystals and nanofibers from Green Fluorescent Protein chromophore derivatives via the reprecipitation method. The properties of these microcrystals and nanofibers, especially in relation to the powder obtained from organic solvents, are also explored. Additionally, it is demonstrated that the size and shape of the microcrystals and nanofibers can be modulated with varying experimental conditions for RP.[3]

A new class of AIE-active GFP chromophores are reported in chapter 4. These chromophores contain a benzoxazole group on the phenyl ring and varying lengths of alkyl chains on the imidazolidinone nitrogen. These benzoxazole-based chromophores exhibit unique properties in the solid state not previously observed for GFP chromophore derivatives, namely, a broadening of the excitation spectrum and red-shifting of the

emission, likely caused by excimer formation. The crystal structure also reveals a unique "hot-dog" stacking motif. A publication on this subject is currently in preparation.[4]

5.2 Future Work

A GFP-based polymer which was not discussed in the previous chapters was also synthesized (**Figure 5.1**). The aim of this work was to produce a material that under stress, particularly stretching, would exhibit some kind of fluorescence response.

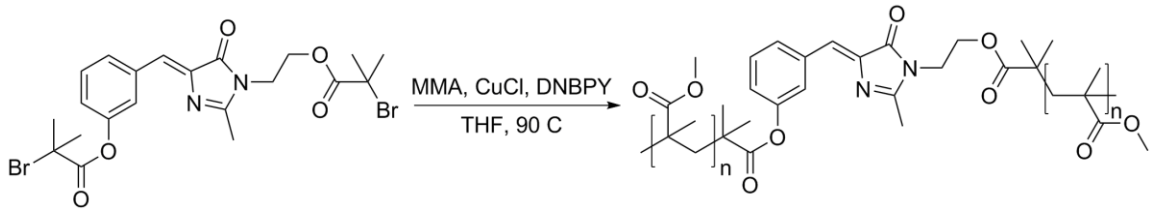

Figure 5.1: Poly(methyl methacrylate) synthesis using a GFP-based initiator.

Unfortunately, upon isolation of the material and spin-coating onto silicone, it was discovered that this material was too brittle and would crack and break after even 1 mm of stretching. Future work can be done to remedy this problem, perhaps by using Bisphenol-A glycidyl methacrylate instead of methyl methacrylate as the monomer, as it is known to be a good elastomer.

A series of quaternary ammonium GFP chromophores were synthesized, based on the interactions observed with certain chromophores and DNA in our group's collaboration with Young-Tae Chang (**Figure 5.2**).[5]

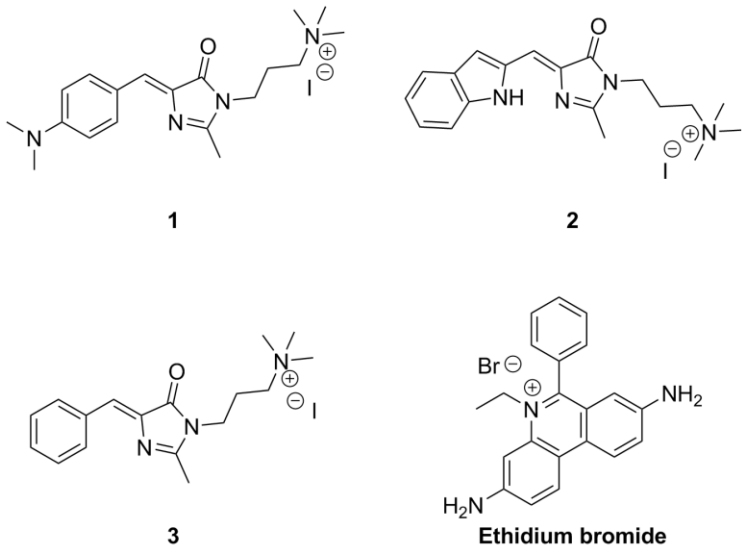

Figure 5.2: Quaternary ammonium GFP chromophores synthesized for DNA binding, alongside ethidium bromide, a common DNA-binding standard.

These chromophores were intended to be DNA binders with potential as fluorescent probes. Through collaboration with the Hud lab, they were tested, but unfortunately, they were not observed to bind to DNA. Future work could be done by testing a wider variety of chromophores currently within our library and derivatizing from those results. This work could provide a new class of fluorescent DNA probing materials.

Additionally, the C-terminus-modified chromophores discussed throughout Chapter 2 are being used in a collaboration with the Williams lab. These chromophores are being tested for binding with various nuclear receptors, such as the Estrogen Receptor alpha and beta and the Retinoic Acid Receptor. The major significance of this work lies in the demonstration that not only does the size and shape of the molecule matter, but the specific derivatization of each R group matters tremendously. These results, while promising, are not yet ready for publication but will be prepared as such soon.

5.3 References

[1] Fellows, W. B.; Kowalik, J.; Tolbert, L. M. "A New Combinatorial Method for C-alkylated GFP and RFP Chromophore Synthesis." *Submitted*.

[2] Baldridge, A.; Kowalik, J.; Tolbert, L. M. *Synthesis* **2010**, *14*, 2424-2436.

[3] Fery-Fogues, S.; Veesler, S.; Fellows, W. B.; Tolbert, L. M.; Solntsev, K. M. *Langmuir* **2013**, *29*, 14718-14727.

[4] Fellows, W. B.; Ghodbane, A.; Ghosh, D.; Fery-Forgues, S.; Tolbert, L. M.; Solntsev, K. M. Solid State Photophysical Properties of a New Class of Benzoxazole-based GFP Chromophores. *In Preparation.*

[5] Lee, J.-S.; Baldridge, A.; Feng, S.; SiQiang, Y.; Kim, Y. K.; Tolbert, L. M.; Chang, Y.-T. *ACS Comb. Sci.* **2011**, *13*, 32-38.

APPENDIX A

CHARACTERIZATION OF SYNTHETIC BDI COMPOUNDS

Table A.1 ^{1}H NMR Spectral Data for Chromophores

Compound #	Proton NMR (ppm), $CDCl_3$, unless otherwise noted
1	DMSO-d_6: 12.36 (s, 1H), 8.04 (d, J = 9 Hz, 1H), 7.28 (t, J = 9 Hz, 1H), 7.21 (s, 1H), 6.87 (d, J = 6 Hz, 1H), 6.85 (t, J = 6 Hz, 1H), 3.10 (s, 3H), 2.67 (t, J = 6 Hz, 2H), 1.75 (sextet, J = 6 Hz, 2H), 1.01 (t, J = 6 Hz, 3H)
2	DMSO-d_6: 9.56 (s, 1H), 7.70 (s, 1H), 7.74 (d, J = 9 Hz, 1H), 7.21 (t, J = 9 Hz, 1H), 6.94 (s, 1H), 6.81 (d, J = 9 Hz, 1H), 3.07 (s, 3H), 2.62 (t, J = 6 Hz, 2H), 1.74 (sextet, J = 6 Hz, 2H), 1.01 (t, J = 6 Hz, 3H)
3	DMSO-d_6: 10.10 (s, br, 1H), 8.08 (d, J = 9 Hz, 2H), 6.87 (s, 1H), 6.82 (d, J = 9 Hz, 2H), 3.06 (s, 3H), 2.59 (t, J = 6 Hz, 2H), 1.74 (sextet, J = 6 Hz, 2H), 1.00 (t, J = 6 Hz, 3H)
4	DMSO-d_6: 8.06 (d, J = 9 Hz, 2H), 6.84 (s, 1H), 6.74 (d, J = 9 Hz, 2H), 3.05 (s, 3H), 2.99 (s, 6H), 2.59 (t, J = 6 Hz, 2H), 1.70 (sextet, J = 6 Hz, 2H), 0.89 (t, J = 6 Hz, 3H)
5	8.69 (d, J = 6 Hz, 1H), 7.38 (s, 1H), 7.26 (m, 3H), 3.18 (s, 3H), 2.58 (t, J = 6 Hz, 2H), 2.49 (s, 3H), 1.87 (sextet, J = 6 Hz, 2H), 1.09 (t, J = 6 Hz, 3H)
6	8.01 (d, J = 6 Hz, 1H), 7.93 (s, 1H), 7.31 (t, J = 9 Hz, 1H), 7.19 (d, J = 6 Hz, 1H), 7.07 (s, 1H), 3.17 (s, 3H), 2.59 (t, J = 6 Hz, 2H), 2.39 (s, 3H), 1.89 (sextet, J = 6 Hz, 2H), 1.11 (t, J = 6 Hz, 3H)
7	8.06 (d, J = 9 Hz, 2H), 7.23 (d, J = 9 Hz, 2H), 7.08 (s, 1H), 3.16 (s, 3H), 2.57 (t, J = 6 Hz, 2H), 2.38 (s, 3H), 1.88 (sextet, J = 6 Hz, 2H), 1.09 (t, J = 6 Hz, 3H)
8	8.63 (d, J = 9 Hz, 1H), 7.37 (s, 1H), 7.10 (d, J = 9 Hz, 1H), 7.02 (s, 1H), 3.17 (s, 3H), 2.57 (t, J = 6 Hz, 2H), 2.45 (s, 3H), 2.33 (s, 3H), 1.87 (sextet, J = 6 Hz, 2H), 1.09 (t, J = 6 Hz, 3H)
9	8.16 (d, J = 9 Hz, 2H), 7.30 (m, 3H), 7.10 (s, 1H), 3.18 (s, 3H), 2.59 (t, J = 6 Hz, 2H), 1.89 (sextet, J = 6 Hz, 2H), 1.11 (t, J = 6 Hz, 3H)
10	8.17 (d, J = 9 Hz, 2H), 1.40 (m, 3H), 7.10 (s, 1H), 3.17 (s, 3H), 2.65 (q, J = 6 Hz, 2H), 1.40 (t, J = 6 Hz, 3H)
11	8.16 (d, J = 9 Hz, 2H), 7.40 (m, 3H), 7.09 (s, 1H), 3.17 (s, 3H), 2.59 (t, J = 6 Hz, 2H), 1.83 (pentet, J = 6 Hz, 2H), 1.40 (m, 8H), 0.90 (t, J = 6 Hz, 3H)
12	DMSO-d_6: 8.62 (s, 1H), 8.18 (d, J = 6 Hz, 1H), 7.74 (d, J = 6 Hz, 1H), 7.23 (t, J = 6 Hz, 1H), 6.90 (s, 1H), 3.73 (t, J = 6 Hz, 2H), 3.45 (t, J = 6 Hz, 2H), 3.23 (s, 3H), 2.37 (s, 3H)
13	DMSO-d_6: 8.64 (s, 1H), 8.18 (d, J = 6 Hz, 1H), 7.74 (d, J = 6 Hz, 1H), 7.23 (t, J = 6 Hz, 1H), 6.90 (s, 1H), 3.09 (s, 3H), 2.36 (s, 3H)

15	DMSO-d_6: 12.41 (s, 1H), 8.03 (d, J = 9 Hz, 1H), 7.27 (t, J = 6 Hz, 1H), 7.19 (s, 1H), 6.86 (d, J = 6 Hz, 1H), 6.84 (t, J = 6 Hz, 1H), 3.09 (s, 3H), 2.72 (q, J = 6 Hz, 2H), 1.22 (t, J = 6 Hz, 3H)
16	DMSO-d_6: 10.08 (s, br, 1H), 8.09 (d, J = 9 Hz, 2H), 6.87 (s, 1H), 6.82 (d, J = 9 Hz, 2H), 3.05 (s, 3H), 2.65 (q, J = 6 Hz, 2H), 1.23 (t, J = 6 Hz, 3H)
17	8.10 (d, J = 9 Hz, 2H), 7.08 (s, 1H), 6.72 (d, J = 9 Hz, 2H), 3.17 (s, 3H), 3.04 (s, 6H), 2.63 (q, J = 6 Hz, 2H), 1.38 (t, J = 6 Hz, 3H)
18	DMSO-d_6: 12.36 (s, 1H), 8.02 (d, J = 6 Hz, 1H), 7.27 (t, J = 6 Hz, 1H), 7.19 (s, 1H), 6.86 (d, J = 6 Hz, 1H), 6.84 (t, J = 6 Hz, 1H), 3.09 (s, 3H), 2.67 (t, J = 6 Hz, 2H), 1.70 (pentet, J = 6 Hz, 2H), 1.36 (m, 4H), 0.88 (t, J = 6 Hz, 3H)
19	DMSO-d_6: 9.56 (s, 1H), 7.69 (s, 1H), 7.54 (d, J = 6 Hz, 1H), 7.20 (t, J = 6 Hz, 1H), 6.84 (s, 1H), 6.80 (d, J = 6 Hz, 1H), 3.07 (s, 3H), 2.63 (t, J = 6 Hz, 2H), 1.72 (pentet, J = 6 Hz, 2H), 1.37 (m, 4H), 0.89 (t, J = 6 Hz, 3H)
20	DMSO-d_6: 10.09 (s, br, 1H), 8.08 (d, J = 9 Hz, 2H), 6.87 (s, 1H), 6.81 (d, J = 6 Hz, 2H), 3.05 (s, 3H), 2.60 (t, J = 6 Hz, 2H), 1.70 (pentet, J = 6 Hz, 2H), 1.37 (m, 4H), 0.88 (t, J = 6 Hz, 3H)
21	8.09 (d, J = 9 Hz, 2H), 7.07 (s, 1H), 6.72 (d, J = 9 Hz, 2H), 3.16 (s, 3H), 3.05 (s, 6H), 2.57 (t, J = 6 Hz, 2H), 1.82 (sextet, J = 6 Hz, 2H), 1.42 (m, 4H), 0.95 (t, J = 6 Hz, 3H)
22	8.06 (d, J = 9 Hz, 2H), 7.23 (d, J = 9 Hz, 2H), 7.07 (s, 1H), 3.16 (s, 3H), 2.58 (t, J = 6 Hz, 2H), 2.38 (s, 1H), 1.83 (pentet, J = 6 Hz, 2H), 1.43 (m, 4H), 0.94 (t, J = 6 Hz, 3H)
23	7.78 (s, 2H), 7.04 (s, 1H), 7.01 (s, 1H), 3.17 (s, 3H), 2.61 (t, J = 6 Hz, 2H), 2.35 (s, 6H), 1.82 (pentet, J = 6 Hz, 2H), 1.51 (sextet, J = 6 Hz, 2H), 1.01 (t, J = 6 Hz, 3H)
24	8.16 (d, J = 9 Hz, 2H), 7.42 (m, 3H), 7.10 (s, 1H), 3.18 (s, 3H), 2.61 (t, J = 6 Hz, 2H), 1.82 (pentet, J = 6 Hz, 2H), 1.50 (sextet, J = 6 Hz, 2H), 1.01 (t, J = 6 Hz, 3H)
25	DMSO-d_6: 10.11 (s, br, 1H), 8.07 (d, J = 6 Hz, 2H), 6.87 (s, 1H), 6.82 (d, J = 9 Hz, 2H), 3.07 (s, 3H), 2.61 (t, J = 6 Hz, 2H), 1.69 (sextet, J = 6 Hz, 2H), 1.43 (pentet, J = 6 Hz, 2H), 0.93 (t, J = 6 Hz, 3H)
26	8.00 (d, J = 9 Hz, 1H), 7.94 (s, 1H), 7.31 (t, J = 9 Hz, 1H), 7.19 (d, J = 6 Hz, 1H), 7.07 (s, 1H), 3.17 (s, 3H), 2.61 (t, J = 6 Hz, 2H), 2.39 (s, 3H), 1.82 (pentet, J = 6 Hz, 2H), 1.53 (sextet, J = 6 Hz, 2H), 1.01 (t, J = 6 Hz, 3H)
27	8.07 (d, J = 9 Hz, 2H), 7.06 (s, 1H), 6.68 (d, J = 9 Hz, 2H), 3.43 (q, J = 6 Hz, 4H), 3.16 (s, 3H), 2.58 (t, J = 6 Hz, 2H), 1.80 (pentet, J = 6 Hz, 2H), 1.48 (sextet, J = 6 Hz, 2H), 1.21 (t, J = 6 Hz, 6H), 1.00 (t, J = 6 Hz, 3H)
28	8.66 (d, J = 6 Hz, 1H), 7.38 (s, 1H), 7.23 (m, 3H), 3.19 (s, 3H), 2.60 (t, J = 6 Hz, 2H), 2.49 (s, 3H), 1.80 (pentet, J = 6 Hz, 2H), 1.51 (sextet, J = 6 Hz, 2H), 1.00 (t, J = 6 Hz, 3H)
29	DMSO-d_6: 12.39 (s, 1H), 8.01 (d, J = 9 Hz, 1H), 7.27 (t, J = 9 Hz, 1H), 7.19 (s, 1H), 6.87 (d, J = 9 Hz, 1H), 6.84 (t, J = 9 Hz, 1H), 3.10 (s, 3H), 2.68 (t, J = 6 Hz, 2H), 1.68 (pentet, J = 6 Hz, 2H), 1.40 (sextet, J = 6 Hz, 2H), 0.93 (t, J = 6 Hz, 3H)

30	DMSO-d_6: 9.56 (s, 1H), 7.70 (s, 1H), 7.54 (d, J = 9 Hz, 1H), 7.21 (t, J = 9 Hz, 1H), 6.84 (s, 1H), 6.81 (d, J = 9 Hz, 1H)
31	8.06 (d, J = 9 Hz, 2H), 7.23 (d, J = 9 Hz, 2H), 7.08 (s, 1H), 3.17 (s, 3H), 2.60 (t, J = 6 Hz, 2H), 2.38 (s, 3H), 1.81 (pentet, J = 6 Hz, 2H), 1.49 (sextet, J = 6 Hz, 2H), 1.00 (t, J = 6 Hz, 3H)
32	8.71 (d, J = 9 Hz, 1H), 7.39 (s, 1H), 7.25 (m, 3H), 3.19 (s, 3H), 2.65 (q, J = 6 Hz, 2H), 2.49 (s, 3H), 1.38 (t, J = 6 Hz, 3H)
33	8.02 (d, J = 9 Hz, 1H), 7.94 (s, 1H), 7.31 (t, J = 9 Hz, 1H), 7.20 (d, J = 9 Hz, 1H), 7.08 (s, 1H), 3.18 (s, 3H), 2.63 (q, J = 6 Hz, 2H), 2.39 (s, 3H), 1.40 (t, J = 6 Hz, 3H)
34	8.08 (d, J = 9 Hz, 2H), 7.07 (s, 1H), 6.69 (d, J = 9 Hz, 2H), 3.40 (q, J = 6 Hz, 4H), 3.17 (s, 1H), 2.60 (q, J = 6 Hz, 2H), 1.38 (t, J = 6 Hz, 3H), 1.22 (t, J = 6 Hz, 6H)
35	7.95 (d, J = 9 Hz, 2H), 7.19 (d, J = 9 Hz, 2H), 7.07 (s, 1H), 3.17 (s, 3H), 2.62 (q, J = 6 Hz, 2H), 2.29 (s, 6H), 1.40 (t, J = 6 Hz, 3H)
36	8.16 (d, J = 9 Hz, 2H), 7.38 (m, 3H), 7.10 (s, 1H), 3.18 (s, 3H), 2.60 (t, J = 6 Hz, 2H), 1.83 (pentet, J = 6 Hz, 2H), 1.30 (m, 10H), 0.89 (t, J = 6 Hz, 3H)
37	8.06 (d, J = 9 Hz, 2H), 7.23 (d, J = 9 Hz, 2H), 7.08 (s, 1H), 3.17 (s, 3H), 2.59 (t, J = 6 Hz, 2H), 2.38 (s, 3H), 1.82 (pentet, J = 6 Hz, 2H), 1.29 (m, 10H), 0.89 (t, J = 6 Hz, 3H)
38	8.68 (d, J = 9 Hz, 1H), 7.38 (s 1H), 7.24 (m, 3H), 3.18 (s, 3H), 2.60 (t, J = 6 Hz, 2H), 2.49 (s, 3H), 1.81 (pentet, J = 9 Hz, 2H), 1.29 (m, 10H), 0.89 (t, J = 9 Hz, 3H)
39	7.99 (d, J = 6 Hz, 1H), 7.94 (s, 1H), 7.30 (t, J = 9 Hz, 1H), 7.19 (d, J = 6 Hz, 1H), 7.07 (s, 1H), 3.17 (s, 3H), 2.60 (t, J = 6 Hz, 2H), 2.39 (s, 3H), 1.83 (pentet, J = 6 Hz, 2H), 1.29 (m, 10H), 0.88 (t, J = 6 Hz, 3H)
40	7.90 (d, J = 6 Hz, 1H), 7.88 (s, 1H), 7.17 (d, J = 9 Hz, 1H), 7.04 (s, 1H), 3.15 (s, 3H), 2.57 (t, J = 6 Hz, 2H), 2.28 (s, 6H), 1.80 (m, 2H), 1.30 (m, 10H), 0.87 (m, 3H)
41	7.76 (s, 2H), 7.03 (s, 1H), 7.00 (s, 1H), 3.15 (s, 3H), 2.58 (t, J = 6 Hz, 2H), 2.33 (s, 6H), 1.82 (pentet, J = 6 Hz, 2H), 1.28 (m, 10H), 0.87 (t, J = 6 Hz, 3H)
42	8.07 (d, J = 9 Hz, 2H), 7.06 (s, 1H), 6.68 (d, J = 9 Hz, 2H), 3.42 (q, J = 6 Hz, 4H), 3.16 (s, 3H), 2.57 (t, J = 6 Hz, 2H), 1.81 (pentet, J = 6 Hz, 2H), 1.30 (m, 10H), 1.19 (t, J = 6 Hz, 6H), 0.89 (t, J = 6 Hz, 3H)
43	DMSO-d_6: 7.46 (d, J = 9 Hz, 1H), 7.00 (s, 1H), 6.26 (d, J = 9 Hz, 1H), 6.04 (s, 1H), 3.36 (q, J = 6 Hz, 4H), 3.08 (s, 3H), 2.64 (t, J = 6 Hz, 2H), 1.68 (pentet, J = 6 Hz, 2H), 1.25 (m, 10H), 1.09 (t, J = 6 Hz, 6H), 0.85 (t, J = 6 Hz, 3H)
44	8.09 (d, J = 9 Hz, 2H), 7.07 (s, 1H), 6.72 (d, J = 9 Hz, 2H), 3.16 (s, 3H), 3.04 (s, 6H), 2.57 (t, J = 6 Hz, 2H), 1.81 (pentet, J = 6 Hz, 2H), 1.30 (m, 10H), 0.89 (t, J = 6 Hz, 3H)
45	7.31 (m, 2H), 7.18 (s, 1H), 6.97 (d, J = 9 Hz, 1H), 6.85 (t, J = 9 Hz, 1H), 3.22 (s, 3H), 2.62 (t, J = 6 Hz, 2H), 1.83 (pentet, J = 6 Hz, 2H), 1.28 (m, 10H), 0.88 (t, J = 6 Hz, 3H)

46	DMSO-d_6: 9.54 (s, 1H), 7.68 (s, 1H), 7.54 (d, J = 6 Hz, 1H), 7.19 (t, J = 9 Hz, 1H), 6.83 (s, 1H), 6.80 (d, J = 9 Hz, 1H), 3.06 (s, 3H), 2.62 (t, J = 6 Hz, 2H), 1.71 (pentet, J = 6 Hz, 2H), 1.24 (m, 10H), 0.83 (t, J = 6 Hz, 3H)
47	DMSO-d_6: 10.08 (s, 1H), 8.07 (d, J = 9 Hz, 2H), 6.86 (s, 1H), 6.81 (d, J = 9 Hz, 2H), 3.05 (s, 3H), 2.60 (t, J = 6 Hz, 2H), 1.69 (pentet, J = 6 Hz, 2H), 1.24 (m, 10H), 0.83 (t, J = 6 Hz, 3H)
48	DMSO-d_6: 9.62 (s, 1H), 7.71 (s, 1H), 7.54 (d, J = 6 Hz, 1H), 7.23 (t, J = 9 Hz, 1H), 7.00 (s, 1H), 6.84 (d, J = 9 Hz, 1H), 4.47 (s, 2H), 3.37 (s, 3H), 3.10 (s, 3H)
49	8.09 (d, J = 9 Hz, 2H), 7.19 (s, 1H), 6.71 (d, J = 9 Hz, 2H), 4.44 (s, 2H), 3.45 (s, 3H), 3.26 (s, 3H), 3.06 (s, 6H)
50	7.24 (s, 1H), 7.16 (d, J = 9 Hz, 1H), 6.24 (dd, J = 9 Hz, 3Hz, 1H), 6.17 (d, J = 3Hz, 1H), 4.42 (s, 2H), 3.41 (s, 3H), 3.39 (q, J = 6 Hz, 4H), 3.30 (s, 3H), 1.21 (t, J = 6 Hz, 6H)
51	DMSO-d_6: 9.56 (s, 1H), 7.73 (s, 1H), 7.55 (d, J = 9 Hz, 1H), 7.21 (t, J = 9 Hz, 1H), 6.85 (s, 1H), 6.81 (d, J = 9 Hz, 1H), 3.07 (s, 3H), 2.68 (q, J = 6 Hz, 2H), 1.25 (t, J = 6 Hz, 3H)
52	8.07 (d, J = 6 Hz, 2H), 7.23 (d, J = 6 Hz, 2H), 7.09 (s, 1H), 3.17 (s, 3H), 2.65 (q, J = 6 Hz, 2H), 2.38 (s, 3H), 1.39 (t, J = 6 Hz, 3H)
53	7.14 (m, 2H), 6.20 (m, 2H), 3.20 (s, 3H), 2.64 (q, J = 6 Hz, 2H), 1.38 (t, J = 6 Hz, 3H)
54	7.79 (s, 2H), 7.05 (s, 1H), 7.01 (s, 1H), 3.18 (s, 3H), 2.66 (q, J = 6 Hz, 2H), 2.35 (s, 6H), 1.40 (t, J = 6 Hz, 3H)
57	7.77 (s, 2H), 7.05 (s, 1H), 7.01 (s, 1H), 3.17 (s, 3H), 2.58 (t, J = 6 Hz, 2H), 2.35 (s, 6H), 1.89 (sextet, J = 6 Hz, 2H), 1.11 (t, J = 6 Hz, 3H)
58	8.07 (d, J = 9 Hz, 2H), 7.06 (s, 1H), 6.68 (d, J = 9 Hz, 2H), 3.49 (q, J = 6 Hz, 2H), 3.40 (q, J = 6 Hz, 4H), 3.16 (s, 3H), 2.56 (t, J = 6 Hz, 2H), 1.87 (sextet, J = 6 Hz, 2H), 1.19 (t, J = 6 Hz, 6H), 1.09 (t, J = 6 Hz, 3H)
59	7.91 (m, 2H), 7.19 (d, J = 9 Hz, 1H), 7.06 (s, 1H), 3.17 (s, 3H), 2.58 (t, J = 6 Hz, 2H), 2.29 (s, 6H), 1.89 (sextet, J = 6 Hz, 2H), 1.10 (t, J = 6 Hz, 3H)
60	7.13 (s, 1H), 7.11 (d, J = 6 Hz, 1H), 6.20 (m, 2H), 3.37 (q, J = 6 Hz, 4H), 3.20 (s, 3H), 2.56 (t, J = 6 Hz, 2H), 1.88 (sextet, J = 6 Hz, 2H), 1.19 (t, J = 6 Hz, 6H), 1.07 (t, J = 6 Hz, 3H)
61	7.90 (m, 2H), 7.12 (d, J = 6 Hz, 1H), 7.00 (s, 1H), 3.13 (s, 3H), 2.81 (pentet, J = 6 Hz, 1H), 2.23 (s, 6H), 1.32 (d, J = 6 Hz, 6H)
62	8.05 (d, J = 9 Hz, 2H), 7.01 (s, 1H), 6.66 (d, J = 9 Hz, 2H), 3.13 (s, 3H), 2.98 (s, 6H), 2.79 (pentet, J = 6 Hz, 1H), 1.30 (d, J = 6 Hz, 6H)
63	7.97 (d, J = 9 Hz, 1H), 7.89 (s, 1H), 7.24 (t, J = 9 Hz, 1H), 7.13 (d, J = 9 Hz, 1H), 7.01 (s, 1H), 3.14 (s, 3H), 2.81 (pentet, J = 6 Hz, 1H), 1.32 (s, 3H), 1.32 (d, J = 6 Hz, 6H)
64	8.13 (d, J = 9 Hz, 2H), 7.31 (m, 3H), 7.04 (s, 1H), 3.14 (s, 3H), 2.82 (pentet, J = 9 Hz, 1H), 1.33 (d, J = 9 Hz, 6H)
65	8.02 (d, J = 9 Hz, 2H), 7.17 (d, J = 9 Hz, 2H), 7.02 (s, 1H), 3.13 (s, 3H), 2.81 (pentet, J = 6 Hz, 1H), 2.32 (s, 3H), 1.32 (d, J = 6 Hz, 6H)

66	DMSO-d_6: 9.48 (s, br, 1H), 7.66 (s, 1H), 7.48 (d, J = 9 Hz, 1H), 7.14 (t, J = 9 Hz, 1H), 6.80 (s, 1H), 6.75 (d, J = 9 Hz, 1H), 3.04 (s, 3H), 2.93 (pentet, J = 6 Hz, 1H), 1.20 (d, J = 6 Hz, 6H)
67	DMSO-d_6: 8.10 (d, J = 9 Hz, 2H), 6.90 (s, 1H), 6.83 (d, J = 9 Hz, 2H), 3.11 (s, 3H), 2.98 (pentet, J = 6 Hz, 1H), 1.26 (d, J = 6 Hz, 6H)
68	7.77 (m, 2H), 7.49 (m, 3H), 7.28 (s, 1H), 7.17 (d, J = 9 Hz, 1H), 6.26 (dd, J = 9 Hz, 3 Hz, 1H), 6.17 (d, J = 3 Hz, 1H), 3.43 (s, 3H), 3.40 (q, J = 6 Hz, 4H), 1.19 (t, J = 6 Hz, 6H)
69	8.18 (d, J = 9 Hz, 2H), 7.61 (d, J = 9 Hz, 2H), 7.54 (d, J = 9 Hz, 2H), 7.14 (s, 1H), 6.93 (d, J = 9 Hz, 2H), 3.20 (s, 3H), 2.40 (s, 3H)
70	DMSO-d_6: 10.21 (s, br, 1H), 8.18 (d, J = 9 Hz, 2H), 7.93 (d, J = 9 Hz, 2H), 7.61 (m, 3H), 7.10 (s, 1H), 6.87 (d, J = 9 Hz, 2H), 3.25 (s, 3H)
71	DMSO-d_6: 9.56 (s, 1H), 7.88 (d, J = 9 Hz, 2H), 7.78 (s, 1H), 7.73 (d, J = 9 Hz, 1H), 7.51 (m, 3H), 7.17 (t, J = 9 Hz, 1H), 6.99 (s, 1H), 6.77 (m, 1H), 3.18 (s, 3H)
72	7.77 (d, J = 9 Hz, 2H), 7.52 (m, 3H), 7.30 (m, 2H), 7.28 (s, 1H), 6.92 (d, J = 9 Hz, 1H), 6.82 (t, J = 9 Hz, 1H), 3.38 (s, 3H)
73	8.12 (d, J = 9 Hz, 2H), 7.64 (m, 2H), 7.45 (m, 3H), 7.20 (s, 1H), 6.66 (d, J = 9 Hz, 2H), 4.45 (s, 2H), 3.64 (s, 3H), 3.00 (s, 6H)
74	8.25 (d, J = 9 Hz, 2H), 7.87 (m, 2H), 7.56 (m, 3H), 7.40 (m, 3H), 7.27 (s, 1H), 3.37 (s, 3H)
75	8.11 (d, J = 9 Hz, 1H), 7.99 (s, 1H), 7.87 (m, 2H), 7.56 (m, 3H), 7.32 (t, J = 9 Hz, 1H), 7.24 (s, 1H), 7.22 (d, J = 9 Hz, 1H), 3.37 (s, 3H), 2.40 (s, 3H)
76	7.13 (s, 1H), 7.11 (d, J = 9 Hz, 1H), 6.23 (dd, J = 9 Hz, 3 Hz, 1H), 6.18 (d, J = 3 Hz, 1H), 3.40 (q, J = 6 Hz, 4H), 3.20 (s, 3H), 2.57 (t, J = 6 Hz, 2H), 1.81 (pentet, J = 6 Hz, 2H), 1.30 (m, 8H), 1.20 (t, J = 6 Hz, 6H), 0.89 (t, J = 6 Hz, 3H),
77	DMSO-d_6: 8.08 (d, J = 9 Hz, 2H), 6.87 (s, 1H), 6.82 (d, J = 9 Hz, 2H), 3.05 (s, 3H), 2.60 (t, J = 6 Hz, 2H), 1.70 (pentet, J = 6 Hz, 2H), 1.27 (m, 8H), 0.86 (t, J = 6 Hz, 3H)
78	8.00 (d, J = 9 Hz, 1H), 7.94 (s, 1H), 7.31 (t, J = 9 Hz, 1H), 7.19 (d, J = 9 Hz, 1H), 7.07 (s, 1H), 3.17 (s, 3H), 2.60 (t, J = 6 Hz, 2H), 2.39 (s, 3H), 1.83 (pentet, J = 6 Hz, 2H), 1.31 (m, 8H), 0.90 (t, J = 6 Hz, 3H)
79	8.68 (m, 1H), 7.38 (s, 1H), 7.24 (m, 3H), 3.18 (s, 3H), 2.59 (t, J = 6 Hz, 2H), 2.48 (s, 3H), 1.81 (pentet, J = 6 Hz, 2H), 1.31 (m, 8H), 0.90 (t, J = 6 Hz, 3H)
80	7.77 (s, 2H), 7.04 (s, 1H), 7.01 (s, 1H), 3.17 (s, 3H), 2.60 (t, J = 6 Hz, 2H), 2.35 (s, 6H), 1.83 (pentet, J = 6 Hz, 2H), 1.31 (m, 8H), 0.89 (t, J = 6 Hz, 3H)
81	7.93 (d, J = 9 Hz, 1H), 7.91 (s, 1H), 7.19 (d, J = 9 Hz, 1H), 7.06 (s, 1H), 3.17 (s, 3H), 2.59 (t, J = 9 Hz, 2H), 2.29 (s, 6H), 1.83 (pentet, J = 6 Hz, 2H), 1.32 (m, 8H), 0.90 (t, J = 6 Hz, 3H)
82	8.09 (d, J = 9 Hz, 2H), 7.07 (s, 1H), 6.72 (d, J = 9 Hz, 2H), 3.16 (s, 3H), 3.04 (s, 6H), 2.57 (t, J = 6 Hz, 2H), 1.82 (pentet, J = 6 Hz, 2H), 1.32 (m, 8H), 0.90 (t, J = 6 Hz, 3H)

83	7.31 (m, 2H), 7.17 (s, 1H), 6.97 (d, J = 9 Hz, 1H), 6.85 (t, J = 9 Hz, 1H), 3.22 (s, 3H), 2.62 (t, J = 6 Hz, 2H), 1.83 (pentet, J = 6 Hz, 2H), 1.30 (m, 8H), 0.89 (t, J = 6 Hz, 3H)
84	8.29 (s, 4H), 7.79 (m, 1H), 7.61 (m, 1H), 7.38 (m, 2H), 7.13 (s, 1H), 3.21 (s, 3H), 2.43 (s, 3H)
85	8.29 (s, 4H), 7.79 (m, 1H), 7.60 (m, 1H), 7.37 (m, 2H), 7.11 (s, 1H), 3.61 (t, J = 6 Hz, 2H), 2.43 (s, 3H), 1.26 (m, 20H), 0.88 (t, J = 6 Hz, 3H)
86	8.29 (s, 4H), 7.79 (m, 1H), 7.61 (m, 1H), 7.37 (m, 2H), 7.10 (s, 1H), 3.61 (t, J = 6 Hz, 2H), 2.43 (s, 3H), 1.64 (pentet, J = 6 Hz, 2H), 1.35 (m, 4H), 0.91 (t, J = 6 Hz, 3H)
87	8.29 (s, 4H), 7.79 (m, 1H), 7.60 (m, 1H), 7.37 (m, 2H), 7.11 (s, 1H), 3.62 (t, J = 6 Hz, 2H), 2.43 (s, 3H), 1.62 (m, 2H), 1.40 (sextet, J = 6 Hz, 2H), 0.97 (t, J = 6 Hz, 3H)
89	8.23 (d, J = 9 Hz, 2H), 8.10 (d, J = 15 Hz, 1H), 7.63 (m, 2H), 7.41 (m, 3H), 7.15 (s, 1H), 6.99 (d, J = 9 Hz, 2H), 6.86 (d, J = 15 Hz, 1H), 3.88 (s, 3H), 3.33 (s, 3H)
90	8.18 (d, J = 9 Hz, 2H), 7.37 (doublet of quartets, J = 15 Hz, 9 Hz, 1H), 7.20 (s, 1H), 6.80 (d, J = 9 Hz, 2H), 6.28 (d, J = 15 Hz, 1H), 3.31 (s, 3H), 3.09 (s, 6H), 2.10 (d, J = 6 Hz, 3H)
91	8.34 (d, J = 9 Hz, 2H), 8.25 (d, J = 9 Hz, 2H), 7.49 (doublet of quartets, J = 15 Hz, 9 Hz, 1H), 7.06 (s, 1H), 6.32 (d, J = 15 Hz, 1H), 3.25 (s, 3H), 2.10 (d, J = 6 Hz, 3H)
92	8.40 (d, J = 9 Hz, 2H), 8.30 (d, J = 9 Hz, 2H), 8.24 (d, J = 15 Hz, 1H), 7.67 (m, 2H), 7.46 (m, 3H), 7.11 (s, 1H), 6.89 (d, J = 15 Hz, 1H), 3.36 (s, 3H)
95	8.18 (d, J = 9 Hz, 2H), 8.06 (d, J = 15 Hz, 1H), 7.63 (m, 2H), 7.41 (m, 3H), 7.16 (s, 1H), 6.88 (d, J = 15 Hz, 1H), 6.76 (d, J = 9 Hz, 2H), 3.33 (s, 3H), 3.07 (s, 6H)
96	DMSO-d_6: 10.18 (s, br, 1H), 8.19 (d, J = 9 Hz, 2H), 7.99 (d, J = 15 Hz, 1H), 7.85 (m, 2H), 7.44 (m, 3H), 7.24 (d, J = 15 Hz, 1H), 6.96 (s, 1H), 6.87 (d, J = 9 Hz, 2H), 3.26 (s, 3H)

Table A.2 Mass Spectrometry and ^{13}C Data for a Representative Selection of Chromophores

Compound #	^{13}C NMR data (ppm), $CDCl_3$, unless otherwise noted	*m/z* $[M+H]^+$
11	171.06, 165.64, 138.84, 134.32, 132.22, 129.94, 128.63, 127.02, 31.69, 29.29, 28.99, 28.86, 26.48, 25.44, 22.62, 14.10	Calculated: 285.1961 Found: 285.1958
15	168.14, 161.53, 158.57, 136.42, 134.09, 132.68, 130.25, 119.69, 119.41, 119.16, 26.53, 21.75, 8.73	Calculated: 231.1128 Found: 231.1125

20	In DMSO-d_6: 170.45, 165.29, 159.96, 136.66, 134.57, 125.99, 125.86, 116.14, 31.31, 28.22, 26.50, 24.58, 22.29, 14.32	Calculated: 273.1598 Found: 273.1595
25	In DMSO-d_6: 170.45, 165.30, 159.97, 136.64, 134.57, 126.00, 125.85, 116.16, 28.02, 27.31, 26.50, 22.31, 14.17	Calculated: 259.1441 Found: 259.1439
30	In DMSO-d_6: 170.52, 167.23, 157.73, 139.18, 135.67, 129.93, 125.47, 123.78, 118.53, 117.78, 28.11, 27.20, 26.55, 22.32, 14.16	Calculated: 259.1441 Found: 259.1439
34	171.07, 162.42, 149.11, 134.55, 134.45, 128.85, 121.62, 111.24, 44.51, 26.31, 22.15, 12.64, 9.75	Calculated: 286.1914 Found: 286.1911
37	171.12, 164.95, 140.51, 138.11, 132.24, 131.62, 129.45, 127.34, 31.82, 29.34, 29.29, 29.16, 28.86, 26.48, 25.51, 22.65, 21.65, 14.10	Calculated: 313.2274 Found: 313.2272
38	171.09, 165.82, 139.36, 138.77, 132.75, 132.20, 130.37, 129.89, 126.30, 124.05, 31.81, 29.36, 29.26, 29.15, 28.92, 26.52, 25.57, 22.64, 20.14, 14.10	Calculated: 313.2274 Found: 313.2272
42	171.07, 161.64, 149.08, 134.54, 134.51, 128.73, 121.66, 111.23, 44.51, 29.32, 29.19, 28.80, 26.43, 25.67, 22.67, 14.11, 12.64	Calculated: 370.2853 Found: 370.2847
45	168.16, 160.77, 158.63, 136.40, 134.08, 132.72, 130.22, 119.71, 119.38, 119.18, 31.76, 29.15, 29.13, 29.12, 28.25, 26.67, 24.73, 22.61, 14.09	Calculated: 315.2067 Found: 315.2064
47	In DMSO-d_6: 170.44, 165.26, 159.96, 136.65, 134.57, 125.98, 125.86, 116.13, 31.70, 29.16, 29.10, 29.06, 28.23, 26.49, 25.15, 22.54, 14.41	Calculated: 315.2067 Found: 315.2067
57	171.10, 165.00, 138.50, 138.05, 134.16, 131.99, 130.06, 127.60, 30.72, 26.44, 21.32, 18.98, 13.93	Calculated: 257.1648 Found: 257.1646
61	171.51, 168.68, 139.38, 137.95, 136.78, 133.52, 132.08, 130.06, 130.04, 127.69, 27.74, 26.54, 19.97, 19.87, 19.56	Calculated: 257.1648 Found:257.1645
62	171.40, 166.07, 151.39, 134.91, 134.30, 128.63, 122.52, 111.71, 40.06, 27.63, 26.49, 19.69	Calculated: 272.1757 Found: 272.1754
66	In DMSO-d_6: 171.11, 170.86, 157.72, 139.02, 135.66, 129.94, 125.76, 123.87, 118.66, 117.83, 27.27, 26.66, 19.84	Calculated: 245.1285 Found: 245.1283

68	168.51, 161.31, 153.39, 152.08, 139.05, 133.04, 131.12, 128.93, 128.42, 128.09, 127.93, 110.16, 104.90, 99.17, 44.70, 29.26, 12.80	Calculated: 350.1863 Found: 350.1859
80	171.12, 165.18, 138.48, 138.05, 134.15, 131.99, 130.06, 127.63, 31.71, 29.29, 29.04, 28.77, 26.47, 25.42, 22.64, 21.30, 14.08	Calculated: 313.2274 Found: 313.2273
83	168.09, 160.83, 158.59, 136.39, 134.04, 132.71, 130.04, 119.68, 119.37, 119.14, 31.64, 29.10, 28.85, 28.20, 26.61, 24.65, 22.58, 14.06	Calculated: 301.1911 Found: 301.1908
92	In DMSO-d_6: 170.43, 163.66, 147.56, 142.76, 142.65, 141.55, 135.43, 133.11, 131.01, 129.41, 129.06, 124.02, 121.57, 114.25, 27.04	Calculated: 334.1186 Found: 334.1184
96	In DMSO-d_6: 170.41, 160.22, 159.19, 139.89, 137.33, 136.74 135.66, 134.96, 130.45, 129.35, 128.71, 126.41, 126.24, 116.33, 26.84	Calculated: 305.1285 Found: 305.1282

APPENDIX B

SUPPLEMENTAL FIGURES

Figure B.1: Steady-state fluorescence (left) and absorbance (bottom, black) spectra for compound 86 in solution. Also shown are the absorbance in the solid state (bottom, blue), the 3D solid state spectrum (center), and the excitation spectrum at 600 nm emission extracted from the 3D plot (bottom, red).

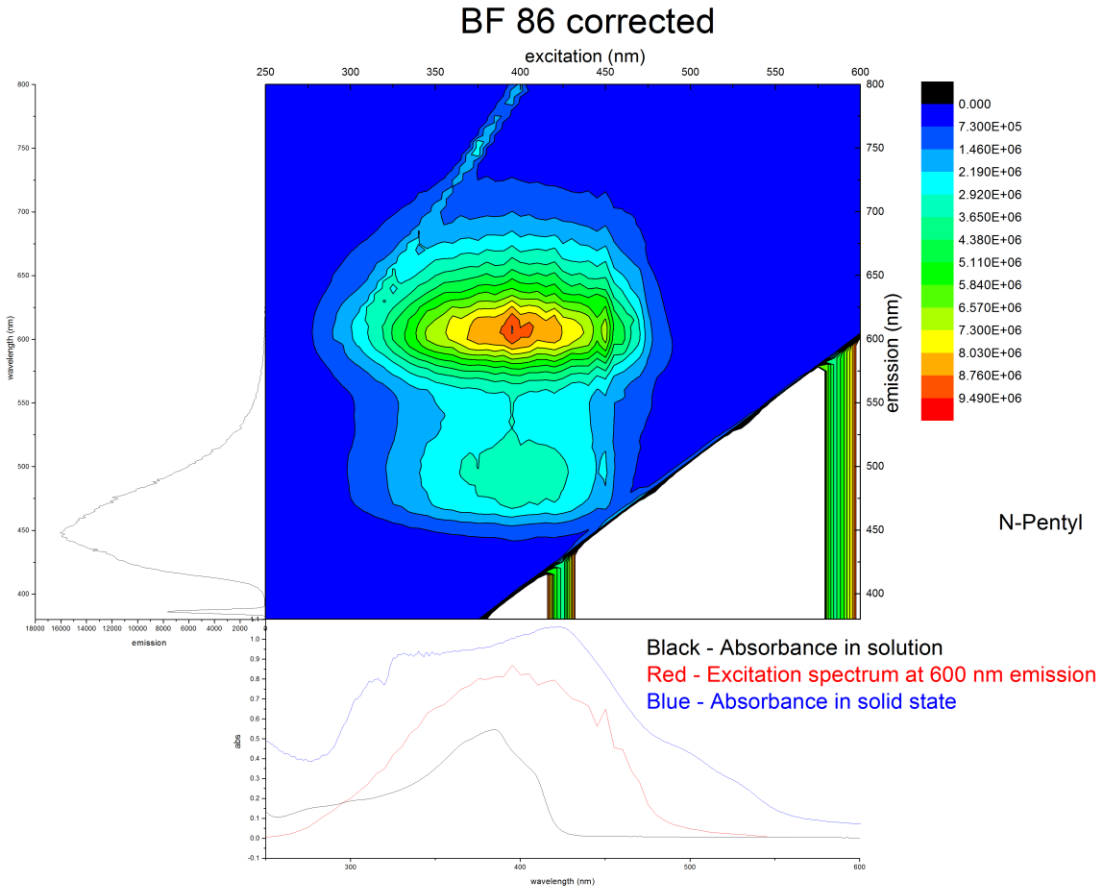

Figure B.2: Steady-state fluorescence (left) and absorbance (bottom, black) spectra for compound 87 in solution. Also shown are the absorbance in the solid state (bottom, blue), the 3D solid state spectrum (center), and the excitation spectrum at 600 nm emission extracted from the 3D plot (bottom, red).

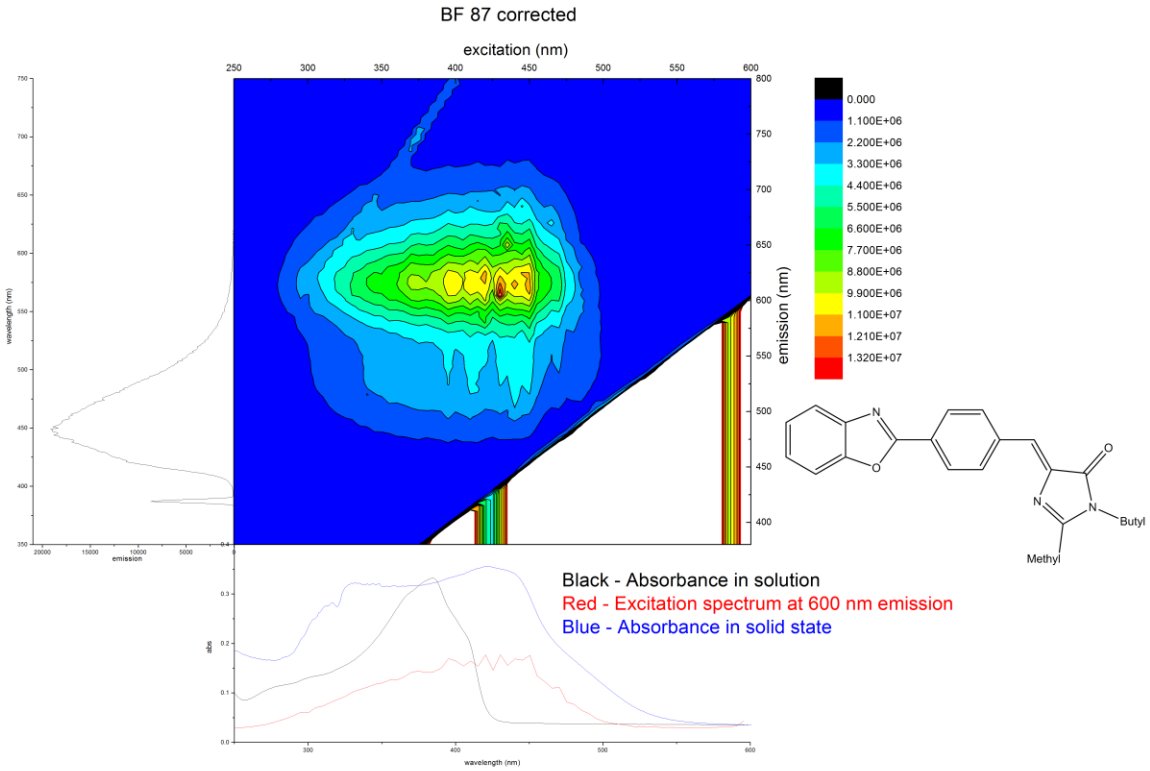

Figure B.3: Fluorescence decay spectrum of compound 86, taken with 372 nm laser excitation.

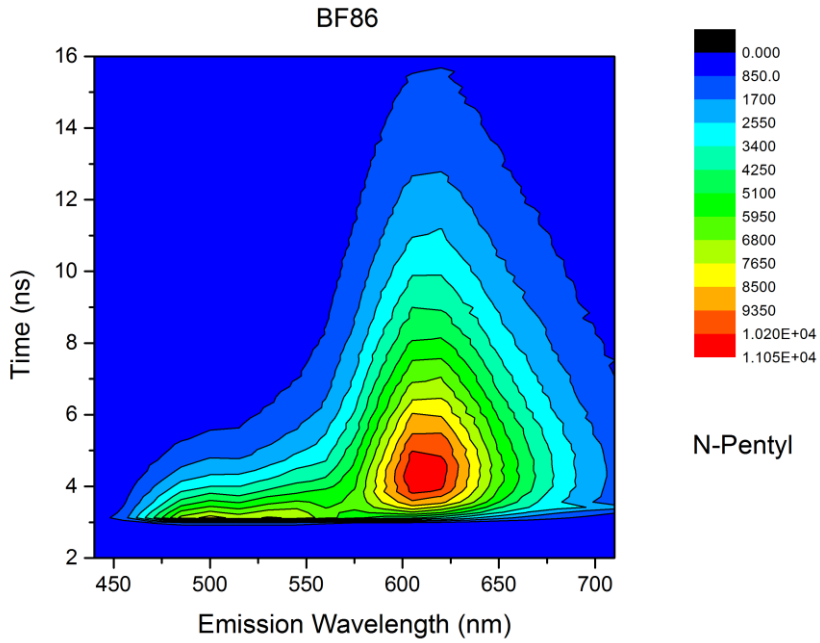

Figure B.4: Fluorescence decay spectrum of compound 87, taken with 372 nm laser excitation.

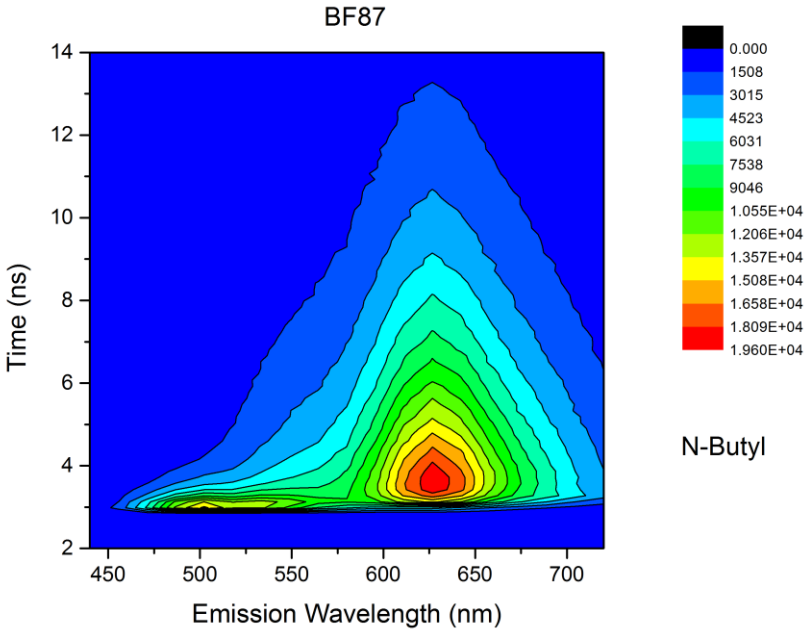

Figure B.5: UV-Vis spectrum for BDI 90 in DCM

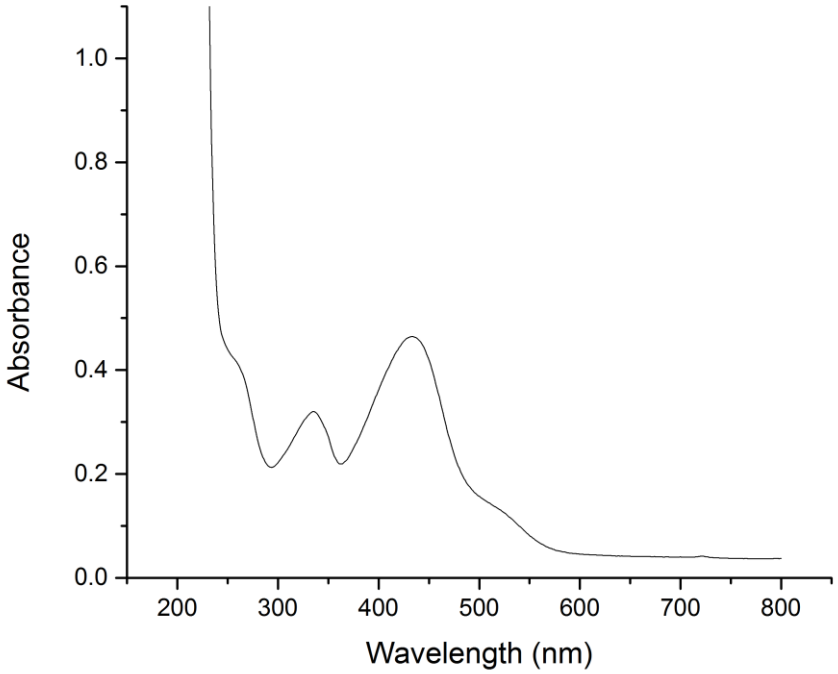

Figure B.6: UV-Vis spectrum for BDI 95 in DCM

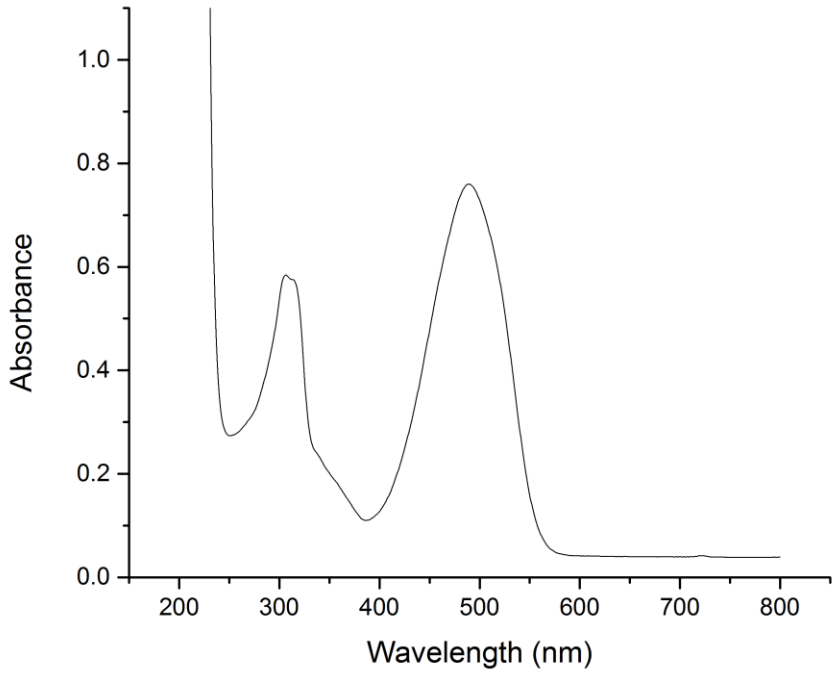

Figure B.7: UV-Vis spectrum for BDI 96 in DCM

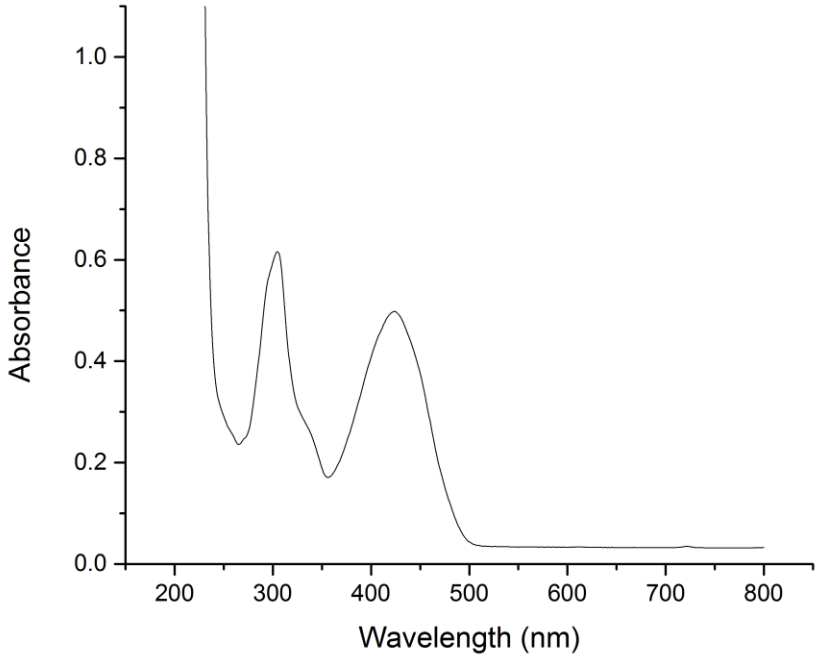

Figure B.8: Emission spectrum of BDI 90 in DCM

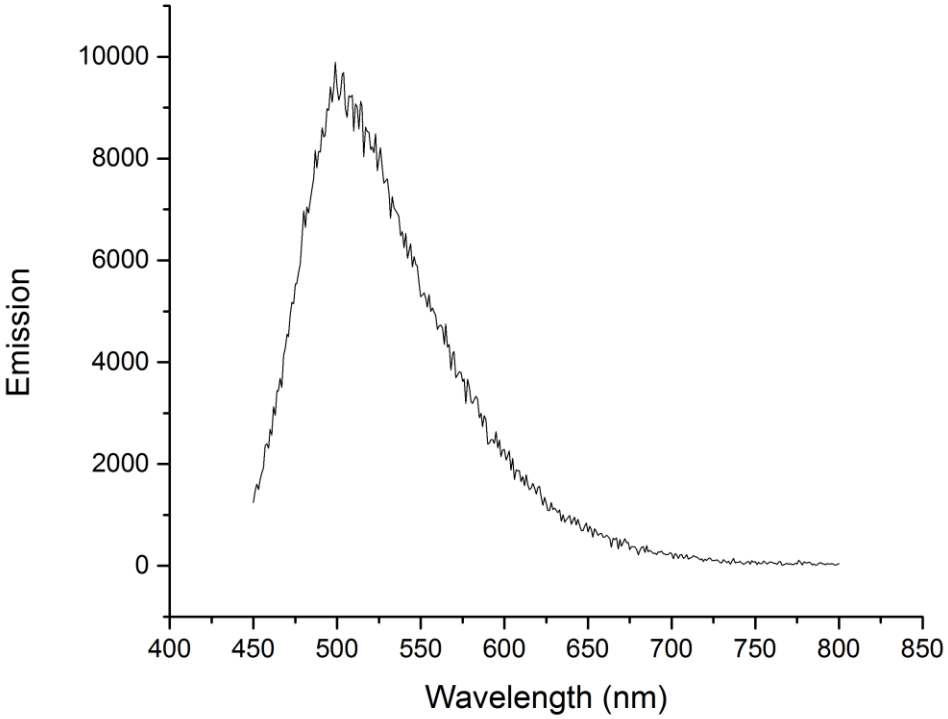

Figure B.9: Emission spectrum of BDI 91 in DCM

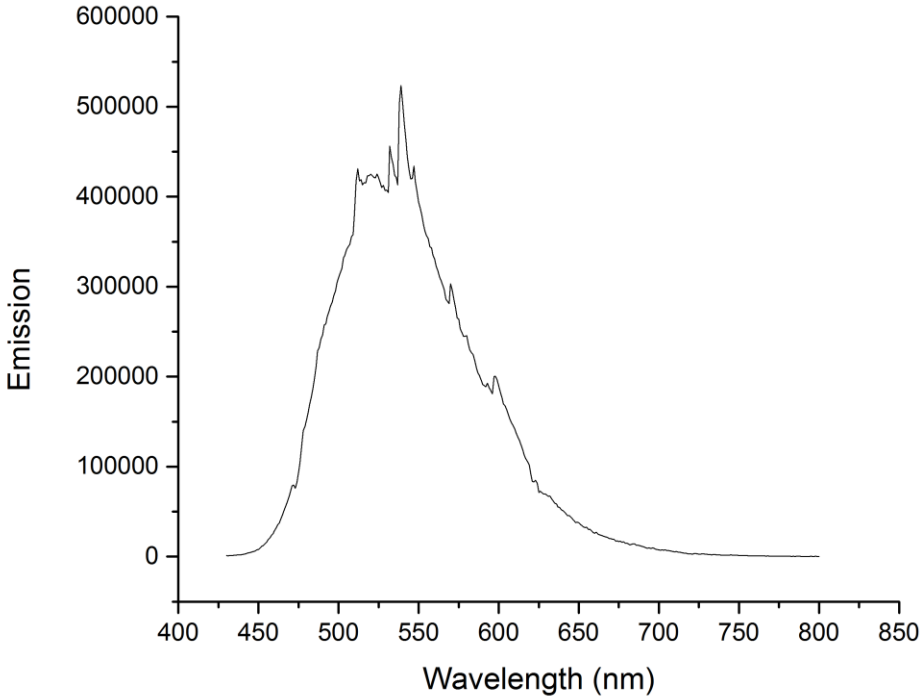

Figure B.10: Emission spectrum of BDI 92 in DCM

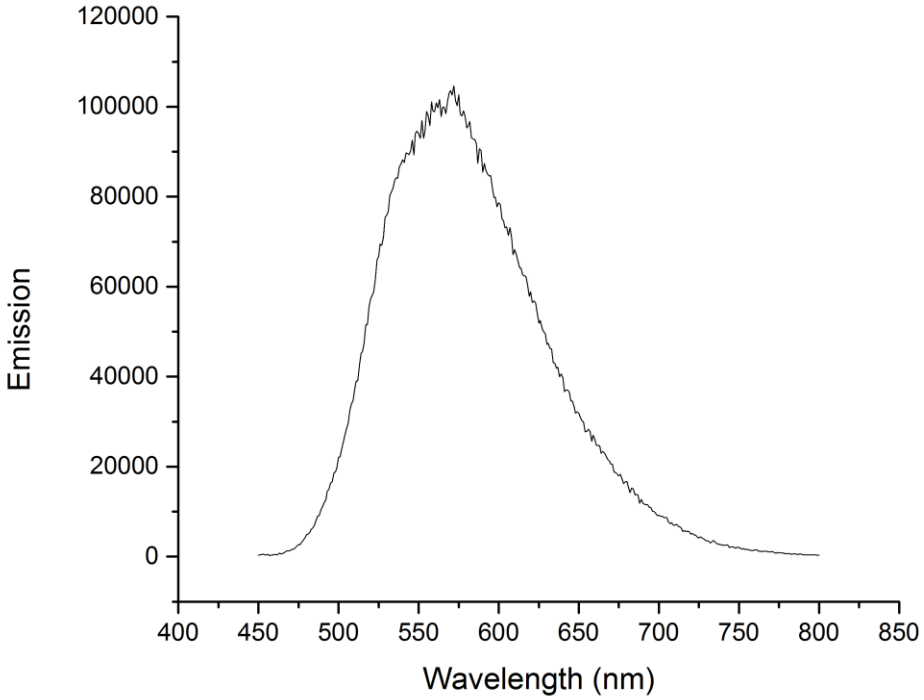

Figure B.11: Emission spectrum of BDI 95 in DCM

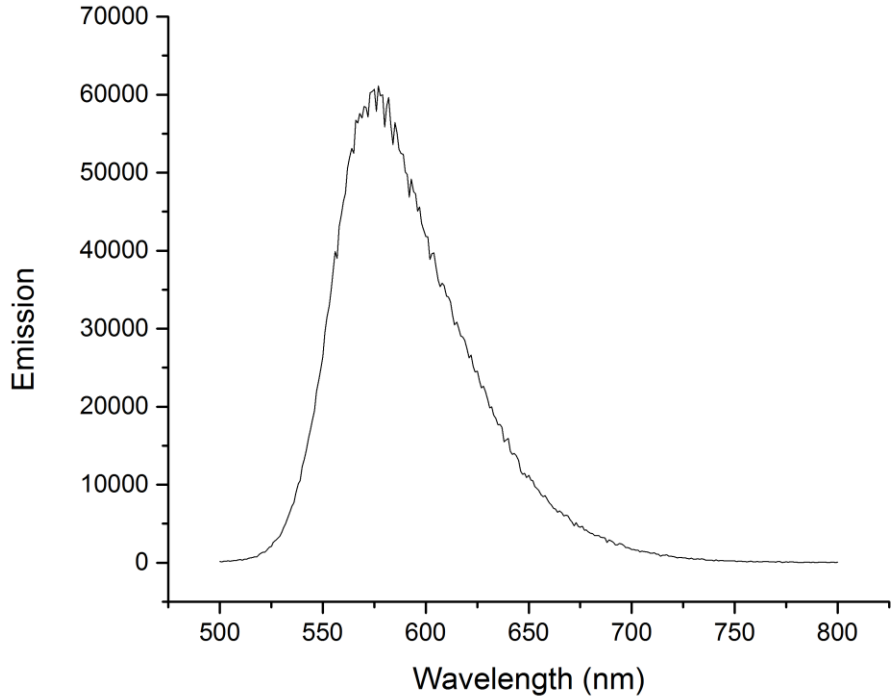

Figure B.12: Emission spectrum for BDI 96 in DCM